Experimental Evaluation of Solids and Ash Removal Pathways of Fast Pyrolysis Bio-oils

Dillon Mazerolle

Thesis submitted to the faculty of graduate and postdoctoral studies at the University of Ottawa in partial fulfillment of the requirements for the degree

MASTER OF APPLIED SCIENCE IN CHEMICAL ENGINEERING

Executive Summary

Biomass liquefaction by fast pyrolysis is considered to be a key technology in future biorefineries for the production of low-carbon renewable liquids. These liquids may be used as a fuel for heat and power, as an intermediate for catalytic upgrading to distillate transportation fuels (such as renewable diesel or biojet) and as a raw material for advanced bioproducts. With the estimated supply of bioenergy required to meet international GHG reduction targets, the use of high ash (mineral-containing) biomass sources, such as harvest residues, hog fuels, and other unmerchantable wood sources is also expected to increase.

However, the elevated presence of suspended char particulate (solids), as well as minerals and other ash components contained in pyrolytic liquids resulting from the conversion of these lower quality biomass residues may create new challenges for end-users. In light of this, two treatment pathways were investigated in this work: biomass pretreatment through sieving and acid washing, and post-condensation microfiltration of fast pyrolysis bio-oils. Selection of these two pathways was prioritized based on scarcity of published data, as well as the technical potential of both approaches for suspended char particulate and ash reduction in fast pyrolysis bio-oils.

For biomass sieving and acid washing carried out at pilot scale, it was found that removing up to 80% of the ash contained in a hog fuel feedstock was possible by sieving out a fraction of the fines and subsequently washing with 0.1M nitric acid provided up to 40% increase in organic liquid yield after fast pyrolysis. Reaction water in the product was minimized when acid leaching was performed, while the solids content and ash content of the produced liquids were reduced by up to 80% and 87%, respectively.

Cross-flow microfiltration of fast pyrolysis bio-oils produced principally from non-pretreated mill and harvest residues in the 1-40 µm range was performed. Microfiltration was found to remove between 80-95% of suspended solid particles, while only removing 4-45% of ash, presumably in the solid phase. To achieve high ash removal (>90%), microfiltration was combined with use of solid-phase adsorbents, such as Amberlyst 15, to remove cationic ash elements such as magnesium, calcium, iron, etc.

The flux profiles from bio-oil cross-flow microfiltration were analyzed and consistently demonstrated a transient rapid and intermediate decline operating region, followed by a pseudo steady-state operating region. It was found that the initial flux of permeate in the transient operating region ranged from 100-1000 L m^{-2} h^{-1}, while the pseudo steady-state flux ranged from 20-50 L m^{-2} h^{-1} for the experimental trials included in this study. It was determined that bio-oil temperatures of 50-60 ˚C, transmembrane pressures

less than 1 bar and the addition of diluent solvents provided the highest pseudo steady-state fluxes of such a process. To improve the throughput of the process, different fouling remediation strategies were experimentally evaluated. The use of permeate, solvent and air backflushing confirmed that on-line cleaning strategies are suitable for active flux remediation, as fouling was found to be reversible over continuous operating periods up to 10 hours. Furthermore, it was found that the use of non-optimized on-line air backflushing resulted in increased throughput of low solids fast pyrolysis bio-oil from cross-flow microfiltration by 100%.

Ultimately, the data produced from this work is intended to be used to generate design parameters and associated cost estimates for biomass washing and post-condensation microfiltration as processing strategies to generate high quality bio-oils from low cost biomass feedstocks.

Résumé

La pyrolyse rapide est un procédé qui convertit la biomasse en bio-huile. Cette technologie est appelée à jouer un rôle déterminant dans les futures bioraffineries pour la production de biocarburants renouvelables à faible taux d'émissions. Ces bio-huiles peuvent être utilisées pour la production de chaleur, d'électricité, ou comme produits intermédiaires pour des procédés de raffinage catalytique. Ces procédés peuvent générer des distillats pour le transport (tels que le diésel renouvelable ou le biocarburant pour avions) ou encore une variété de bioproduits. L'atteinte des cibles internationales de réduction des GES implique une demande accrue pour la bioénergie, cette croissance devrait également se refléter sur l'utilisation de biomasses dont le taux de cendre est élevé. Par exemple, ceci inclut les résidus forestiers, les résidus des usines de pâtes et papier et d'autres sources de bois non commercialisables.

La pyrolyse rapide d'une biomasse de qualité inférieure entraîne une augmentation des particules solides ainsi qu'un taux de cendre élevé dans la bio-huile. La présence de ces solides peut rendre l'utilisation des bio-huiles plus difficile. En réponse à ce problème potentiel, deux processus furent investigués pour la réduction du taux des cendres et des particules solides contenus dans la bio-huile pyrolytique. Le premier est le prétraitement de la biomasse par tamisage et lavage à l'acide, et puis le second est la microfiltration de la bio-huile pyrolytique. La sélection de ces deux processus a été priorisée en fonction de la rareté des données publiques et le potentiel technique de ces deux approches.

Les résultats des expériences démontrent que le tamisage et le lavage par acide nitrique d'un résidu forestier («*hog fuel*»), dérivé de l'opération d'une usine de pâtes et papier, ont réduit le taux de cendre de ce résidu jusqu'à 80 %. Également, ce prétraitement améliore le rendement en bio-huile jusqu'à 40 %, obtenue suite à une pyrolyse rapide. De plus, la quantité d'eau contenue dans la bio-huile est moindre lorsqu'un lavage de la biomasse a été effectué. La teneur en cendre et en particules solides fut réduite de 80 % et 87 %, respectivement.

Par ailleurs, la microfiltration à flux croisés de la bio-huile pyrolytique a été effectuée avec des filtres/membranes dont la taille des pores était de 1 à 40 micromètres. Il fut observé que la microfiltration peut retirer 80 à 95 % des particules solides, mais seulement 4 à 45 % des cendres. Afin d'enlever plus de cendre (>90 %), incluant des éléments cationiques comme le magnésium, le calcium, le fer, etc., la microfiltration a été combinée à des adsorbants en phase solide, comme l'Amberlyst 15.

Le profil des flux volumiques, obtenu de la microfiltration de la bio-huile pyrolytique, a été analysé et a démontré une zone de déclin rapide et transitoire, suivie par une zone d'opération en état de pseudo-équilibre. Il a été constaté que le flux initial du filtrat dans la région transitoire était très variable entre 100 et 1000 L m^{-2} h^{-1}, tandis que le flux à l'état de pseudo-équilibre était moins variable entre 20 et 50 L m^{-2} h^{-1} dans la plupart des cas. Il a été observé qu'une température de la bio-huile entre 50 et 60 °C, des pressions transmembranaires sous 1 bar et l'ajout de solvants diluants permettaient des flux plus élevés à l'état pseudo-équilibre. Afin d'améliorer l'efficacité de la microfiltration, plusieurs stratégies furent évaluées afin d'éviter l'encrassement («*fouling*») des membranes ou filtres. Parmi ces stratégies, le rétro lavage utilisant le filtrat, l'utilisation d'une variété de solvants et de l'air. Ces stratégies de nettoyage sont convenables pour la régénération du flux. Notamment, le rétro lavage avec de l'air à basse pression a doublé la productivité de la microfiltration de la bio-huile pyrolytique.

En fin de compte, les données produites à partir de ce travail ont pour but de guider la formation de paramètres d'estimation de coûts pour les processus de lavage de la biomasse et la microfiltration de la bio-huile. Ces traitements permettent de produire des bio-huiles de hautes qualités à partir d'une matière première (biomasse) à faible coût.

Acknowledgements

I would like to express my gratitude to my supervisors, Benjamin Bronson and Dr. Boguslaw Kruczek, for their time, patience and expertise. These proved to be invaluable in planning the scope of work, executing trials, interpreting experimental data and reviewing this thesis.

The aid of many other colleagues at CanmetENERGY-Ottawa Bell's Corners Complex was required for the completion of this work. I would like to thank Dr. Fernando Preto and Dr. Sebnem Madrali for their guidance and expertise in planning and review. Supply of suitable quantities of fast pyrolysis bio-oil over the past few years would not have been possible without the contributions of Frank Leclair, Leslie Nguyen, Evan Shuparski, Éric Robert, Jaden Murphy, Simon Lalonde, Chad Scobie, Berney Chan and Andrew Jewlal. Many of these individuals also assisted in some other capacity over the course of this project. I would like to acknowledge and thank Al Vaillancourt for manufacturing the customized cells that were used for bio-oil microfiltration.

I would also like to thank the staff of the characterization laboratory at CanmetENERGY-Ottawa Bell's Corners Complex, as well as Hooman Rezaei, Serge Genest and the characterization laboratory at FPInnovations Pointe-Claire. Their specialized analytical services for the characterization of pyrolysis liquids and biomass feedstocks were critical in the delivery of this work.

I would like to express my gratitude to the leadership and management at CanmetENERGY-Ottawa for their support for the completion of this thesis. Funding for the research was provided by Natural Resources Canada's Office of Energy Research & Development through the Program for Energy Research and Development as well as Canadian Forestry Service's Forestry Innovation Program.

For their continuous encouragement, sacrifice and support, I would like to express my sincere appreciation to Michelle, Lori, Mark, Kyle and Carter. This would not have been possible without you.

Table of Contents

List of Figures

List of Tables

Nomenclature

Abbreviation	Definition	Notes
>35M	Interior Hog Fines > 35 Mesh	Biomass feedstock used in chapter 2 study
AAEM	Alkali and alkaline earth metal	used to represent sodium, potassium, magnesium and calcium in biomass
ASTM	American Society for Testing and Materials	
AW >35M	Nitric Acid-Washed Interior Hog Fines > 35 Mesh	Biomass feedstock used in chapter 2 study
BRDL	Below reportable detection limit	
FPBO	Fast pyrolysis bio-oil	also called bio-oil, pyrolysis oil
CE-O	CanmetENERGY-Ottawa	
daf	Dry, ash-free basis	
DEGMME	Diethylene glycol monomethyl ether	
GCMS	Gas Chromatography Mass Spectroscopy	
HB	Hydrophobic	
HXL	Heat exchanger liquids	secondary fraction of liquid collected in CE-O's fluidized bed fast pyrolysis system
ICP-OES	Inductively Coupled Plasma Optical Emission Spectrometry	
IHF	Interior Hog Fuel	Biomass feedstock used in chapter 2 study
LMH	Liters per meters squared per hour	
LPH	Liters per hour	
LPM	Liters per minute	
MF	Microfiltration	
NCG	Non-Condensable Gas	gas produced from fast pyrolysis of biomass
odt	Oven-dry tonnes	
PCL	Primary condensation liquids	principal fraction of liquid collected in CE-O's fluidized bed fast pyrolysis system
PCTE	Polycarbonate	
PRESS	Predictive error sum of squares	
PTFE	Polytetrafluoroethylene (Teflon)	Filtration media material used
Solids	Suspended char particulate in fast pyrolysis bio-oils	
SS	Stainless steel	
S-S	Steady-state	
TEA	Technoeconomic assessment	
UF	Ultrafiltration	
WIS	Water-insoluble fraction	characteristic fraction of pyrolysis oil produced from phase separation. Also called "organic" fraction
WS	Water-soluble fraction	characteristic fraction of pyrolysis oil produced from phase separation. Also called "aqueous" fraction
XRF	X-Ray Fluorescence	

Variables

Abbreviation	Definition	Units
μ	Fluid kinematic viscosity	$mm^2\ s^{-1}$ (cSt, $m^2\ s^{-1}$)
A	Active filtration surface area	m^2
J	Permeate flux	$L\ m^{-2}\ h^{-1}$ ($m^3\ m^{-2}\ h^{-1}$)
l	membrane thickness	m (mm)
n_p	number of pores per unit area	m^{-2}
θc	Solid volume fraction in cake	
θs	Solid volume fraction in fluid suspension	
$\hat{R}_C$	Specific cake resistance	m^{-2}
R_C	Cake resistance	m^{-1}
R_M	Membrane resistance	m^{-1}
R_p	Pore plugging resistance	m^{-1}
R_T	Total filtration resistance	m^{-1}
S_M	specific surface area	$m^2\ m^{-3}$
t	Processing time	s (h, min)
TMP	Transmembrane pressure	Pa (bar, psi)
V	Volume of low solids permeate processed	m^3 (L)
ΔP	See TMP	
ε_C	Cake porosity	
ε_M	Membrane porosity	

Chapter 1. Introduction

1.1. Background

The growth of the bioenergy sector will require diversification of numerous key technologies to help provide the energy volumes, security, diversity, socio-economic benefits and fuel flexibility required to meet the GHG reduction targets set in the 2015 Paris Agreement [1]. Information on greenhouse gas emission reduction targets and the urgent need to transition to clean, low-carbon or renewable energy technologies is thoroughly conveyed in publically-available reports [1,2]. One of the bioenergy conversion pathways which has the potential to significantly contribute to this future outlook is the fast pyrolysis liquefaction of lignocellulosic biomass to produce fast pyrolysis bio-oil (FPBO).

This thesis dissertation focusses on evaluating two different treatment pathways to resolve a technical challenge associated with the utilization of fast pyrolysis bio-oils produced from low quality forestry residues containing elevated levels of suspended char particulate (solids) and ash. The reduction of solids and ash in FPBO to levels below 0.25 wt% and 0.15 wt%, respectively, may be viewed as a critical requirement prior to its use as a low-carbon, renewable fuel for heat and power generation, or similarly as an intermediate product for the catalytic upgrading into low-carbon, renewable distillate transportation fuels [3].

In the context of this thesis, solids are defined as the suspended char particulate contained in the liquid matrix of bio-oil, originating from imperfect separation of fast pyrolysis biochar by-products. Meanwhile, ash is defined as mineral matter contained in the liquid matrix of bio-oil and can be present as water or oil soluble compounds as well as extraneous, non-carbonaceous solids [4].

An internal review was previously carried out on evaluating the performance of numerous pilot or bench scale solids/ash reduction strategies in biomass pyrolysis liquids produced from low quality/high ash Canadian biomass feedstocks [5]. This included, but was not limited to: biomass pretreatment (washing), hot vapour filtration, membrane separation, centrifugation, distillation, staged condensation, emulsification, water-induced phase separation, esterification, etc. Hot vapour filtration is a solids/ash reduction pathway that has been studied in a number of publications [6–11]. Emulsification of low concentrations (< 50%) of FPBO with diesel has been demonstrated to add minor incremental costs (cents/litre) and incur combustion advantages (ex. reduced NOx) and disadvantages (ex. denser smoke) relative to use of pure diesel fuel [12,13]. Vacuum and molecular distillation, as well as staged

condensation and water-induced phase separation have all been studied for water removal in heavy, energy-rich fractions, as well as concentration of chemical components of raw bio-oil in light fractions [14–18]. Esterification reduces the acidity of bio-oil by reacting low chain alcohols with components such as carboxylic acids [19,20].

The development of technoeconomic assessments (TEAs) associated with the aforementioned treatment pathways as a selection tool for determining the optimal pretreatment approaches was first considered. However, it became clear that there is significant lack of publically-available scientific or design data that could be used to generate cost and energy estimates for each treatment pathway.

Ultimately, biomass pretreatment and post-condensation microfiltration were the two treatment pathways that were selected for study within the scope of this dissertation. This selection was greatly influenced by the fact that while there had been previously-published literature highlighting the technical feasibility of these two approaches, challenges existed for these two approaches, whether related to high energy requirements of feedstock drying in the case of biomass pretreatment, or the potential for fouling during microfiltration of fast pyrolysis bio-oils [21]. Furthermore, additional work was required to generate comparative cost estimates with existing solids and ash reduction pathways.

1.2. Thermochemical Conversion of Forestry Residues

Alternative thermochemical conversion pathways exist which differ from fast pyrolysis by the targeted product outputs. Among a few include synthesis gas (syngas, reformer gas), which is the main output from gasification; biochar (bio-carbon, among many other aliases) is the targeted output from slow pyrolysis, carbonization and torrefaction; bio-crude, which has many similar properties to fast pyrolysis bio-oil, is the main liquid product from hydrothermal liquefaction. It is recommended to review additional literature to learn more about these biomass thermochemical conversion technologies [22]. A commonality exists between the objective of all these conversion pathways, which is aimed at the valorization and utilization of raw biomass for energy and product applications.

Clean, woody biomass is typically favoured by the end-user relative to lower grades of biomass feedstocks which may contain a combination of the following: high nitrogen content, high mineral content, low ash melting temperatures, high moisture contents, high fraction of contaminants including heavy metals, high extractives contents, etc. [23]. However, cost and availability of clean stem wood, or merchantable wood, often render vast supplies of this material challenging for bioenergy applications. Forestry residues are a leading opportunity feedstock alternative for bioenergy applications. Forestry residues, a broad term, can

be used to describe various output streams from forestry harvesting which are considered by-products from the purchase of merchantable wood. It may include, but not limited to, harvest residues (roadside residues, logging residues, etc.), hog fuel, thinnings, dead or unmerchantable wood (standing timber, insect and fire kill), etc. [24–26]. It has been predicted that there will be approximately 19-35 EJ/yr of forestry residues available for bioenergy around the world in 2050 [27].

Harvest residues have long been identified as a critical biomass feedstock in large supply for future use, but largely lack an economic incentive for collection from harvesting sites [26,28]. Numerous studies have been performed to estimate the quantity of harvest residues available in Canada. A general rule of thumb is that harvest residues compose around 15-25% (by mass) of the forest harvest cut block, with 20% being a typical reference value [28–30]. By considering annual cut allowances, availability estimates range from 10-20 million oven-dry tonnes (odt) of harvest residues annually in Canada.

Hog fuel is a common term for wood waste residues from pulp and paper mills and can include a combination of bark, sawdust, shavings, fines, dirt, etc. Hog fuels represent another opportunity feedstock that are usually located directly at the mill as a by-product from primary operations, and thus are likely available at low collection costs relative to harvest residues. Historically, hog fuel has been incinerated on site to provide heat to boilers located at the mill [26,28]. A 2013 Canadian Bioenergy survey including 39 cogeneration plants found up to 165 MW was produced from hog fuel [31].

Biomass is typically a highly variable resource. The physicochemical properties of residue streams can be even more difficult to predict based on the silviculture practices, level of contamination, age, geospatial and temporal conditions, etc. However, forestry residues are typically of lower quality relative to merchantable wood. Contextually, one of the leading indicators of quality is the ash content of the residues. Ash content of biomass can be defined as the inorganic fraction of the original material which does not combust, and for biomass is typically composed of silica, alkali and alkaline earth metals (AAEMs), heavy metals, etc. [32]. To demonstrate this concept, a summary of different exemplary Canadian forestry-based residual feedstock samples analyzed at CanmetENERGY-Ottawa are included in Figure 1.1. A detailed set of properties of these residual feedstocks is also presented in Table A. 1.

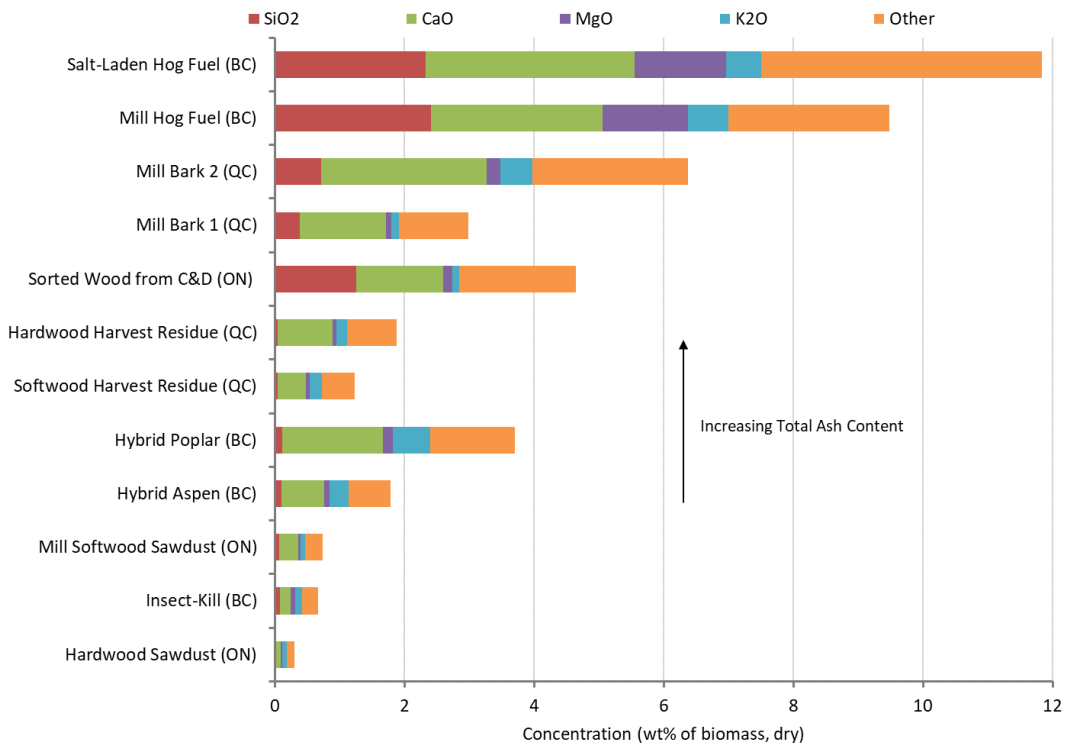

Figure 1.1: Concentration of select ash compounds for various exemplary Canadian forestry residues measured by ASTM D4326, as well as total ash

There is significant variability in the measured total ash from the range of woody-based biomass feedstocks. For example, the amount of soil contamination, which can be partially represented by the total SiO_2 content, is of high variability. The amount and composition of AAEMs also varies quite significantly. It can be generally stated that the number of potential technical challenges associated with conversion or utilization of products from biomass increases with the total ash content, and specifically AAEMs. The impact of ash on biomass thermochemical conversion is further detailed in Chapter 2.

1.3. Fast Pyrolysis Bio-oil and Applications

Biomass fast pyrolysis is a thermochemical conversion pathway in which the main objective is to maximize the production of a "liquid biomass", termed fast pyrolysis bio-oil. To satisfy the requirements for fast pyrolysis and maximize liquid yield, a few operational requirements exist, which include: (i) reaction temperatures ranging from 400-600 ˚C (450-550 ˚C is optimal); (ii) short vapor residence times (typically less than 5 seconds, although 1-2 is preferred); (iii) rapid quenching of condensable vapours to produce fast pyrolysis bio-oil; and (iv) performed in the absence of oxygen [21].

In the case of biomass liquefaction by fast pyrolysis, many processing advantages exist when comparing the properties of FPBO to raw biomass. Energy densification is the most prominent advantage. To demonstrate this concept, Figure 1.2 shows the relative volume of different materials required to produce 1 GJ of thermal energy. Based on the relative differences in bulk density between FPBO and biomass, increases in volumetric energy density as high as an order of magnitude can be realized through fast pyrolysis. Since biomass is usually a geographically-dispersed resource, significant savings in energy transportation costs to centralized processing facilities can be realized through a biomass liquefaction process [21]. Material handling and storage is also typically much easier and less prone to operational issues for a liquid relative to a low bulk density solid, which is another advantage for liquefaction relative to utilization of raw biomass.

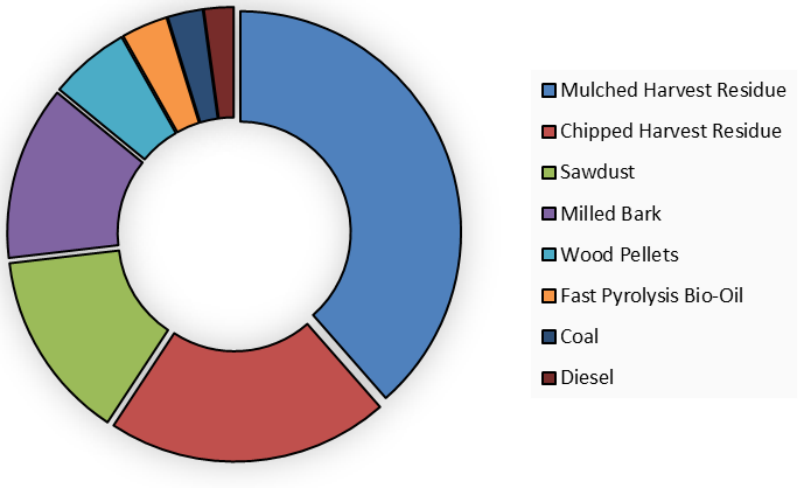

Figure 1.2: Relative volume of material required to produce same amount of thermal energy demonstrating the benefit of biomass densification [33,34]

In many cases, petroleum fuel oil (such as diesel or number 2 fuel oil) is used for the reliable production of heat and power. Producing a low-carbon renewable liquid capable of displacing petroleum fuel oil creates many opportunities for bio-oil. However, the properties of petroleum fuel oil and fast pyrolysis bio-oil are quite distinct. In addition to the presence of solids and ash, which will be discussed further, some of the major differences between the two fuels is that FPBO contains water at concentrations of 20-30 wt%, is acidic with a pH of 2.5-3, has a higher bulk density by about 50%, and is approximately half the energy density [35,36]. An image of a fast pyrolysis bio-oil produced from bark is shown in Figure 1.3 for reference.

Figure 1.3: Image of fast pyrolysis bio-oil produced from bark at CanmetENERGY-Ottawa

In regards to energy, there are two major applications for FPBO. The first is to directly use the liquid as a fuel, typically in stationary heat and power generation, including furnaces, boilers, turbines or engines. The second application is to further transform the FPBO by catalytic upgrading of fast pyrolysis bio-oils to produce fungible transportation fuels, including renewable diesel and biojet fuel [10]. Co-processing of fast pyrolysis bio-oil with heavy gas oil has also been demonstrated in conventional refinery units [37–42]. Other potential applications for bio-oils include extraction of high-value chemicals [43–45], replacement of heavy fuel oil in the marine sector [46,47], and use as a biogenic binder in applications such as asphalting [48,49].

A study performed in 2010 found that the North American pulp and paper, as well as sawmill industries had a biomass pyrolysis production potential of up to 9.5 million tons of oil equivalent per year (Mtoe/yr) by 2020 as an alternative to heavy fuel oil (HFO) [50]. Biofuel consumption in the global transport sector was also expected to rise from 5-10 EJ/year in 2015 up to 30-40 EJ/year by 2060. Biojet and renewable diesel, which can be produced from catalytic upgrading of fast pyrolysis bio-oils, could contribute approximately 20 EJ/year globally by 2060 [1]. This represents the dominant share of anticipated biofuel usage in the transportation sector. It is estimated that biofuels will provide as much as 40% of air transport and 30% of bunker fuel for shipping globally by 2060. The required biomass supply to meet these targets will be extremely large. As such, the use of secondary and tertiary biomass feedstocks, which may include forestry residues, short-rotation crop and post-use wood residues, among others, are likely to be a critical element of this long-term solution [51].

1.3.1. Challenges with Solids and Ash

With respect to clean, low ash stem wood, the properties of these secondary and tertiary biomass residues typically lead to additional challenges during thermochemical and catalytic conversion. It has previously been defined that solids are the suspended char particles within the liquid matrix originating from imperfect separation of fast pyrolysis by-products. Meanwhile, ash is defined as mineral matter contained in the liquid matrix, either in the solid or liquid phase, originating from the converted biomass material. Numerous transport mechanisms exist for the transport of biomass ash to FPBOs during fast pyrolysis [52]. It can be deduced that higher ash-containing biomass feedstocks will lead to higher ash-containing FPBOs under the same operating conditions. Although the elevated presence of suspended char particles in FPBO is largely related to mechanical separation equipment and operating conditions, increased concentrations of suspended solids in FPBOs can be correlated to the presence of soil contaminants and other ash species in biomass [53].

One such issue related to elevated ash levels in the biomass feedstock are incremental reductions in organic liquid yield and potential for multiphase behaviour based on increased water yield from fast pyrolysis [54,55]. For use in direct heat and power, the presence of suspended char particulate in fast pyrolysis bio-oil are linked to the formation of sludge layers in vessels, erosion of mechanical components (pumps, mixers, atomizers, etc.), increased particulate emissions, inconsistent spray/entry patterns, and have been theorized to promote polymerization reactions of the bio-oil leading to irreversibility viscosity increases (also known as “ageing”) [21,51,56,57]. Sediment formation on furnace walls originating from volatile and non-volatile components is another potential issue [58]. The presence of char particles accelerates the occurrence at which micro-explosions occur during spray atomization combustion, which was found to be undesirable since the micro-explosions do not effectively disperse the droplet mass, leading to severe coking tendencies [59]. In addition to many of these issues, the presence of ash in bio-oil may also cause corrosion on heat transfer surfaces, slag formation, etc. In regards to catalytic upgrading, the presence of char particles and ash in fast pyrolysis bio-oils is associated with catalyst poisoning, catalyst blockage and packed bed plugging/fouling [11,21].

1.4. Principles of Microfiltration

The use of cross-flow and dead-end microfiltration is studied extensively in Chapters 3-5 of this work. To visually compare the two processing modes for microfiltration, simple diagrams are included in Figure 1.4. The driving force for both process configurations is pressure differential. Dead-end microfiltration

typically passes the liquid feed perpendicularly to the active filtration surface, and as a result there is usually only one feed and permeate (low-solids product) stream. Alternatively, cross-flow microfiltration actively passes the concentrated feed tangentially to the filtration surface, such that an addition outlet streams exists, which is called the retentate (or reject) stream. This retentate stream is usually recycled back into the process and subsequently re-introduced across the filtration surface.

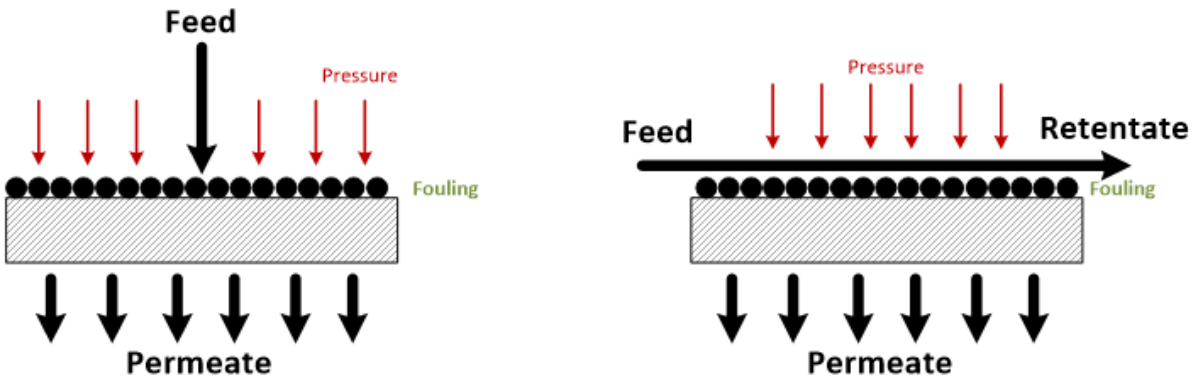

Figure 1.4: Visual representation of dead-end filtration (left) and cross-flow filtration (right)

Both filtration configurations have advantages and disadvantages. Dead-end microfiltration may be viewed as a simpler approach, and would typically represent lower costs relative to a similar scale cross-flow microfiltration system. However, more interruptions in processing is required in dead-end microfiltration since the accumulation of fouling is theoretically infinite. Meanwhile, cross-flow microfiltration is a process that may incur higher capital/operational costs, but can offer significant increases in overall throughput relative to dead-end microfiltration. This is largely caused by the shear forces acting tangentially to the accumulated fouling layer by the circulating feed stream. This effect limits the deposited fouling thickness to a theoretical constant value as the rate of fouling accumulation stabilizes with the rate of fouling layer removal. As a result, steady-state permeation rates are often observed in cross-flow microfiltration assuming the bulk solids concentration also remains constant. A summary of operational differences between dead-end and cross-flow microfiltration are also located in Table 1.1.

Table 1.1: Summary of operational advantages/disadvantages of microfiltration configurations [60,61]

Microfiltration Configuration	Advantages	Disadvantages
Cross-flow	Theoretical ability to reach steady-state High filtration areas possible with advanced configurations Low waste generation relative to dead-end microfiltration More flexibility with operating parameters exist to improve process	Higher capital costs Operational costs sensitive to circulation rate Limit of solids loading of feed for practical operability exists Higher equipment maintenance costs anticipated On-line or off-line cleaning and regeneration strategies required for continuous systems
Dead-end	Low capital cost Simple System	Operating costs directly linked to solids loading in feed Frequent interruptions in feed required for cleaning

To help explain the permeate flux and fouling accumulation, Figure 1.5 demonstrates the differences in operability between a dead-end and cross-flow microfiltration system by using simulated values. Additional key principles, terms and guidelines for membrane separation technologies, and in particular cross-flow microfiltration, have been detailed elsewhere [60–62].

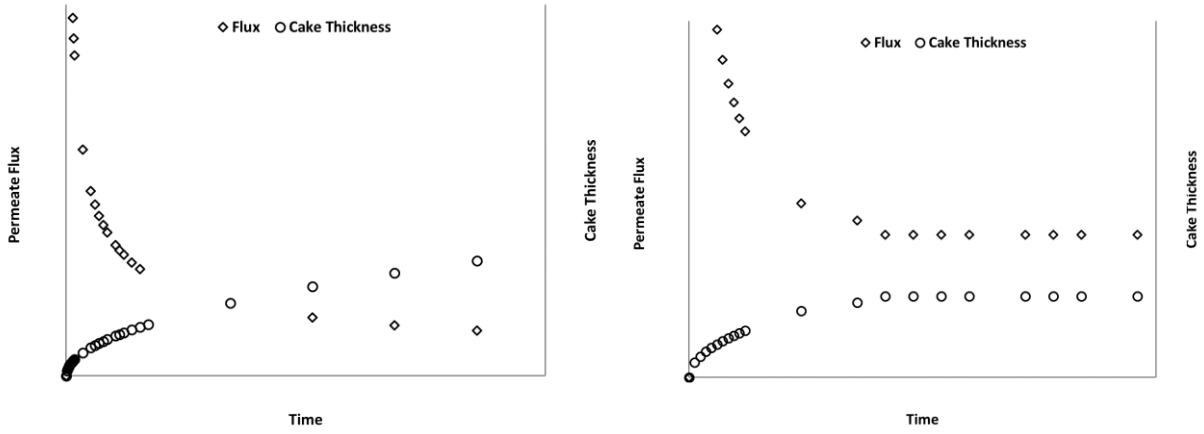

Figure 1.5: Exemplary plots of permeate flux and fouling accumulation thickness as a function of processing time for uninterrupted dead-end microfiltration (left) and cross-flow microfiltration (right)

Permeate flux is defined as the volumetric flow rate of low-solids permeate, normalized by the active area of the filtration media as demonstrated in Eq. (1).

$$J = \frac{1}{A}\frac{dV}{dt} \tag{1}$$

where *J* is the flux, *V* is the volume of permeate produced, *A* is the active filtration area and *t* is the processing time.

In this work, the term *throughput* is used as a general measure for production potential of low-solids permeate from microfiltration, and may be approximated as the average flux over a specified time period as demonstrated in Eq. (2).

$$\bar{J} = \frac{1}{A}\frac{\Delta V}{\Delta t} \tag{2}$$

where $\bar{J}$ is the throughput.

The steady-state flux for a cross-flow microfiltration process is often described by Darcy's law, and is shown in Eq. (3) [60].

$$J = \frac{1}{A}\frac{\Delta P}{\mu_o R_T} = \frac{1}{A}\frac{\Delta P}{\mu_o(R_m + R_c + R_p)} \tag{3}$$

where ΔP is the transmembrane pressure, μ_o is the fluid bulk kinematic viscosity, R_T is the total resistance to filtration, R_m is the membrane resistance, R_c is the cake resistance, and R_p is the pore plugging resistance.

The use of the term "pseudo steady-state" may be used to represent an operating region in which an apparent constant permeate flux is observed, although the operating parameters (such as bulk solids content) have not yet completely stabilized. In most cases of this work, the term "pseudo" steady-state is used because of these reasons.

As Darcy's law states, the steady-state flux is directly proportional to the transmembrane pressure (TMP), and inversely proportional to the fluid kinematic viscosity and total resistance. The kinematic viscosity of FPBO, similar to many fluids, is related to its temperature. The total resistance, which may include membrane, cake and pore plugging, can be a challenging term to define and is a function of many operating parameters, including fluid properties and operating conditions, such as temperature, pressure

and circulation rate. Discussion related to the different bio-oil microfiltration resistances are included in Chapters 3 and 4.

1.5. Objectives of Thesis

The principal objectives of this graduate thesis can be summarized as follows:

1. With the use of pilot and bench scale systems, generate the necessary design data to have the ability to inform process and technoeconomic models for the use of biomass washing and/or post-condensation microfiltration for the reduction of solids and ash in bio-oils produced from lower quality forestry residues.

   Some examples of key parameters for biomass pretreatment include mineral removal efficiency of hog fuel by sieving and nitric acid washing, water consumption rates, mass/energy balances from biomass washing and pyrolysis conversion and properties of fast pyrolysis bio-oils from nitric acid-washed hog fuel. Examples of key parameters for FPBO cross-flow microfiltration include low-solids bio-oil flux, optimal operating parameters (including temperature of fluid and transmembrane pressure), solids/ash removal efficiency by microfiltration, etc.

2. Augment and expand the limited data that is publically-available related to biomass pretreatment and post-condensation microfiltration of bio-oils for amelioration of its physicochemical properties prior to direct utilization, catalytic upgrading or other applications.
3. Identify new challenges, and solutions, to the investigative study of cross-flow microfiltration for solids/ash reduction of fast pyrolysis bio-oils.

It is intended that the accomplishment of these objectives will aid in the advancement of this field of research through:

- Adoption of laboratory, engineering and analytical procedures and methodologies conveyed through information exchange from one institution to another to aid in the advancement of the state-of-the-art.
- Informed decisions, based on scientific and design data, may be made related to the subject of study, or alternatively, on a related subject of study.
- The data that was generated may be used in technoeconomic assessments which can be powerful tools for identifying the commercial relevancy of many of these processes and technologies.

- Those that see opportunity in the work may adopt and continue the work based on missed, partially fulfilled or new opportunities.

1.6. Thesis Format

This thesis dissertation was designed to be manuscript-based, and thus the core of the report includes three manuscripts that were prepared for refereed journal publication, included in Chapters 2 - 4.

Chapter 2 contains a journal manuscript detailing the use of biomass sieving and washing pretreatment as a solids and ash reduction pathway for fast pyrolysis bio-oils. The manuscript was submitted to the journal Energy & Fuels on March 7th, 2019, and was successfully published on May 22nd, 2019 [63]. However, the format of the manuscript that appears in this work is the internal version following successful publication to respect journal publication copyright. Minor modifications to the text has also been performed, namely the replacement of the term biomass pyrolysis oil (BPO) with fast pyrolysis bio-oil (FPBO) for consistency throughout this dissertation.

Chapter 3 includes a prepared journal manuscript which outlines the use of an experimental cross-flow microfiltration system for the removal of solids and ash from fast pyrolysis bio-oil. The impact of several key operating parameters were investigated in both the transient and steady-state operating regions. This chapter is intended to be submitted to the Journal of Membrane Science at the successful completion of the thesis defence.

Chapter 4 is a prepared journal manuscript which evaluates the occurrence of fouling in cross-flow microfiltration of fast pyrolysis bio-oils, and is an extension to the work that was performed in Chapter 3. Furthermore, the use of experimental on-line and off-line filtration media cleaning strategies are explored to reduce fouling and improve the throughput of the process. This chapter is intended to be submitted to the Journal of Membrane Science or Energy & Fuels at the successful completion of the thesis defence.

Chapter 5 was included in this dissertation as a standalone short communication to explore the technical feasibility of combined solid-phase adsorbents with bio-oil microfiltration. For a full-length journal article, additional tests would be necessary. Chapter 6 comprises of the concluding remarks and recommendations.

Supplementary information, graphics and data are included in the appendices of this report. Additional information related to the properties of Canadian residual forestry materials is provided in Appendix A. Detailed information on the design and layout of the various cross-flow microfiltration systems also used

in the work is located in Appendix B. Supplementary information to the Chapter 2 manuscript is found in Appendix C. Appendix D contains supplementary information to the Chapter 3 manuscript, including the properties of the filtration media used, additional data from the results and discussion, a description on the use of diascopic bright field microscopy to qualitatively evaluate solids removal in FPBO after microfiltration, a summary of properties of low-solids bio-oil compared to unfiltered bio-oil, and additional information related to the multi-linear modelling approach used in the work. Appendix E contains a short communication regarding the use of a forced settling apparatus for the agglomeration of solids in fast pyrolysis bio-oils.

1.7. Statement of Contributions

This thesis, including the introduction, each individual chapter, and the appendix, is a result of my individual authorship. Review of the work was performed by my supervisors Dr. Boguslaw Kruczek and Benjamin Bronson, as well as Dr. Fernando Preto and Dr. Sebnem Madrali from CanmetENERGY-Ottawa. Unless otherwise specified below, I was the individual contributor to experimental planning, feedstock/material preparation for the experiments, experimental operation, data capture and compilation, and data analysis for Chapters 2-5.

For Chapter 2, Benjamin Bronson, Dr. Fernando Preto and Dr. Hooman Rezaei led the experimental planning, contributed to data analysis after experimental operation and performed review of the prepared manuscript for publication. Feedstock/material preparation assistance was provided by Benjamin Bronson and Dr. Hooman Rezaei. Benjamin Bronson and Leslie Nguyen assisted with experimental operation and data capture.

For Chapters 3-5, Dr. Boguslaw Kruczek and Benjamin Bronson assisted with experimental planning and data analysis. Benjamin Bronson also assisted in experimental operation of the extended duration microfiltration trials described in Chapter 4. Additionally, some assistance in experimental operation was required from Evan Shuparski, Jaden Murphy, Simon Lalonde, Berney Chan and Andrew Jewlal, who were COOP students at the time with the Bioenergy group at CanmetENERGY-Ottawa.

Chapter 2. Sieving and Acid Washing as Pretreatment to Fast Pyrolysis of a High Ash Hog Fuel

Dillon Mazerolle[a], Hooman Rezaei[b], Benjamin Bronson[a], Leslie Nguyen[a], Fernando Preto[a]*

[a]Natural Resources Canada, CanmetENERGY-Ottawa, 1 Haanel Drive, Ottawa ON, K1A 1M1, Canada

[b]FPInnovations, 2665 East Mall, Vancouver, BC, V6T 1Z4, Canada

Abstract

Mineral matter can negatively influence liquid yield and product properties from the fast pyrolysis of woody biomass residuals. Biomass pretreatment approaches to reduce the ash content represent a potential pathway to expand the feedstock flexibility of fast pyrolysis. In this work, ash reduction in fast pyrolysis bio-oil via sieving the fines portion of a hog fuel, as well as washing the fractionated hog fuel with nitric acid was investigated prior to conversion in CanmetENERGY-Ottawa's 5-10 kg h^{-1} fast pyrolysis system. It was found that sieving the material was much less influential on the liquid yield and product properties relative to nitric acid washing. Product analysis showed up to 40% increase in organic liquid yield and up to 30% decrease in biochar yield on a dry, ash-free basis by nitric acid washing the fractionated hog fuel. Pyrolysis reaction water was minimized when nitric acid washing the feedstock, which has important implications for phase separation of the pyrolysis liquids. Through nitric acid washing, ash content in the liquid was reduced up to 87% relative to liquid produced from pyrolysis of untreated material. The chemical quantification of the produced pyrolysis liquids demonstrated that the chemical composition was significantly altered after nitric acid washing the hog fuel, indicating that the removal of the ash species impacted the pyrolysis reaction chemistry.

Keywords

fast pyrolysis; ash removal; biomass pretreatment, biomass acid washing; fast pyrolysis bio-oil

2.1. Introduction

Biomass fast pyrolysis is a thermochemical conversion process in which biomass is rapidly heated and condensed in the absence of oxygen to produce a densified liquid, biochar and pyrolysis gases. The densified liquid intermediate, called fast pyrolysis bio-oil (FPBO), can be used as a fuel oil replacement for retrofitted heating equipment and has garnered interest as a potential blendstock for petroleum refiners [38]. FPBO also shows promise as an input for a variety of other applications including as an intermediate for the production of fungible transportation fuels including diesel and jet fuel, or as a direct fuel in combined heat and power through internal combustion engine or gas turbine applications. Currently, a suitable liquid can be produced from the fast pyrolysis of a clean, low ash and low moisture woody biomass. Significant challenges, and opportunities, exist when utilizing lower quality residual woody feedstocks with high ash content such as bark, harvest residues from forestry operations, hog fuels, etc. When using FPBO as a fuel for heating or prime mover-based applications, the presence of ash can lead to numerous combustion and/or operational difficulties. Examples of such issues include ash deposition on moving parts leading to erosion, ash deposition on heat transfer surfaces, irreversible viscosity effects and elevated particulate emissions [21,52,64]. Ash/inorganics within FPBOs originate primarily from the biomass feedstock. Ash that exists outside of the biomass particle is referred to as *external* ash in this work. External ash is often in the form of soil that is mixed with the biomass during the harvest process. Since soil is a major source of external ash in biomass, typical species of ash that are categorized as external include silica, metals such as iron, nutrients in the soil such as nitrogen and potassium, etc. [65]. Unlike external ash, *inherent* ash is contained within the biomass particle structure. Different mechanisms for inherent ash incorporation include organically-bound species by covalent bonding, ash species that are enveloped by the biomass particle, and ash species in ionic form present in the biomass [66,67].

Inorganic compounds in the biomass may alter the reaction networks occurring during fast pyrolysis, such as additional cracking reactions in the vapour phase, and lead to altered product distribution and chemical properties of the liquid phase product [68]. It has been reported that the inorganic compounds in biomass such as potassium and calcium catalyze and accelerate biomass decomposition and char formation reactions during pyrolysis [21,64,69]. As a result, reductions in liquid yield in favor of biochar and gas yields are observed from the pyrolysis of high ash feedstock relative to low ash feedstock.

It is important to highlight that in itself, fast pyrolysis may be considered a strategy for ash removal from biomass to the liquid product by concentrating ash in the biochar product. However, ash levels in FPBO can still exceed required limits for immediate energy applications or further upgrading [56]. In pyrolysis,

ash transfer in solid form into the solid or liquid products is typically a result of limitations in gas-solid separation equipment due to reduced efficiency for decreasing biochar particle sizes [52]. A common example includes the adherence of ash to a solid biochar particle during pyrolysis, which may be entrained with the produced vapours and gases through downstream cyclones and deposited into the pyrolysis liquids. Ash transfer in the gaseous phase may occur when inorganics present in the biomass react with organic volatiles in the pyrolysis reactor, form gaseous molecules with sufficiently high vapour pressures, pass through cyclonic separators and condense in the liquid phase. A previously reported example is the formation of volatile salts when ionic sodium reacts with a carboxylic acid-containing organic molecule, which has been demonstrated in the pyrolysis of brown coal [70]. Although the degree of inherent ash transfer from biomass to FPBO is low (typically <10%) [52] for species present in significant quantities, these levels are still sufficiently high to introduce issues for downstream combustion applications and/or upgrading.

Biomass pretreatment strategies may be considered in order to reduce the ash content of FPBO derived from high ash materials and its resulting impact on the reaction chemistry during pyrolysis. External ash components may be removed based on approaches that use the differing physical properties of the biomass particles and inorganic particles within the bulk feedstock. This may include water flotation or sieving, where the ash may concentrate in the fines or denser particles [71]. Many of the techniques to remove inherent ash are based on leaching. Water leaching methods are the ones most commonly used [72]. The main objective of biomass washing is to efficiently maximize the removal of inorganic elements from the original biomass to limit the transfer of inorganics downstream during processing. Due to its effectiveness compared to water washing, dilute inorganic acid washing pretreatment has the potential to be more widely adopted at the commercial scale [73,74]. Increased oil yield and decreased water, gas and biochar yields have been reported when acid-washed biomass undergoes pyrolysis compared to the untreated biomass [75].

Few available scientific articles describe the effect of biomass washing on the resulting fast pyrolysis product yields and properties. Available literature has identified consistency in the impact of inorganic acid washing on low ash woody feedstocks (ash <1 wt%), including increases in overall liquid yield (up to 10%) and decreases in biochar (up to 30%) and gas (up to 40%) yields on a dry, ash-free basis [71,76,77]. It has also been reported that levoglucosan levels in FPBO increased dramatically after inorganic acid washing [64]. However, there is a lack of information on the effect of acid washing wood-based residual materials with high ash contents (such as >5 wt%). As such, experimental work at CanmetENERGY-Ottawa

(CE-O) was performed to determine how biomass ash removal pretreatment would influence the fast pyrolysis of a high ash forestry hog fuel.

2.2. Materials and Methods

2.2.1. Materials

Interior hog fuel, obtained from a pulp mill in the northern interior of British Columbia, was used as the base material for this study. Hog fuel is a common term for wood waste residues from pulp and paper mills and can include bark, sawdust, shavings, fines, dirt, etc. An initial particle size reduction of the hog fuel was performed, followed by sieving using a 3.2 mm (1/8") screen for comminution. The fraction of material that passed through the 3.2 mm screen was the parent material interior hog fuel (IHF) for further sieving, washing, and fast pyrolysis outlined in this study. The properties of the parent material are presented in Table 2.1.

Two pretreatment methods for the removal of ash from the IHF material were investigated. First, to remove external ash that was present as a fine material, the parent IHF was further fractionated using a 0.5 mm (35 mesh) screen rotary sieve shaker at a residence time of 1–2 minutes. Thus, the majority of the finest fraction of material was separated and removed. This procedure yielded approximately 83 wt% of material which was retained above the 35 mesh screen (*>35 M*). It is important to note that approximately 10 wt% of the sieved material contained particles with a diameter still below 35 mesh, which was due to limitations in the operability of the large-scale sieve shaker used. To further remove ash, the >35 M material was washed in dilute nitric acid, which is referred to as the acid-washed hog fuel (*AW>35 M*). Preliminary studies concluded that nitric acid at a concentration of 0.1 M was an effective washing medium for woody material [78]. Further investigation on the IHF feedstock material used in this study confirmed the effectiveness of sieving followed by 0.1 M nitric acid for the removal of many key ash components. Upon completion of the bench-scale tests, the washing procedure was scaled-up to produce larger quantities for pilot scale pyrolysis testing.

Acid washing was performed at ambient temperature conditions, where a slurry of 12.5 wt% of >35 M material in 0.1 M nitric acid was mixed in a stainless steel tank using a 1/3 HP mixer at 1725 rpm for 30 minutes. The slurry was centrifuged and filtered with a 0.16 mm (90 mesh) screen to remove all free liquid. The biomass was rinsed with distilled water at a 12.5 wt% slurry and similarly mixed for 15 minutes and centrifuged to remove all excess liquids. Distilled water washing was repeated once more to ensure that all excess acids were removed from the biomass structure. The washed material was then oven-dried to

remove the majority of moisture in the feedstock. The organic biomass recovery after nitric acid washing was not captured in this work.

2.2.2. Experimental Procedures

2.2.2.1. Description of Fast Pyrolysis System

The IHF, >35 M and AW > 35 M materials were used as the feedstock in CanmetENERGY-Ottawa's 5– 10 kg h^{-1} bubbling fluidized bed fast pyrolysis system operated at nominal reaction temperatures of 400 and 480 °C. Thus, six fast pyrolysis trials were completed in this study. Although there were some reactor temperature variabilities over the duration of a trial, temperatures were always ±10 °C of the temperature objective during biomass feeding. Lower reactor bed pressures, at approximately 171 mm (6.7") above the gas distributor plate, varied marginally from 6.5 to 7.5 kPa (26–30 in. H_2O). Lower reactor freeboard pressures, at approximately 457 mm (18.0") above the gas distributor plate, varied between 4.2 and 5.2 kPa (17–21 in. H_2O). The height of the reactor was 1.0 m, while the diameter was 0.11 m. Reactor bed fluidization was maintained with a supply of pre-heated nitrogen, which varied from 12.5 ± 0.6 kg h^{-1} for operation at 480 °C and 12.9 ± 0.6 kg h^{-1} at 400 °C. Vapor residence time until primary quench was approximately one second for all temperature levels. External electric heaters maintained the set point temperature in the reactor, whereas external heating tape controlled downstream process temperatures until the reaction products were quenched. Olivine sand (magnesium iron silicate), with an approximate Sauter mean diameter of 613 µm, was used as the bed material. Biomass was fed to the reactor through a sealed feed hopper/metering auger system at a feed rate of 6.5–8 kg h^{-1}. The products exiting from the fluidized bed reactor are categorized as non-condensable gases (NCGs), condensable vapours and biochar. As the products exited the reactor, biochar was immediately removed by two cyclones in series that drained solids into sealed biochar reservoirs. Primary condensation of FPBO occurred as the gaseous and condensable products proceeded through a direct contact co-current immiscible hydrocarbon quench spray at approximately 30-50 °C, followed by direct contact with a counter-current spray in a wet scrubber. These primary condensation liquids (PCLs) were filtered using coarse strainers and filters in series (100 µm and 5 µm nominal, respectively) prior to final recovery in a settling tank. A second stage of condensation occurred as remaining gases and vapours were cooled from 30 °C to 10 °C in a single-pass shell-and-tube heat exchanger. This second fraction is termed heat exchanger liquids (HXLs) in this work. A process schematic of the pyrolysis system at CE-O is displayed in Figure 2.1. An image of the experimental pilot system is located in Appendix C. A small quantity of FPBO was lost as fine aerosolized

droplets entrained by the NCGs. To quantify the amount of liquids lost as fine droplets, a slipstream of the NCG was sampled through a refrigerated methanol column.

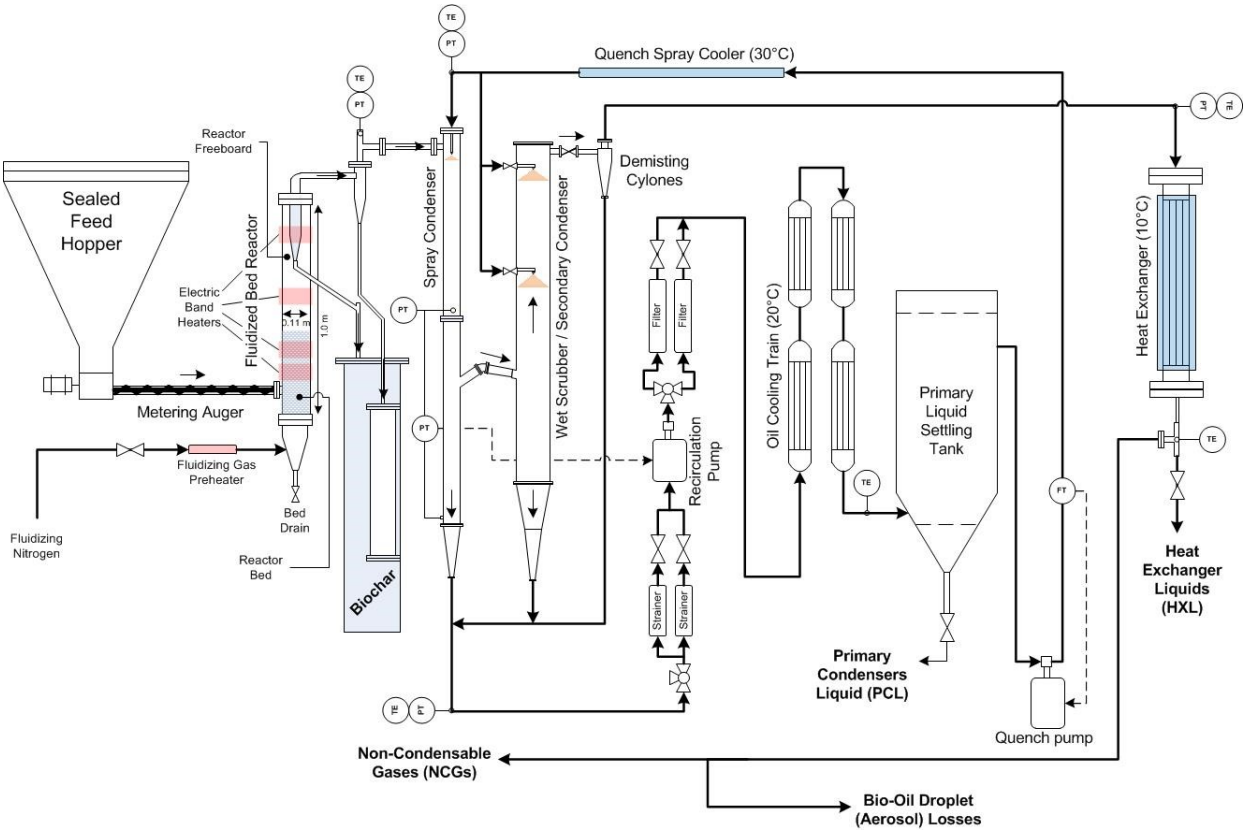

Figure 2.1: Process schematic of 5-10 kg h^{-1} fluidized bed fast pyrolysis system operated at CanmetENERGY-Ottawa

All experimental trials that are included in this study were performed as singlicates due to the resource intensity required to perform repeat trials at the pilot scale. As such, no experimental repeatability analysis is provided for recovered product yields in the context of this study. Variation in operating conditions were minimized to prevent unintended variations in product yield distributions between trials.

2.2.2.2. Material Sampling, Handling and Physicochemical Analysis

Generated FPBO samples were immediately stored below 0 °C after production. Representative, whole FPBO mixtures were generated from the individually collected fractions (PCL and HXL) according to the total amount of each fraction obtained. A single sample of each pyrolysis liquid fraction was characterized for each trial and thus sampling repeatability is not available in this study. If multiphase liquid products were generated, the bulk properties were calculated from the individual properties of the organic and aqueous fractions, which were characterized separately. Prior to characterization, the organic and

aqueous fractions were separated at 5 °C and ambient pressure using a 60 mesh screen, where the organic phase retained on the screen and was collected separately from the aqueous phase which immediately passed through the screen. Reported physicochemical properties of the liquid samples were analyzed according to ASTM D7544 testing specifications.

Biochar samples were collected the day following the experiment and quenched in water upon collection (approximately 20 wt% moisture) to stabilize the biochar and prevent self-heating once exposed to an oxygen-containing environment. Representative biochar samples were obtained by coning and quartering the biochar once complete stabilization was observed. A single biochar sample was characterized for each trial and thus sampling repeatability is not available in this study. Representative biochar samples were ground to 200 mesh prior to analysis. Proximate analysis of solid samples followed ASTM D7582 for fixed carbon and ash, while ISO 562 was used for volatiles. Ultimate analysis followed ASTM D5373 for carbon, hydrogen, and nitrogen while ASTM D4239 was used for sulfur. Biomass feedstock analysis had the same testing protocols as biochar samples. Ash compositional analysis was performed by X-ray fluorescence (XRF) complying with ASTM D4326.

Chemical quantification by GCMS was performed based on previous round robin study [79]. In preparation for analysis, a sample aliquot of 0.5 g was added to 0.5 mL of an internal standard solution containing isoamyl ether (30mg), 1-octanol (30mg), methyl laurate (30mg), and acetonitrile (25 mL), then diluted with 5 mL acetonitrile. The diluted sample was sonicated at 30 °C for a period of 20 minutes and subsequently filtered through a 0.45 µm filter. Filtered samples were injected into the gas chromatograph with injection volume of 1 µL and a 30:1 split ratio. The injector temperature was set at 250 °C. The chromatography column was an RTX-1701 with a length of 60 m, an inner diameter of 250 µm, a stationary phase with a film thickness of 0.25 µm of 14%-Cyanopropyl-phenyl-methylpolysiloxane, and constant helium flow of 1.0 mL min^{-1}. After injection, the temperature of the chromatograph was ramped from 45 °C to 250 °C at a rate of 3 °C min^{-1}. External standardization was carried out for calibration, and quantification of each compound was based on Selective Ion Monitoring (SIM) using calibration solutions diluted in acetonitrile certified by SigmaAlrich (via Supelco). The samples were run for calibration yielding internal standard calibration curves and a relative response factor for each compound. Repeatability was assessed through triplicate injections with all target compounds meeting a relative standard deviation (RSD) less than 5%.

2.3. Results and Discussion

2.3.1. Feedstock Properties

A summary of the physicochemical properties of all three materials is shown in Table 2.1. Overall ash reduction from IHF improved from 57% by sieving alone up to 79% with the inclusion of nitric acid washing of the fractionated hog fuel.

Table 2.1: Physicochemical properties of hog fuel-based feedstocks used in this experimental study

Feedstock ID	IHF	>35M	AW >35M
Water Content (wt %)	11.6	9.4	6.0
Ash (wt%, dry)	9.5	4.1	2.0
Volatile (wt%, dry)	71.6	76.1	83.1
Fixed Carbon (wt%, dry)	19.0	19.9	14.9
C (wt%, daf)	52.9	52.1	52.0
H (wt%, daf)	6.1	6.1	6.2
N (wt%, daf)	0.4	0.4	0.2
S (wt%, daf)	0.2	0.1	< 0.05
O (wt%, daf)	40.4	41.3	41.6

Ash reduction from the hog fuel by means of sieving was successful in removing 18–65% of metallic species including manganese, iron, aluminum, and silica, 43–60% of non-metal species including sulfur and phosphorus, and 40–60% of alkali and alkaline earth metals (AAEMs). The nitric acid washing step incrementally removed 50% of the total ash remaining in the >35M material. Metallic species present in quantities above 100 mg kg^{-1} (such as iron and aluminum) showed an additional incremental reduction in concentration after nitric acid washing. Non-metals quantified by X-ray fluorescence, including sulfur and phosphorus, were reduced by more than 95% from washing and sieving combined. The concentration of AAEMs also decreased substantially after nitric acid washing as most components had a removal efficiency greater than 90% from the IHF, with the exception of sodium at 77%. The inorganic compositions of the various feedstock samples present in quantities greater than 100 mg kg^{-1} in the untreated IHF are summarized in Figure 2.2.

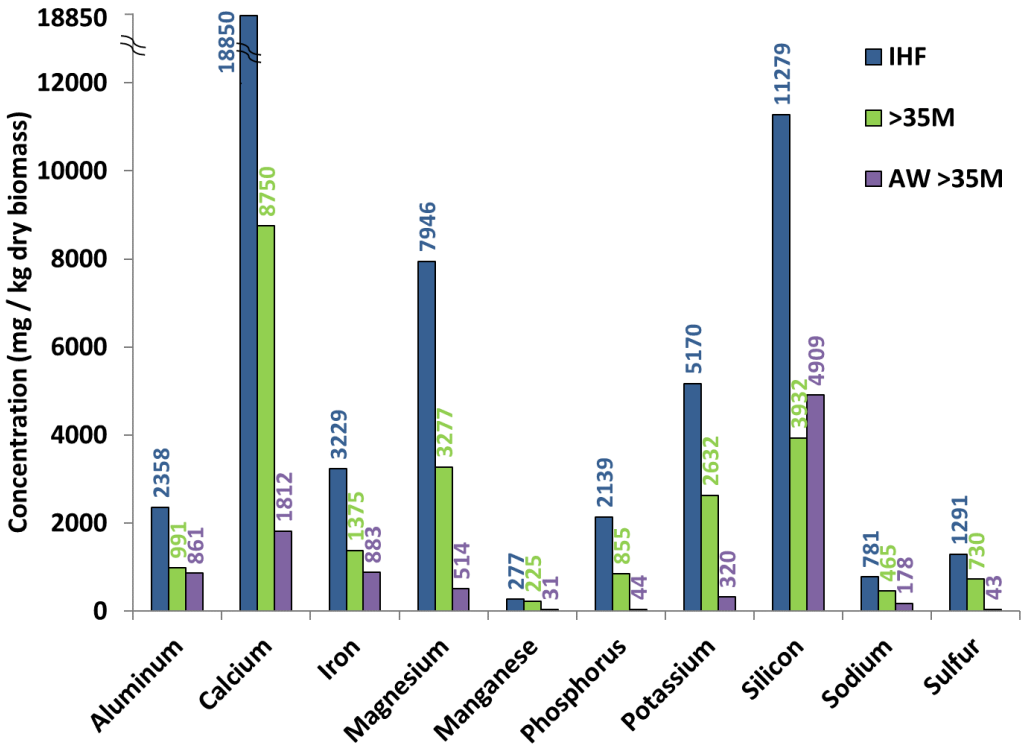

Figure 2.2: Inorganic content of prevalent mineral species of *IHF*, *>35M*, and *AW >35M*

In addition to the removal of ash components, the results also show a reduction in sulfur and nitrogen content of the acid-washed material relative to the parent feedstock. Of note is the slight variability in water content between the three materials, which represents a limitation in material preparation. For this reason, product yields described below are presented both on an as-received basis and on a dry, ash-free basis.

2.3.2. Product Yields

As previously mentioned, experiments were carried out at 400 °C and 480 °C to assess the effect of biomass pretreatment on the yield and quality of different products at two different temperature levels. Product yields on an as-received basis at both pyrolysis temperatures are shown in Figure 2.3. Note that primary liquids are defined as total liquid material recovered during the first stage of condensation (PCL), while secondary liquids are defined as total liquid material recovered from the final heat exchanger (HXL) and liquid losses as aerosolized droplets.

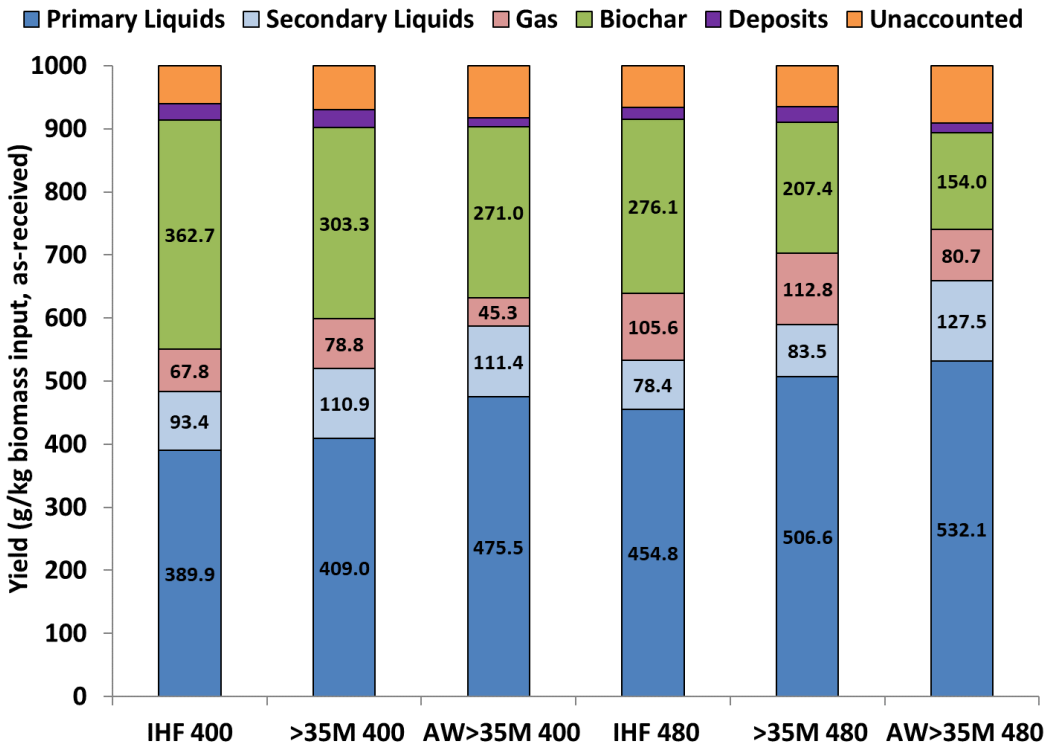

Figure 2.3: Mass product yields (on an as-received basis) from the series of fast pyrolysis trials at 480 °C and 400 °C

On an as-received (wet) basis, an increase in total liquid yield up to 24% was achieved at both temperature levels when acid washing the sieved material compared to the untreated IHF, whereas increases in total liquid yield up to 10% were measured for the sieved material. Gas yields demonstrated increases up to 16% after sieving and decreased by as much as 33% after nitric acid washing. Biochar yield reduction up to 25% was observed after sieving, and up to 44% by nitric acid washing relative to the untreated IHF. The expected result from reducing the reactor temperature was also observed; at the lower reactor temperatures, the total liquid and gas yields were reduced, with an increase in biochar yield. Deposits recovered from various locations in the system after an experimental trial accounted for 1–3% of the recovered mass over the range of trials and include solid materials adhering to condensation points in the experimental system, either of solid or liquid origin. Approximately 6–9% of the total mass balance for each trial was unaccounted, due to experimental limitations in full recovery of all materials in the small pilot scale system. Due to the variation in moisture and ash content in the feedstock materials, normalization on a dry, ash-free (daf) basis was performed to assess true changes in mass yield for the liquid, solid and gaseous products after fast pyrolysis and is demonstrated in Figure 2.4. Reaction water was calculated as the difference in total water between the produced liquids and the input biomass feedstock. Note that the dry, ash-free yields do not account for complete recovery; this is because the

estimated yield contribution of aerosol liquids, accumulations and product losses were excluded in the plot.

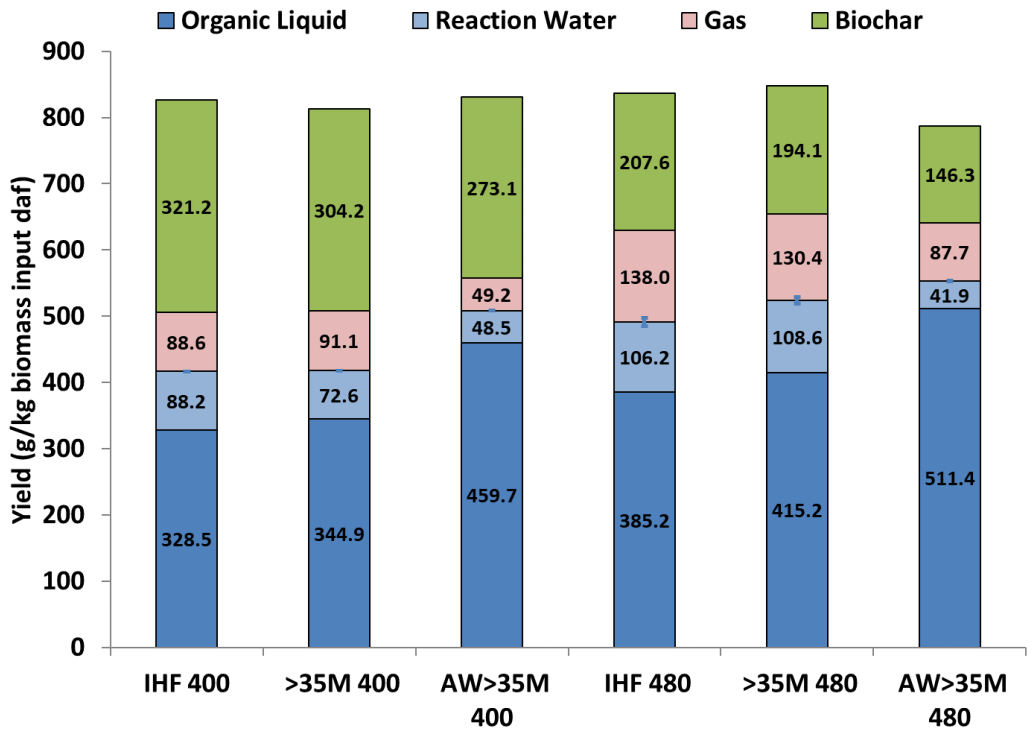

Figure 2.4: Mass yields of organic liquid, reaction water, gas and biochar from the series of fast pyrolysis trials at 480 °C and 400 °C

On a dry, ash-free basis, the trends in mass yield are similar to the as-received basis as the biochar yield decreases, whereas the total liquid yield increases with the pretreatment severity. By sieving, the dry, ash-free biochar yield decreased within 5%, whereas the gas yield varied within ±5% relative to the parent hog fuel at both temperature objectives. The organic liquid yield after sieving increased within 8% of the yield relative to the untreated IHF, whereas the reaction water decreased by up to 18% at 400 °C. The reaction water produced from the sieved material at 480 °C, as presented, actually slightly increased relative to the untreated IHF. This deviation in trend is believed to be a result of the pyrolysis liquid moisture content analytical variance from the pyrolysis liquid samples from trials IHF 480 and >35 M 480, which was not observed in any other trial in this study. Nonetheless, the minor incremental changes to organic liquid, gas, and biochar product yields between the sieved material and parent hog fuel support the notion that the external ash that is removed by sieving would have mostly reported to the biochar product in a fast pyrolysis process when evaluating the product yields on an as-received basis. It also suggests that the

external ash only has a small impact on the pyrolysis reaction kinetics and/or chemistry when evaluating the product yields on a dry, ash-free basis.

Comparing the relative difference in liquid, gas and char yields after sieving and nitric acid washing demonstrates substantially different results. On a dry, ash-free basis, the reduction in gas yields was observed at approximately 40%, while the reduction in char yields was 15-30% at the two operating temperatures. The organic liquid yield after nitric acid washing increased by 33-40% relative to the *IHF* material, while the reaction water decreased by 45-60%. Thus, not only did the total liquid yield increase with pretreatment severity, but so did the organic content of the liquids produced from fast pyrolysis. One of the suggested mechanisms for char yield reduction in the case of washed biomass is the role inorganic minerals in catalyzing the dehydration reaction of cellulose. It has been suggested that this results in weakening the hydrogen bonds in the cellulose structure, inherently increasing char-forming reactions and producing water as a by-product [52,71].

2.3.3. Liquid Properties

2.3.3.1. Solids and Ash Content

From the perspective of liquid properties, the analysis of total ash content in the total primary liquids demonstrated significant change after sieving and nitric acid washing. As seen in Figure 2.5, sieving the *IHF* resulted in a 20 and 60% reduction of measured ash in the total primary liquids at 480 °C and 400 °C, respectively. Sieving and nitric acid washing yielded superior results, as the total ash removal was 70 and 87% in the primary liquids at 480 °C and 400 °C, respectively.

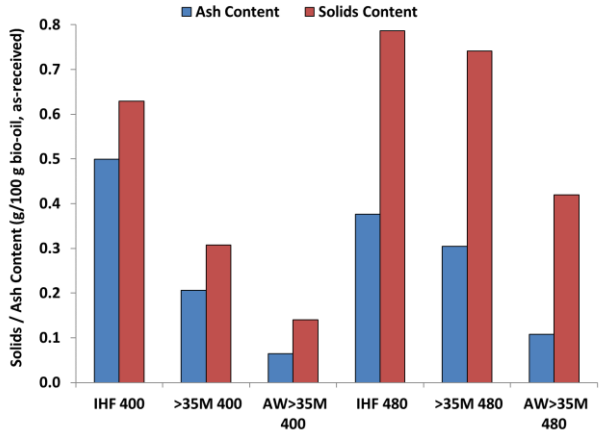

Figure 2.5: Solids and ash content of FPBOs as a function of demineralization severity and reaction temperature

The 400 °C trials generated primary liquids with lower ash content relative to the 480 °C condition for the *>35M* and *AW >35M* materials. This is believed to be an effect of heating rate on the volatilization of inorganics present in the biomass, which has been suggested as an ash reduction strategy in pyrolysis liquids [52]. It was unexpected that a higher ash content was measured in the liquids at the lower temperature condition (*IHF 400*) for the untreated *IHF* material, as the opposite was expected such as was observed for the sieved and washed materials.

The solids content in the primary liquids also decreased as much as 50 and 80% when comparing the untreated IHF trials with the sieved and acid-washed trials, respectively. The reduction in solids could be attributed to the removal of fines in the feedstock by sieving as well as the incremental reduction of fines by water separation as in the case for nitric acid washing. Since smaller biomass particles are more likely to be entrained through the cyclones with the gases and vapors, the removal of fines would aid in the reduction of elutriated solids in the process. The reduction in char yields by sieving and nitric acid washing also likely contributed to the reduced solids content in the pyrolysis liquids. It is believed that one of the main reasons for this observed trend is the adherence of ash within the solid char particles, which would reasonably cause an increase in the ash content as a function of the increased solid content in the pyrolysis liquids [52]. Supplementary data on the ash composition of the pyrolysis liquids included above are also found in Appendix C. Virtually complete removal of aluminum, calcium, phosphorus, potassium and sulfur were found after nitric acid washing, while significant reductions (> 75%) of magnesium was also found.

2.3.3.2. Phase Stability

The liquid product of a fast pyrolysis process, especially when obtained from residual materials with high ash and/or water content, is known to undergo phase separation into an aqueous (water-soluble [WS]) phase and an organic (water-insoluble [WIS]) phase [21]. Analysis of the primary liquids from the various pyrolysis trials showed visually distinct two-phase heterogeneous behaviour for the trials including the untreated and sieved materials, while the primary liquids of the sieved + washed *IHF* was found to be visually homogeneous and stable after collection. Microscopic images of the liquids from the untreated *IHF* and sieved + washed *IHF* are shown in Figure 2.6.

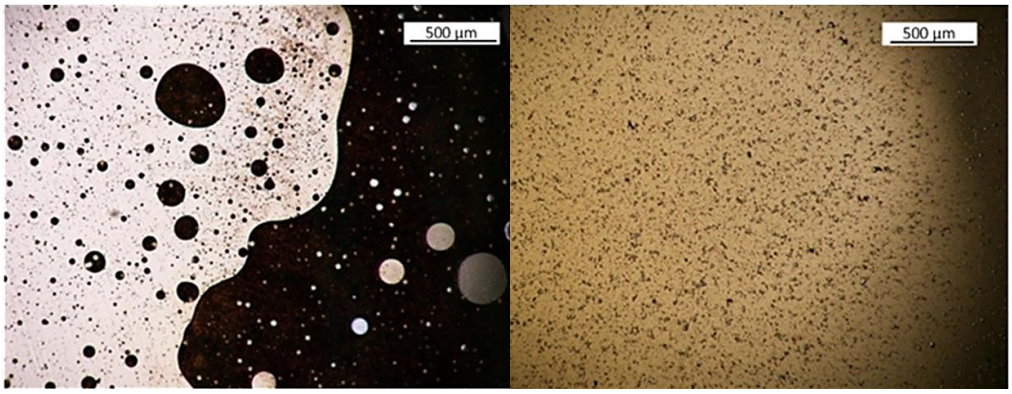

Figure 2.6: Optical microscopy images of the mixed primary liquids collected from fast pyrolysis trials *IHF 480* (left) and *AW >35M 480* (right)

The presence of additional minerals in the untreated and sieved IHF, which had caused more reaction water to be produced under pyrolytic conditions (as per Figure 2.4) could be an explanation for the occurrence of phase separation in the produced primary liquids, in contrast to the nitric acid-washed material. However, the impact of the higher feedstock water content in the untreated and sieved IHF (as per Table 2.1) should not be ignored, as 35–60 g of additional water per kilogram of feedstock was introduced into the pyrolysis process by the parent and sieved IHF compared to the washed material. As previously stated, this was a limitation in humidity control of the three hog fuel materials at the pilot scale. Thus, under the current operational constraints, it is difficult to conclude that the removal of minerals alone eliminates the possibility of the phase separation. Rather, it may be concluded that the demineralization of a given feedstock will increase its moisture tolerance as a feedstock for pyrolysis, given that significantly less reaction water may be expected to be produced compared to a high ash-containing parent material.

Although not directly investigated in this work, it is also expected that the removal of minerals and ash within the bio-oils produced from nitric acid-washed hog fuel would contribute to enhanced storage stability and reduce the effects of storage “ageing” relative to the untreated hog fuel bio-oil. Previous accelerated ageing tests of raw and hot gas-filtered bio-oil have demonstrated significant reductions in measured viscosity change of the demineralized bio-oil [6].

2.3.3.3. Chemical Quantification

Chemical quantification by GCMS was performed on all liquid samples to determine the impact of selected pretreatment methods on reaction chemistry and FPBO composition. The complete dataset from this exercise is included in Table A. 3. For data analysis and interpretation, detected compounds in FPBO by

GCMS were classified together in groups including furans, levoglucosan, phenols, guaiacols/syringols, "other' volatile oxygenates and volatile acids. A summary of the chemical quantification results are shown in Figure 2.7 for the recovered primary liquids.

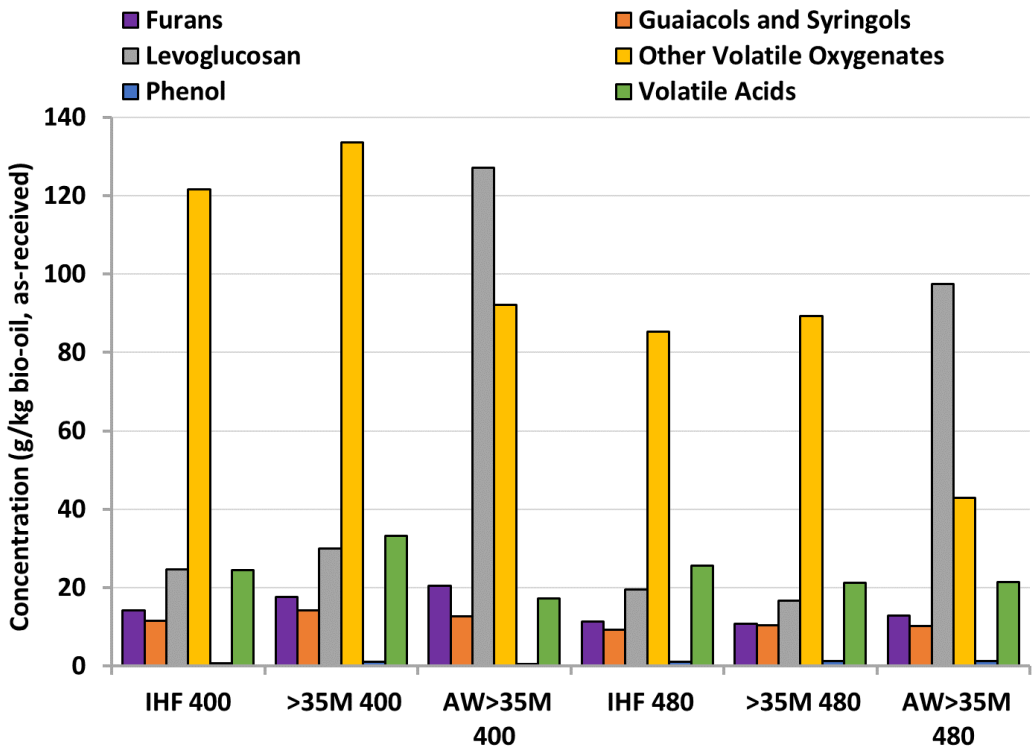

Figure 2.7: Comparative plot of major groups from GCMS quantification of primary liquids

Levoglucosan concentrations quadrupled at both 480 °C and 400 °C when comparing the liquids generated from the nitric acid-washed material relative to the untreated and sieved material. The notable increase in levoglucosan after acid washing has previously been reported [64,71]. Levoglucosan yield was favorable at the lower temperature trials relative to the higher temperature trials by a considerable margin. A reduction of up to 50% in hydroxyacetone and glycoaldehyde was experienced for the demineralized material, which comprised the majority of the classification "other volatile oxygenates". The overall level of furans, guaiacols/syringols, phenols and volatile acids were quite comparable between the three feedstock materials when comparing the components present in quantities greater than 10 mg kg^{-1}. Most notably, the levels of acetic acid in the liquid products of the nitric acid-washed feedstock were approximately 50% lower at 400 °C while only slightly lower at 480 °C.

The chemical composition similarity of the FPBOs recovered from the untreated *IHF* and the sieved *IHF* strongly suggests that the removal of external ash elements in the biomass does not necessarily affect

pyrolysis kinetics or reaction chemistry. As such, components which tend to concentrate in the external ash fines such as silica appear to be quite inert in the pyrolysis reaction, and will simply concentrate in the biochar. Furthermore, it is interesting to note that the reduction in AAEMs (up to 60%) in the sieved *IHF* did not have any significant effects on GCMS results from the FPBO samples, whereas an appreciable impact was found when removing approximately 90% of the AAEMs in the nitric acid-washed samples. This implies that the nature of the inherent ash species in the biomass feedstock could play a more significant role in affecting fast pyrolysis reaction networks than simply the amount contained within the biomass. For example, it is possible that potassium bound within the structure of biomass is more active than potassium which is contained within silicate or other relatively stable minerals that is found in the bulk feedstock due to soil or other contamination forms.

2.3.4. Biochar Properties

The biochar from the 400 °C series of experimental trials were representatively sub-sampled and analyzed, and the physicochemical properties are summarized in Table 2.2.

Table 2.2: Comparison of biochar properties (proximate and ultimate) from pyrolysis trials using *IHF*, *>35M*, and *AW >35M* at 400 °C

Trial ID, Temperature (°C)	IHF, 400	>35M, 400	AW >35M, 400
Measured Ash (wt%, dry)	40.8	22.5	15.8
Theoretical Ash (wt%, dry)	34.9	14.0	5.5
Volatiles (wt%, dry)	33.1	35.0	43.1
Fixed Carbon (wt%, dry)	26.1	42.5	41.1
C (wt%, daf)	71.2	72.0	68.3
H (wt%, daf)	4.6	4.5	4.7
N (wt%, daf)	0.7	0.4	0.3
S (wt%, daf)	0.7	0.2	<0.05
O (wt%, daf)	23.0	22.9	26.6

In the context of this work, it is important to distinguish between the measured and theoretical ash in the biochar. The measured ash was obtained by subsampling the bulk biochar that was produced and analyzing according to ASTM methods. However, due to the nature of the fluidized bed reactor operation,

a considerable amount of bed material (sand) was ejected from the freeboard and reported to the biochar, which would increase the observed bulk ash content. As a result, the theoretical ash content of the biochar may be used to better understand the true ash content of the char if no bed contamination were to occur.

As expected, the ash content of the biochars decreased considerably with pretreatment severity. This result is intuitive, since much of the external ash is removed from the starting material upon sieving, resulting in less ash reporting to the biochar after pyrolysis. Significant reductions of nitrogen and sulfur were also measured. Aside from ash, one of the other major differences appeared to be that the acid-washed feedstock trial led to a more volatile biochar with a lower carbon content.

2.4. Conclusions

Two approaches for ash removal from a high ash forestry residue used as a feedstock for fast pyrolysis were assessed to determine the impacts on product yields and properties. Sieving the material to remove fines (concentrated in external ash) generated some measurable benefit on the properties of the FPBO including reduced solids and ash content of the liquid. Dilute nitric acid washing combined with sieving had more profound impacts on the product yields and properties of the liquids generated from fast pyrolysis. Organic liquid fraction yields increased as much as 40% compared to the untreated hog fuel. The FPBO produced from the acid-washed hog fuel had substantially lower ash and solids content than the FPBO produced from the parent and sieved hog fuel.

This work confirmed some additional trends found by others for acid washing of woody biomass used as a feedstock in a fast pyrolysis processes, and held true for the high ash forestry residue used in this study. Reductions in biochar, reaction water and hydroxyacetone/glycolaldehyde yields were observed, along with increases in levoglucosan yield after nitric acid washing. This study also found that although sieving was capable of reducing the ash content of the bulk feedstock as high as 57%, the impact on the pyrolysis conversion performance was minor. This suggests that in order to observe the benefits of ash reduction for fast pyrolysis processes, removal techniques should target inherent ash rather than simply external ash.

Overall, this study confirms that from a technical perspective, ash leaching strategies may offer a route towards the production of high quality fast pyrolysis bio-oil from high ash forestry residues. Further work is needed to verify the general applicability of these conclusions with other high ash forestry residues of varying origins, to optimize washing/drying conditions based on selected feedstocks and to generate cost assessments to establish economic viability of the approach.

Acknowledgements

Funding for this work was supported by Natural Resources Canada's Office of Energy Research & Development through the Program for Energy Research and Development (Project title: Pyrolysis Liquids for Immediate Heat and Power Applications). The authors would like to thank Wenli Duo, Stacey Kus, Emma Harrison, Dr. Boguslaw Kruczek, Phil Bulsink and the Characterization Laboratory at CanmetENERGY-Ottawa for their assistance in completing this work.

Chapter 3. Evaluation and Modelling of Fast Pyrolysis Bio-oil Cross-flow Microfiltration

D. Mazerolle[1,2], B. Bronson[1], B. Kruczek[2]*

[1]CanmetENERGY, Natural Resources Canada, 1 Haanel Drive, Nepean, ON, K1A 1M1, Canada

[2]Department of Chemical and Biological Engineering, University of Ottawa, 161 Louis Pasteur Drive, Ottawa, ON, K1N 6N5, Canada

Abstract

The presence of suspended char particulate and ash in bio-oil produced from the fast pyrolysis of low quality or high ash forestry materials poses a significant technical challenge for the direct utilization or catalytic upgrading of these low-carbon renewable fuels. Cross-flow microfiltration is a physical upgrading process strategy that can remove suspended solids and ash from the bio-oil. To develop datasets on operational characteristics of bio-oil cross-flow microfiltration, experimental research was undertaken. Using a variety of filtration media with nominal pore sizes between 1-40 µm, typical solids and ash rejection ranged from 80-95% and 4-45%, respectively. Key operating parameters were also studied, and it was found that transmembrane pressures less than 1 bar and fluid pre-heat temperatures up to 60 °C were ideal for maximizing the pseudo steady-state flux of the process. Furthermore, the use of low viscosity, miscible solvents and/or initial solids reduction pathways prior to microfiltration offered interesting routes to potentially improve the throughput of such a process. Multi-linear models constructed from a range of experimental data identified that the bulk solids content, fluid kinematic viscosity (at operating temperatures) and transmembrane pressure were the most influential parameters on cake resistance in the transient operating range, while fluid temperature, bulk solids content and fluid circulation velocity were the most critical for pseudo steady-state performance.

Keywords:

fast pyrolysis bio-oil; cross-flow microfiltration, transient microfiltration, specific cake resistance, biorefinery membrane processes

3.1. Introduction

Successes in medium-large scale fast pyrolysis bio-oil (FPBO) heating projects, such as in Fortum/Valmet [36], Bates College & Memorial Hospital (Ensyn) [80], and FrieslandCampina (BTG-BTL) [81] highlight the potential in displacing the use of non-renewable fuels (ex. natural gas and/or heavy fuel oil) with low-carbon renewable FPBO. However, the production of FPBO by the thermochemical conversion of low quality forestry residues, such as hog fuel or harvest residue, are believed to create new technical issues that must be addressed prior to direct utilization of the fuel such as in heat or power production [82]. Of note, the presence of elevated suspended char particulate (solids) and ash contained in pyrolysis liquids derived from these low quality biomass residues are of concern.

The presence of char and mineral ash contained within fast pyrolysis bio-oils can create a number of technical and quality issues. Firstly, the presence of mineral ions contained within the suspended char complex may act as a catalyst for further polymerization reactions in the liquid during storage [83]. The presence of suspended char in the liquid can lead to a number of technical issues associated with direct combustion applications (such as furnaces, boilers and turbines) including nozzle plugging/fouling, inconsistent atomization spray patterns, severe erosion, increased particulate emissions, corrosion, etc. [36,57,83]. Finally, if producing fast pyrolysis bio-oil as an intermediate product for catalytic upgrading to transportation fuels or for co-processing in petroleum refineries, the presence of solids and ash can lead directly to reactor plugging and/or catalyst deactivation [52,84].

In the context of this work, bio-oil solids content is defined as the concentration of solid particulate contained within the continuous phase of bio-oil, and is typically associated with char particulate, but depending on the style of reactor utilized, may also contain a small concentration of ejected bed material. For a standardized measurement technique, the American Society for Testing and Materials (ASTM) defines the measurement method for solids content in pyrolysis liquids as methanol-insoluble materials [85]. Previous microscopic analysis, along with particle detection software, has demonstrated that the particle size distribution of char particulate contained in pyrolysis oils primarily ranged from 0.5-50 µm at a solids loading of 0.45-0.75 wt% [86,87]. However, this is certainly sensitive to the total solids content. Previous round robin study has shown that the solids content may vary as widely as 0.05-2.25 wt% under the same operating conditions using poplar with a variety of experimental systems with and without hot vapour filtration (HVF) [88]. The authors are not aware of any published literature evaluating the particle size distribution of suspended char in FPBO as a function of total solids content.

In literature, there are a few processes which have been explored to remove char particulate from FPBO at the bench, lab and pilot scale. Almost every fast pyrolysis system will include some level of char removal from the hot reaction products before the vapours are condensed. These are most often cyclonic separators which remove char via inertial separation prior to condensation in a pyrolysis conversion unit. The efficiency of cyclones drastically reduces when char particulate diameter drops below 100 µm [84,86] causing those small particles to be collected in the condensed liquid product. There is currently no widely accepted technology for the economic removal of suspended char particles below 10 µm in particle diameter [83,84] at the commercial scale.

Hot vapour filtration (HVF) was found to be the most investigated technique for removal of fine particulate and ash prior to FPBO condensation at the lab and pilot scale. Multiple data sources from open literature show agreement on the high efficacy of solids removal using HVF with ceramic elements in the 1-5 µm range, while mineral removal is usually high but can vary depending on the source of biomass [6–11]. Additional observations from HVF include reductions in liquid yield by 4-10%, increase stabilisation of liquid FPBO, as well as minor reductions in molecular weight distributions of produced liquids resulting from additional cracking reactions occurring either through more intimate contact of vapours with char and ash on the surface of the filter, longer vapour residence times, or a combination thereof. Another potential method to remove fine particulate and ash from bio-oil prior to condensation is electrostatic precipitation [84], although no publicly available data has been found on this approach.

It should be recognized and acknowledged that given the issues related to solids and ash, current commercial producers of fast pyrolysis bio-oil have likely implemented their own strategies for maintaining adequate quality control prior to sale of fuel in direct utilization applications. Public information on these quality control measurements is limited. This could represent a key barrier for new adapters looking to convert lower quality forestry materials using similar technologies. Thus, the objective of this work is to generate data on the cross-flow microfiltration of FPBO for suspended char particulate and ash removal, while investigating the impact of key operating parameters on the performance and flux of the process. In turn, this may lead to the identification of new opportunities to reduce processing costs of FPBOs, with higher levels of suspended char particulate and ash, produced from progressively lower quality forestry materials.

3.1.1. Microfiltration of Fast Pyrolysis Bio-oils

Use of membrane separation technology in the petroleum refining and pulp/paper industry suggests that processes such as microfiltration and ultrafiltration will play key roles in future biorefinery operations for the production of biofuels and bioproducts [84]. Key principles, terms and guidelines for membrane separation technologies, and in particular cross-flow microfiltration, have been detailed elsewhere [60–62]. Filtration and/or microfiltration has previously been reported as an undesirable treatment pathway for solids removal from FPBO based on the degree of technical challenges associated with the formation of gel-like "cake" fouling layers [21,89]. Previous investigative studies on solids removal from pyrolysis oil by microfiltration have been performed with 0.5 µm and 0.8 µm tubular membranes [90]. Microscope imaging visually revealed a high level of solids removal from the FPBO after microfiltration. Furthermore, ash content in the permeated liquids was reduced by approximately 60%. Cake fouling formation was determined to be the primary resistance for permeation, as the permeance (the transmembrane pressure-normalized flux) decreased from an initial value of 25-55 L h^{-1} m^{-2} bar^{-1} to 5-20 L h^{-1} m^{-2} bar^{-1} after several hours of operation for both pore sizes. The authors acknowledged the need for process development for larger scale use, as well as more detailed studies required for understanding the fouling mechanisms that were occurring on the surface of the membrane. Additionally, existing patents indicate that bio-oil filtration using pore sizes ranging from 5-50 µm can achieve permeate flux rates ranging from 10-500 L m^{-2} h^{-1} [91,92], although the exact filtration strategy is largely unknown. Further details in these patents include examples of operating parameters, including fluid pre-heating and the transmembrane pressures employed.

Declines in permeate flux in cross-flow microfiltration due to a combination of developing resistance mechanisms is well-documented in literature [60,62,93]. The main resistance mechanisms include filter/membrane resistance, pore blockage and cake formation (fouling). "Fouling" is a term commonly used to describe the most common technical challenge associated with liquid filtration technologies – the accumulation of materials on the active filtration surface. Depending on the properties of the filtration media, the liquid that is being filtered, and the properties of the rejected particulate, fouling may be reversible, irreversible or a combination thereof.

3.2. Materials and Methods

To study the microfiltration of fast pyrolysis bio-oils for solids and ash removal, a bench scale cross-flow microfiltration system (version: MRK II in Appendix B) was designed and assembled at CanmetENERGY-

Ottawa (CE-O). Supplemental pictures and information related to the design of the system is included in Appendix B. A schematic of the experimental system is included in Figure 3.1.

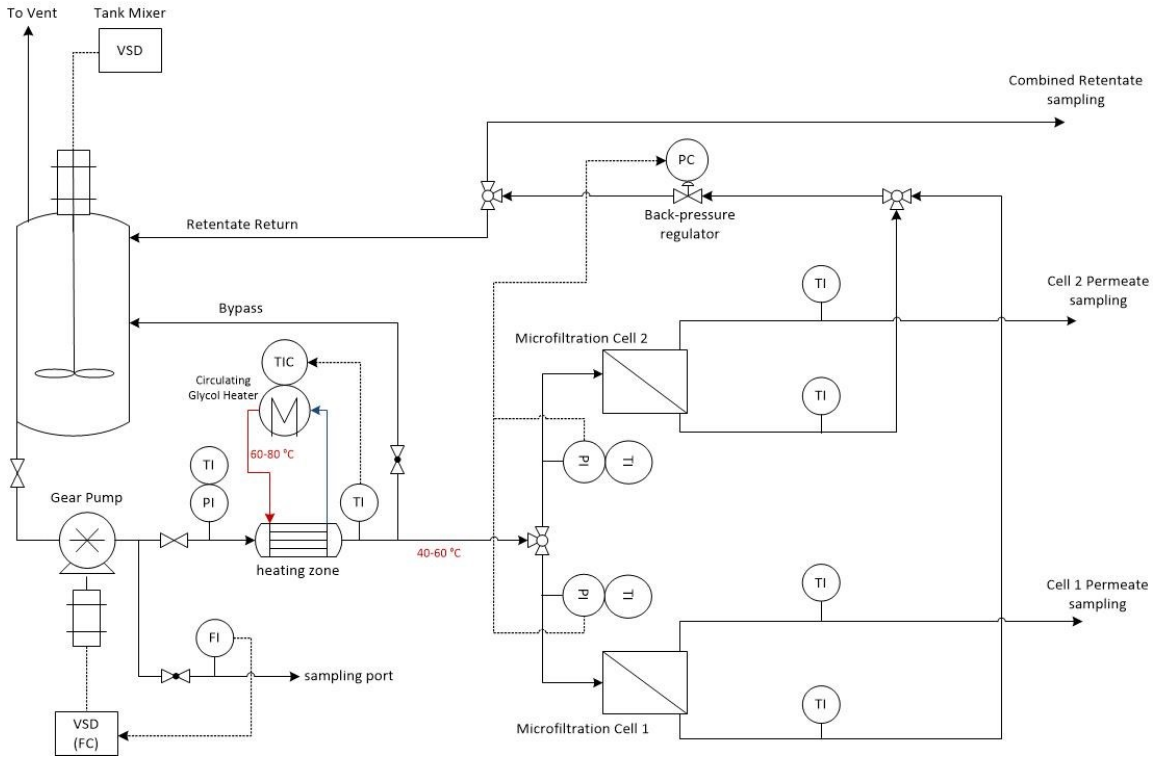

Figure 3.1: Schematic of MRK II version of FPBO cross-flow microfiltration system

The experimental system comprised of parallel filtration cells, which could be operated simultaneously to allow for different flow or filtration configurations under the same operating conditions. A prototype microfiltration cell was designed and assembled at CE-O. Of note, the cell was oriented such that the feed flow came from the bottom and the permeate was collected from the top of the cell. An image of the microfiltration cell is shown in Figure 3.2. The shear forces of the fluid acting upon the fouling layer at the active surface of the filtration media was inherently difficult to calculate. Thus, the fluid injection velocity was used as a relative parameter to compare the shear forces occurring at the fouling layer between different trials. The fluid injection velocity was calculated from the measured circulation rate of bio-oil through the system and the cross-sectional area of the injection tubes at the active filtration surface.

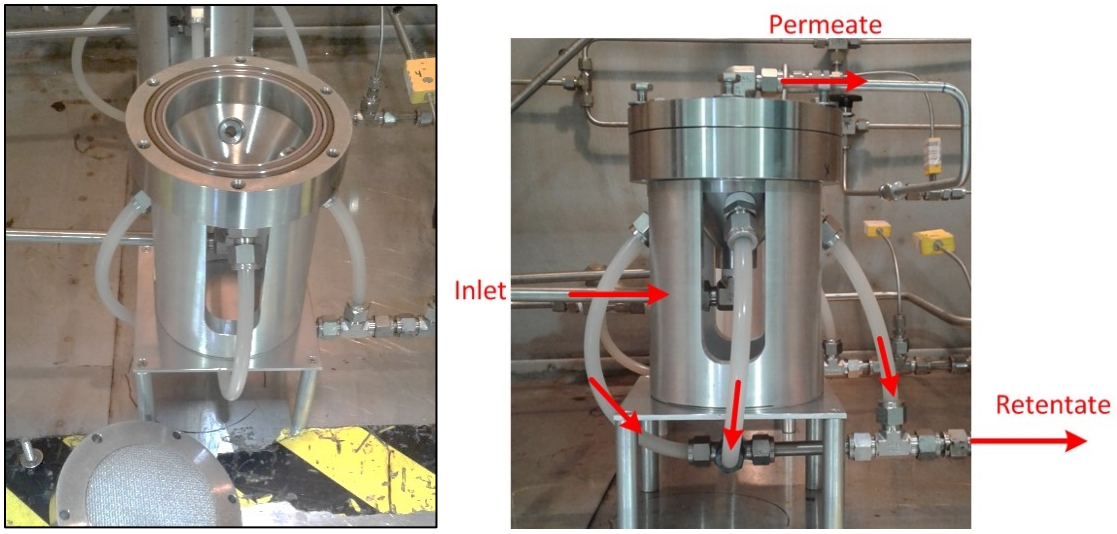

Figure 3.2: Top view (left) and side view (right) of filtration cell used in FPBO cross-flow microfiltration trials

The filtration media used in experiments varied between 1 µm and 40 µm 316 stainless steel mesh, 5 µm nylon and 5 µm polycarbonate. These materials were selected due to their relative preferred compatibility with carboxylic acids, ketones and aldehydes, among other components in bio-oil, with respect to other commonly-available types of filtration material media. Due to the mechanical weakness of the membrane materials, when used, they were supported by a 40 µm stainless steel mesh filter. The selection of filtration media with FPBO is important as it is known to be incompatible with many elastomers, polymers (causing deterioration or excessive swelling) and metals (corrosion) [94]. A summary of the recorded properties of the different filtration media used in this work is located in Table A. 4.

The other main features of the cross-flow experimental system comprised of a mixing tank, a pump, a heating zone and a back-pressure regulator. The majority of the wetted components in the system were fabricated from 316 or 304 stainless steel. Process connections were made from compression tubing and fittings, with ¼" - ½" nominal internal diameter tube sizes. The mixing tank was a 12 L vessel with an impeller mixer mounted at the top. The mixer was an axial impeller with a diameter of 0.08 m with a typical rotational speed of 350-875 rpm. The pump that was used for the majority of the trials was a helical hear pump connected to an 1150 rpm motor with variable speed drive, which corresponds to a nominal circulation rate of 1.8-7.5 L min^{-1} (LPM) based on manufacturer pump performance diagrams. Pump performance was however significantly below pump curve expectations at higher pressures and observations indicate that this was likely due to erosion of the pump mechanical components over time. Typical FPBO circulation rates during experimental trials ranged from 0.15-1.2 LPM.

Bio-oil heating was achieved in initial experimental trials using low intensity external heat tracing along the tubing at the pump outlet. The low intensity electrical heat tracing was replaced by an indirect shell-and-tube heat exchanger connected to a circulating heated bath with glycol as the shell-side heating fluid in later experiments. The main reason for this transition was from technical experience in the unsuitability of direct electrical heating for bio-oil, which can cause over-heating if sudden loss of flow is encountered. Heating of the fluid was controllable up to 60°C. The liquid temperature was monitored at numerous locations in the system including the pump outlet, the filtration cell inlet/outlet and the permeate outlet. Temperatures were logged using a Graphtec data logger.

System pressures were manually recorded using bourdon tube pressure gauges at the pump outlet and the filtration cell inlets/outlets. A Swagelok KFB model (0-3.45 bar) back-pressure regulator was used to maintain system pressure. The microfiltration cells were operated in parallel such that the retentate stream from each cell re-connected prior to the back-pressure regulator. As a result, both microfiltration cells were operated under the same transmembrane pressure set points.

The vast majority of the fast pyrolysis bio-oils that were used throughout the experimental work were produced at CanmetENERGY-Ottawa from Canadian forestry biomass residual feedstocks. A description of CanmetENERGY-Ottawa's bubbling fluidized bed fast pyrolysis system is available in supplementary literature [53]. Of relevance to this work includes the condensation approach that is used in the experimental system. For maximum recovery of bio-oil at a single condensation temperature, CE-O utilized a hydrocarbon quench fluid which was separable from the produced bio-oil by gravitational settling. However, imperfect separation existed in the system, and thus small amounts (< 5 wt%) of the hydrocarbon quench fluid could be contained in the FPBO. It is believed that the introduction of small concentrations of hydrocarbon quench fluid did not impact the microfiltration performance or properties of the bio-oils.

The fluid properties that were analyzed for direct comparison included solids content by ASTM D7579, fluid kinematic viscosity (at operating temperature) by ASTM D445 and in some cases, ash content by ASTM D482 and water content by ASTM E203. In many cases, the amount of volume required in the cross-flow microfiltration system exceeded the amount of bio-oil produced in a single pilot scale pyrolysis trial, and thus blending of different bio-oils produced from different conditions was necessary to meet the volume requirements for microfiltration study. Blending of bio-oils was catalogued such that the properties of the liquids input into microfiltration experiments were closely monitored at the time of experiment. A summary of the fast pyrolysis bio-oils that were used in the microfiltration studies are

included in Table 3.1. The properties of the forestry-based biomass feedstocks used to generate the FPBOs are included as supplementary data available in Appendix A.

Table 3.1: Summary of production information and properties of FPBOs used for microfiltration studies

Internal Numerical ID	Original Feedstock	Approximate Reactor Temperature (°C)[b]	Age at Use (months)	Solids Content (wt%)[b]	Ash Content (wt%)[b]
1	Coastal Hog Fuel	480	7		0.167
2	Hardwood Flooring Sawdust Residue	480	5	0.3	0.033
3	Hardwood Flooring Sawdust Residue	480	5	2.27	0.092
4	Fines fraction from a Hog Fuel	400	14	0.36 - 0.41	0.364
5	Hardwood Harvest Residue (Forest Slash)	480	16	0.5 - 0.64	
6[a]	confidential	unknown	< 5	0.03 - 0.07	0.045
7	Hardwood Flooring Sawdust Residue	460 - 480	2-12	0.45	0.13
8	Hardwood Harvest Residue (Forest Slash)	480	< 1	0.12 - 0.55	0.135 - 0.14
9	Softwood Sawdust (Sawmill Residue)	480	48	0.41	0.154
10	Hardwood Flooring Sawdust Residue	400 - 480	36	0.37 - 0.48	
11	Hardwood Flooring Sawdust Residue	400 - 480	2 - 36	0.35 - 0.63	0.191

[a]obtained from external supplier; [b]When a range is provided, this indicates that multiple bio-oils under the same feedstock or production conditions were used with the range of properties included

For most feedstocks, a single phase bio-oil could be produced from fast pyrolysis as long as the initial moisture content of the feedstock was appropriately limited to below 10 wt%. However, in the cases that multiphase bio-oils were produced, the liquids were homogenized with the addition of low levels of diluent solvent. Bio-oils used in this work were stored at freezer temperatures when not being utilized.

3.2.1. Experimental Procedures

Prior to each experimental trial, the mixing vessel was manually loaded with 6-10 L of the bio-oil to be processed. Once loaded, the mixing vessel was sealed and the impeller mixer was activated. The gear pump was then activated to circulate the bio-oil through the heating zone, and then returned directly to the tank by bypassing the microfiltration cells. As a result, the entire contents of the mixing vessel were

heated to the set point temperature of the heating zone. A sample of the bio-oil was collected from a sampling port prior to proceeding with the experimental trial.

Once the appropriate fluid temperature was achieved, a valve was used to direct flow to the back-end of the microfiltration system where the filtration cells were located. After passing through the parallel filtration cells, the combined retentate passed through the back-pressure regulator, which was manually adjusted to maintain the desired set point transmembrane pressure (TMP). The combined retentate was then directed back into the mixing vessel.

During processing, the permeate was actively collected in a bottle located on top of a balance. The instantaneous permeate flux was subsequently approximated by taking the forward-finite difference between the cumulative mass of permeate collected over different time intervals. Permeate weight measurements were taken manually by the operator. Given the typical flux profiles in bio-oil microfiltration, permeate weight measurements were recorded every 1-2 minutes for the first ten minutes of operation, followed by every 5-10 minutes for the subsequent hour of continuous operation. Permeate weight measurements were taken much less frequently after a couple hours of continuous operation. Generally, a single bulk permeate sample was collected per experimental trial which was subsequently analyzed for solids content, among other properties. Periodic samples of the circulating liquid medium and retentate (reject) were also collected and weighed to obtain mass flow rates during experimental trials.

3.3. Results and Discussion

3.3.1. Model Development from FPBO Cross-flow Microfiltration

As it pertains to this work, it was decided to model cross-flow microfiltration of bio-oil in such a way that the transient operating region is defined by dead-end microfiltration and constant pressure, while the pseudo steady-state (S-S) operating region is modelled by Darcy's law. The use of "pseudo" steady-state represents the assumption that the permeate output flux has reached a constant value for the purpose of modelling and comparison, although in reality the permeate flux has not truly stabilized due to limitations in continuous processing time durations, as well as eventual concentration of solids in the circulating bio-oil as a function of processing time.

The individual resistance contributions are normally not known *a priori* so that only the total resistance can be evaluated from the steady-state flux, as described by Darcy's law, and is shown in Eq. (3) [60].

$$J = \frac{1}{A}\frac{\Delta P}{\mu_o R_T} = \frac{1}{A}\frac{\Delta P}{\mu_o(R_m + R_c + R_p)} \quad (3)$$

where ΔP is the transmembrane pressure, μ_o is the fluid bulk kinematic viscosity, R_T is the total resistance to filtration, R_m is the membrane resistance, R_c is the cake resistance, and R_p is the pore plugging resistance.

Assuming pore plugging is negligible, the contribution of the remaining individual resistance factors may be approximated by correlations applicable to dead-end microfiltration at constant pressure [60]. Using experimental data, the specific cake resistance can be found by plotting the area-normalized volume to the operating time multiplied by the inverse of the area-normalized volume. The specific cake resistance is conceptually defined as the inverse of the filter cake permeability [60] and is given by Eq. (4).

$$\left(\frac{A}{V}\right)t = \frac{\mu_o \hat{R}_c \theta_s}{2(\theta_c - \theta_s)\Delta P}\left(\frac{V}{A}\right) + \frac{\mu_o R_m}{\Delta P} \quad (4)$$

where θ_c and θ_s correspond to the solid volume fraction in the cake [Eq. (7)] and the fluid suspension [Eq. (8)], respectively, and $\hat{R}_c$ is the specific cake resistance, which is related to the cake resistance by:

$$R_c = \hat{R}_c\, \delta_c(t) \quad (5)$$

where δ_c is the cake thickness. Unlike R_c and δ_c, which both increase with time before steady-state conditions are reached, $\hat{R}_c$ is a constant and independent of time. In the case when the cake resistance dominates, it can be shown that the cake thickness is proportional to the square root of time [50]:

$$\delta_c(t) = \left(\frac{2\theta_s \Delta P t}{(\theta_c - \theta_s)\mu_o \hat{R}_c}\right)^{1/2} \quad (6)$$

$$\theta_s = \frac{x_s}{\rho_f} \quad (7)$$

$$\theta_c = 1 - \varepsilon_c \quad (8)$$

where ε_c is the void fraction of the cake, which may be approximated as 0.4; x_s is the bulk fluid solid content, and p_f is the fluid bulk density which has been approximated as 1200 kg m^{-3}.

Maintaining the assumption of transient microfiltration and cake resistance as the dominant mechanism, the permeate flux and volume collected may be calculated according to Eq. (9) and Eq. (10), respectively.

$$\frac{J(t)}{A} = \frac{1}{A}\left(\frac{(\theta_c - \theta_s)\Delta P}{2\theta_s \mu_o \hat{R}_c t}\right)^{1/2} \quad (9)$$

$$\frac{\mathrm{V}\,(\mathrm{t})}{A} = \left(\frac{2(\theta_c - \theta_s)\Delta P t}{\theta_s \mu_o \hat{R}_c}\right)^{1/2} \quad (10)$$

Knowing $\hat{R}_c$, one can evaluate δ_c at any time, including the time at which cross-flow microfiltration approaches pseudo steady-state. It will also be assumed that once pseudo steady-state is achieved, that a constant cake thickness has also been realized. In turn, knowing the cake thickness at pseudo steady-state and the specific cake resistance allows evaluation of the cake resistance from Eq. (6) and the total resistance (maintaining the assumption that pore blockage is negligible) by calculating the filtration media resistance either from Eq. (3) or Eq.(4).

3.3.1.1. Testing the Model

The developed approach that was described above was applied to existing FPBO cross-flow microfiltration experimental data to determine the suitability of the approach. Four separate trials with similar operating conditions were used for the evaluation to demonstrate repeatability. The range of operating conditions for the independent experimental trials in this dataset are included in Table 3.2.

Table 3.2: Range of operating conditions in cross-flow microfiltration trials presented in Section 3.3.1.1

Bio-oil Internal ID (Table 3.1)	10
Solids Content, kg m^{-3}	4.1 – 4.6
Filtration media	5 µm nylon + 40 µm SS support
TMP, bar	0.69 - 0.83
Fluid temperature, °C	50
Fluid kinematic viscosity at operating temperature, $mm^2 s^{-1}$	25.0
Observed solids rejection range, %	91 - 95
Fluid injection velocity, m s^{-1}	0.48 ± 0.02

Figure 3.3 demonstrates the average flux and volume production, as a function of time, for the four independent experimental FPBO cross-flow microfiltration trials. Error bars are also present, which describe the standard error associated with each data point, and contain between 2-4 data points.

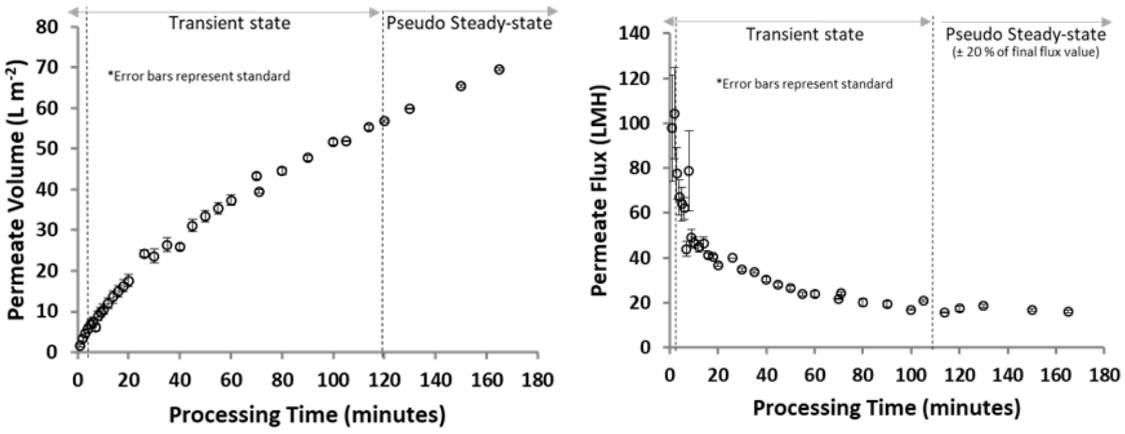

Figure 3.3: Average cumulative volume production (left) and permeate flux (left) from 4 repeat trials as a function of processing time for various FPBO cross-flow microfiltration trials at CanmetENERGY-Ottawa without any operational interference

The profiles from FPBO cross-flow microfiltration resembles that of other common cross-flow microfiltration/ultrafiltration processes, such as whey separation and oily wastewater treatment [60–62,93,95,96]. Evidence of a transient operating region and "steady-state" operating region are observed over the reported time range.

The transient state region of the profile is qualitatively sub-divided into a rapid decline and intermediate decline region, while the pseudo steady-state region shows a very small decline flux profile. In this work, the pseudo steady-state operating region is defined as incorporating all flux data points that are within 20% of the final value. However, minor decreases in flux in the pseudo steady-state region are still apparent. This could be due to subtle changes in operating parameters, such as minor concentration of the bulk solids content of the liquid as a function of processing time, or simply a result of insufficient length of processing to establish true steady-state. By analyzing the standard error with each flux data point, lower repeatability was found in the intermediate decline transient region, and much lower in the initial (rapid decline) transient region relative to the pseudo steady-state operating region.

Manipulation of the experimental data into a plot of tA/V vs. V/A was performed to evaluate the applicability of the cake resistance model, which assumes dead-end microfiltration at constant pressure, and is shown in Figure 3.4.

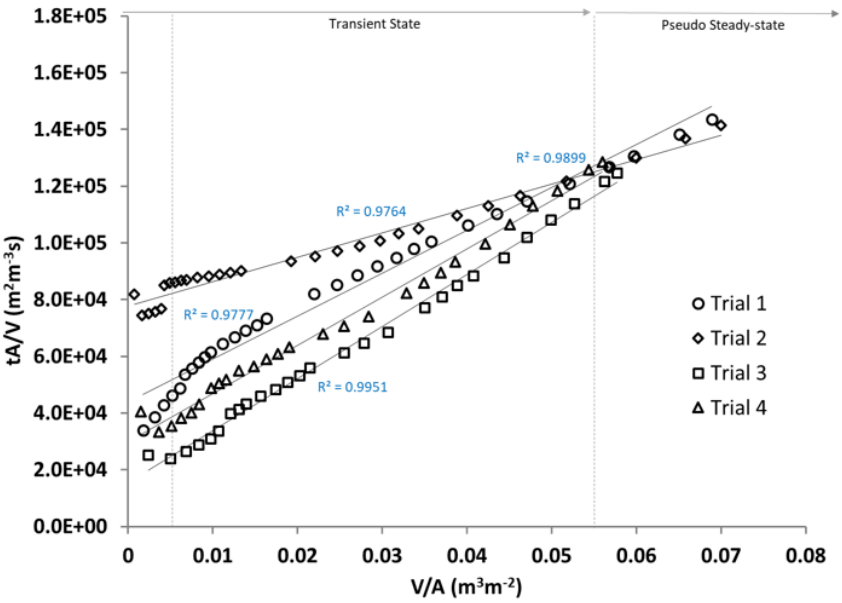

Figure 3.4: Plot of tA/V vs. V/A from four repeat trials to determine the specific cake resistance assuming dead-end microfiltration at constant pressure

The profiles above all appear to fit well under a linear approximation, which demonstrates the applicability of the dead-end model at constant pressure for FPBO cross-flow microfiltration in the transient and pseudo steady-state operating regions. Slight deviations from linearity occur at the beginning of the profiles in the rapid decline transient region, as well as in the pseudo steady-state operating region. The deviations from linearity in the rapid decline transient stage could be caused by other resistance mechanisms, such as pore blockage. Another explanation for the variations in the rapid decline transient region could be experimental limitations, such as trial-to-trial variability in the time required to establish consistent flow patterns in the microfiltration cells, as an example.

Removal of the pseudo steady-state data points from Figure 3.4 may also be performed to incrementally improve the fit of the linear approximation and the calculated specific resistance value. Eventually, the removal of data points in the steady-state operating region would be required to appropriately estimate the specific cake resistance. Various parameters, including specific cake resistance and total resistance at pseudo steady-state from the four trials presented above are summarized in Figure 3.5, along with the associated standard error of each value. It is shown that the total resistance, calculated by Darcy's law and experimental data, is well approximated by the cake resistance as calculated by the model developed in this work. Furthermore, the measured pseudo steady-state flux is well-represented by the modelled flux as presented in Eq. (9).

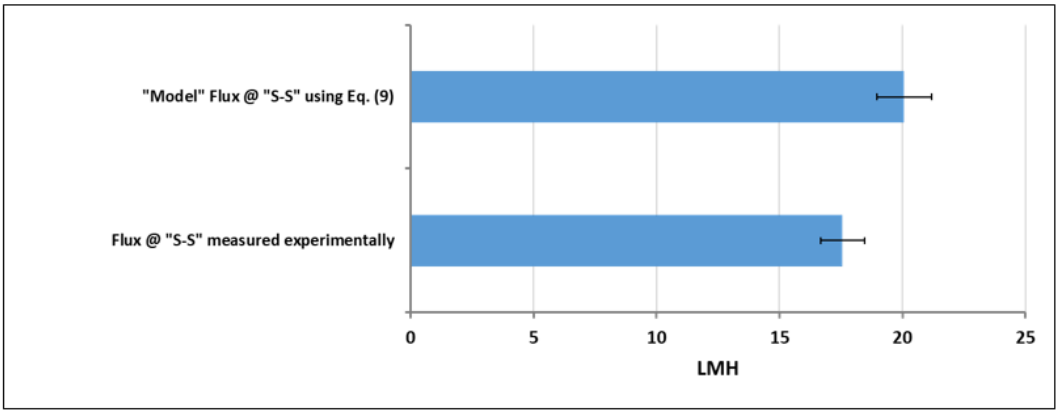

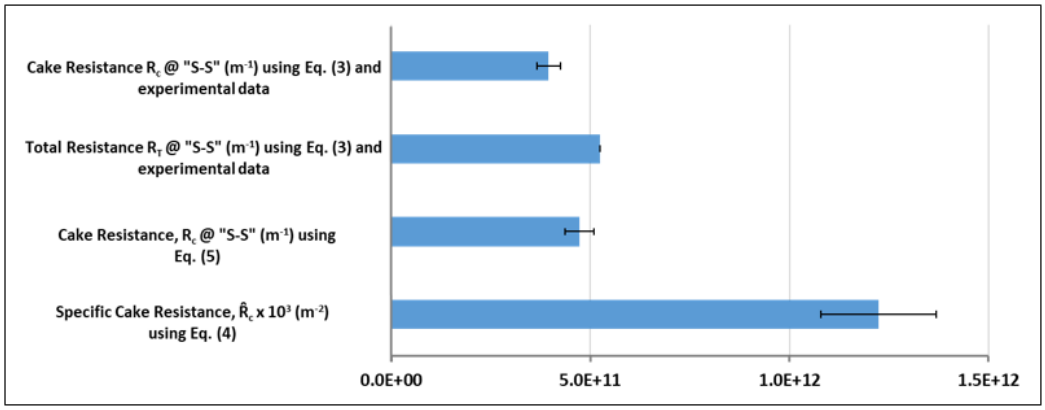

Figure 3.5: Comparison of transient and pseudo steady-state flux (top) and resistance (bottom) with associated standard error obtained from model development using trials 1-4 with range of operating conditions described in Table 3.2

Further model validation has been performed on a wider range of experimental operating conditions for FPBO cross-flow microfiltration using the procedures outlined above. This additional work has been included in Appendix D.

It has been demonstrated that the combined use of dead-end and steady-state correlations to represent the cake resistance and flux in FPBO cross-flow microfiltration in the transient and pseudo steady-state operating regions is appropriate under the operating parameters presented. Thus, the use of the specific cake resistance and model flux will be used as comparable performance metrics when evaluating the impact on operating conditions, which is discussed below. Additionally, the throughput (or cumulative volume production) of low solids bio-oil after a consistent amount of time will be used as a comparative tool for throughput under different operating parameters.

3.3.2. Evaluating Experimental Operating Conditions

3.3.2.1. Effect of Pressure

Transmembrane pressure is the driving force in microfiltration as a pore-size exclusion process. However, relative to smaller pore-size exclusion processes like ultrafiltration or reverse osmosis, microfiltration is often operated at pressures below 3.45 bar (50 psi) since the solute osmotic pressure is often negligible [60]. Diminishing returns associated with increasing transmembrane pressures may exist due to the interacting effects of driving force, cake layer formation and in some cases, cake layer compaction. The impact of TMP up to 3.06 bar was investigated on the resulting performance of FPBO cross-flow microfiltration. The range of operating conditions used in this work are summarized in Table 3.3, with the intentionally-adjusted variable highlighted in grey.

Table 3.3: Range of operating conditions in cross-flow microfiltration trials presented in Section 3.3.2.1

Bio-oil Internal ID (Table 3.1)	10
Solids Content, kg m^{-3}	3.6 - 5.7
Filtration media	5 µm polycarbonate (PCTE) (w/ hydrophobic (HB) layer) + 40 µm SS support
TMP, bar	0.14 – 3.06
Fluid temperature, °C	40
Fluid kinematic viscosity at operating temperature, $mm^2\ s^{-1}$	14.8 - 19.4
Observed solids rejection range, %	83 - 96
Fluid injection velocity, m s^{-1}	1.95 ± 1.32

The calculated specific cake resistance, pseudo steady-state permeance and resulting throughput (defined as total volume produced over specified time limit) from varying transmembrane pressures are show in Figure 3.6. Supplementary data, which includes the flux profiles form this work, are included in Figure A. 13 in Appendix D.

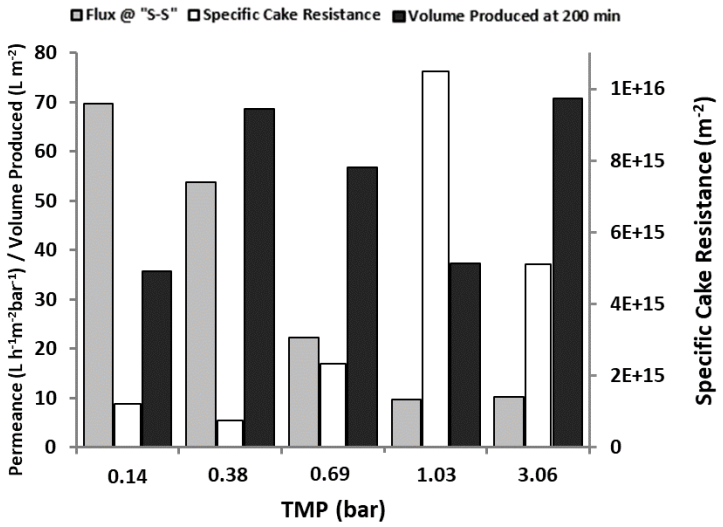

Figure 3.6: Pseudo steady-state permeance, specific cake resistance and volume production (at 200 minutes) from independent trials using different TMPs for FPBO cross-flow microfiltration

There is an indication of increasing specific cake resistance as a function of transmembrane pressure, which suggests that some degree of cake compressibility exists in FPBO cross-flow microfiltration. Correlations exist in literature to quantify the degree of compressibility of the cake as a function of pressure [60], although more data is recommended to complete this exercise. The specific cake resistance calculated in the 1.02 bar trial appears to be significantly higher than that of the trial at 3.06 bar. This result is believed to be due very low circulation rates (leading to lower injection velocities) observed during the 1.02 bar trial, which was a result of poor pump performance for this trial alone.

The permeance, defined as the pressure-normalized flux, is also shown to increase as the transmembrane pressure decreases. This result is indicating that increasing the TMP does not incrementally lead to the similar increases in permeate recovery at pseudo steady-state. However, comparison of the cumulative volume production shows that the most permeate was recovered in the 3.06 bar trial, followed closely by the 0.38 bar trial. This result can be explained by the flux profiles in the transient and steady-state operating regions. Although higher TMPs lead to more permeate recovery in the transient operating region, they have also proven to lead to lower permeate recovery in the pseudo steady-state operating region. Thus, although higher pressures may lead to higher throughput in the short-term, it is expected that the throughput would be surpassed by lower pressure operations as the length of uninterrupted processing time increases.

The results from this dataset would suggest that it is advisable to operate FPBO cross-flow microfiltration systems at lower pressures (0.38-0.69 bar) rather than higher pressures (>1.03 bar) if aiming to operate primarily in the steady-state region. However, if it is desired to operate in the transient region in a FPBO cross-flow microfiltration process, the use of higher pressures (ex. 3.0-3.45 bar) may be recommended. In this processing mode, the cake resistance will eventually become too large and the necessity of higher frequency removal of the accumulated fouling layer is required to maintain acceptable throughput levels. As a result of the observations above, the majority of subsequent FPBO cross-flow microfiltration trials at CE-O were operated at objective pressures of 0.38-0.64 bar.

3.3.2.2. Effect of Fluid Kinematic Viscosity

For this experimental work, two distinct pathways for reducing the fluid kinematic viscosity were investigated. They were:

A. Adjusting fluid kinematic viscosity at constant temperatures by adding a miscible, lower kinematic viscosity solvent to the bio-oil.
B. Increasing fluid temperature

For many fluids, increasing fluid temperatures may be the preferred approach to reduce kinematic viscosity as opposed to the addition of a solvent. However, for FPBO, the preferable route is less obvious. For bio-oil, there is a limit for which the fluid can be pre-heated until irreversible polymerization may occur causing unintended increases to fluid kinematic viscosity [36]. Although this temperature limit may depend on several factors, a rough guideline of 80-100 °C has previously been used [56]. On the other hand, for bio-oils produced from low quality residuals, phase separation (into an organic and aqueous bio-oil fraction) may occur for which solvent addition may represent a necessary pre-requisite prior to processing [21].

Kinematic viscosity reduction of the bulk fluid was investigated using diethylene glycol monomethyl ether (DEGMME), which had a kinematic viscosity of approximately 3.8 $mm^2 s^{-1}$ at 20 °C. Although DEGMME is less common as a diluent for FPBO as compared to light alcohols such as methanol and ethanol, it was selected due to its much higher flash point. The DEGMME concentration of the FPBO was adjusted step-wise by mass concentrations of 5 wt% in four separate trials to evaluate this effect. The range of operating conditions for this dataset are summarized in Table 3.4.

Table 3.4: Range of operating conditions for study of solvent addition in cross-flow microfiltration trials presented in Section 3.3.2.2

Bio-oil Internal ID (Table 3.1)	5
Solids Content, kg m^{-3}	5.7 - 7.5
Filtration media	40 µm SS
TMP, bar	0.34 – 0.68
Fluid temperature, °C	40
Fluid kinematic viscosity at operating temperature, $mm^2\ s^{-1}$	18.8 – 28.5
Observed solids rejection range, %	81 - 90
Fluid injection velocity, m s^{-1}	0.68 ± 0.09
DEGMME concentration, wt%	0 – 20 (5 wt% intervals)

The permeance as a function of processing time for trials where viscosity was reduced by solvent addition are included as supplementary data in Figure A. 14 in Appendix D. The comparative specific cake resistance, cumulative volume production and permeance at pseudo steady-state are shown in Figure 3.7.

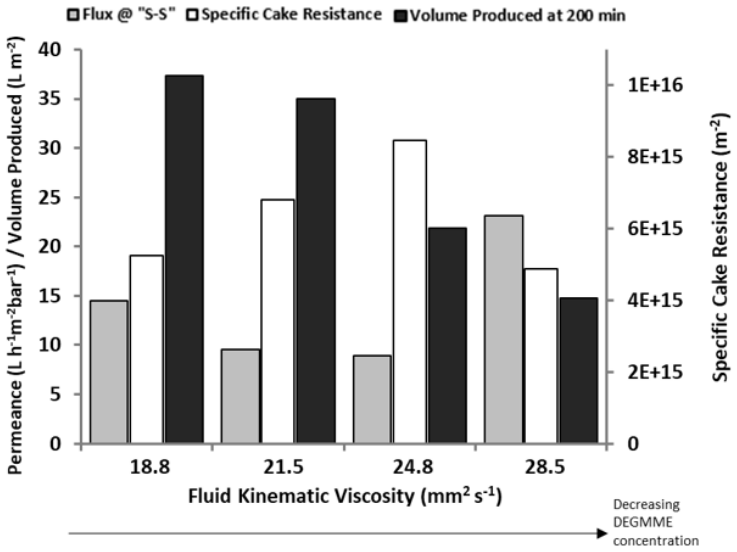

Figure 3.7: Pseudo steady-state permeance, specific cake resistance and volume production (at 200 minutes) from independent trials for different levels of solvent addition for FPBO cross-flow microfiltration

The specific cake resistance generally decreased as a function of increasing solvent concentration. This result lead to increases in pseudo steady-state permeance and permeate recovery. Exceptionally, the trial with the lowest solvent concentration did not follow this trend, where the specific cake resistance was lower than expected. This result is believed to be due to the low initial fluxes that were observed from

this trial leading to less accumulation of fouling, which is likely a function of the higher FPBO viscosity. Although this lead to lower collection volumes of permeate over the specified operating time, the permeance at pseudo steady-state was higher than other trials.

Furthermore, by using GCMS, it was found that the DEGMME concentration did not increase in the filtered permeate samples relative to the unfiltered bio-oils after solvent addition. The results from this analysis indicate that under certain conditions, it may be beneficial to use a low viscosity solvent additive to bio-oil prior to microfiltration to reduce the viscosity of the bulk liquid medium. This may especially be true if solvent is intended to be added to the final bio-oil product prior to utilization. This would depend on several overlaying factors, such as the intended use of the filtered bio-oil or the cost/availability of the solvent, to mention a few.

Following the investigation of solvent addition, the impact of fluid pre-heat temperature at three different levels was studied. For this work, a low-solids FPBO was used. A summary of the processing conditions are included in Table 3.5.

Table 3.5: Range of operating conditions for study of fluid temperature in cross-flow microfiltration trials presented in Section 3.3.2.2

Bio-oil Internal ID (Table 3.1)	6
Solids Content, kg m^{-3}	0.35 – 0.83
Filtration media	5 µm PCTE (w/ HB layer) + 40 µm support
TMP, bar	0.34
Fluid temperature, °C	38, 45, 60
Fluid kinematic viscosity at operating temperature, $mm^2\ s^{-1}$	10.7, 16.8, 28.5
Observed solids rejection range, %	40 - 60
Fluid injection velocity, m s^{-1}	0.36 ± 0.04

The flux profiles from the varying effect of pre-heat temperature is included as supplementary data in Figure A. 15. The specific cake resistance, as well as pseudo steady-state flux and volume production after 200 minutes of processing are presented in Figure 3.8. The specific cake resistance was inversely proportional to the fluid pre-heat temperature, which is analogous to saying that the cake permeability increases with the fluid temperature.

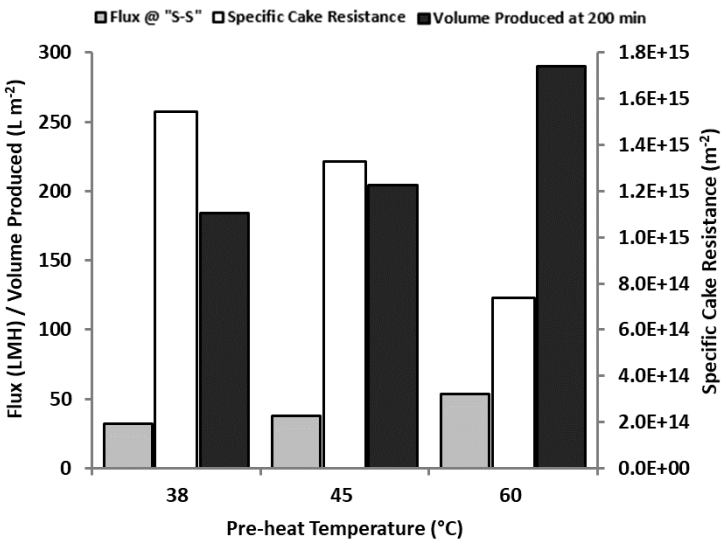

Figure 3.8: Pseudo steady-state permeance, specific cake resistance and volume production (at 200 minutes) from independent trials at three different pre-heat levels for a low solids-containing bio-oil

This result is likely a combination from reductions in fluid viscosity, as well as fouling layer viscosity as the fluid temperature increases. Intuitively, the pseudo steady-state flux and throughput of permeate increases with the fluid temperature. Using pre-heat temperatures of 50-60 °C for FPBO microfiltration is suggested to increase throughput of low solids bio-oil during cross-flow microfiltration. However, it must be verified that pre-heating the bio-oil to these temperatures for the durations required for filtration does not cause significant irreversible changes in viscosity which, depending on the application, would likely be considered a negative impact on the fuel quality.

3.3.2.3. Effect of Solids Content

The final parameter that was experimentally investigated was the bulk solids content of the bio-oil during microfiltration. Under the same operating conditions, higher solids-containing bio-oils should either more rapidly develop cake fouling layers, or develop thicker cake fouling layers on the active microfiltration surface relative to lower ones.

To better understand this concept, the permeance as a function of time for three different experimental trials is represented in Figure 3.9. The permeance, as calculated by Eq. (9), is also included in the plot which shows the similarity between experimental data and established hybrid model outlined in Section 3.3.1. The major difference between the three trials was the bulk solids content in the bio-oil. However, for the case of the high-solids bio-oil, a much higher TMP was used; thus, the permeance profile is

presented in place of the flux profile. A summary of the operating conditions for this investigation is shown in Table 3.6.

Table 3.6: Range of operating conditions for study of fluid temperature in cross-flow microfiltration trials presented in Section 3.3.2.3

Bio-oil Internal ID (Table 3.1)	6 (low solids), 10, 3 (high solids)
Solids Content, kg m^{-3}	0.4 – 26.8
Filtration media	5 µm PCTE (w/ HB layer) + 40 µm SS support **or** 5 µm nylon + 40 µm SS support
TMP, bar	0.34 – 3.06
Fluid temperature, °C	40 - 50
Fluid kinematic viscosity at operating temperature, $mm^2\ s^{-1}$	23 – 28.5
Observed solids rejection range, %	95 - 98
Fluid injection velocity, m s^{-1}	0.43 ± 0.04

To achieve the target solids content for the high solids-containing bio-oil, recovered by-product char from the initial pyrolytic conversion of the hardwood flooring sawdust residue was re-added to the FPBO. The char was ground using a coffee grinder, and sieved such that only char particulate below 40 µm (approximately 50 wt% of the ground char) was re-added to the FPBO. This was done to ensure that the particle size distribution of the suspended char particulate in the bio-oil was not drastically different from what has previously found, where the majority of the suspended char particulate are between 0.5-50 µm in diameter [86,87].

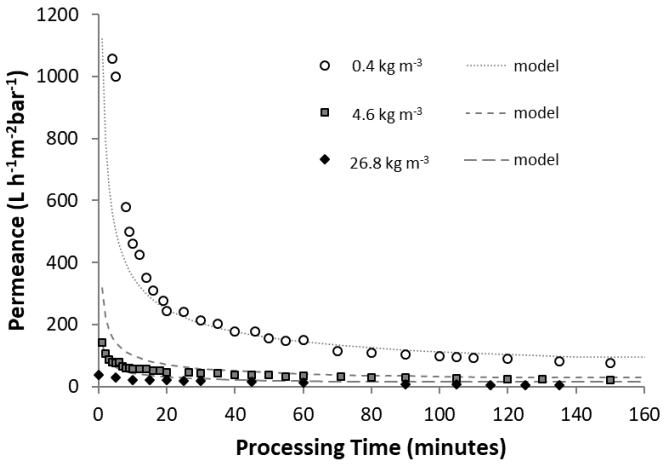

Figure 3.9: Permeance as a function of processing time for three separate trials (along with predictive models) comparing the impact of fluid bulk solids content, as described in Section 3.3.2.3

It is immediately clear upon inspection of the plot that the solids loading has a negative impact on the pressure-normalized flux in both the transient and pseudo steady-state operating regions. The trial with low-solids bio-oil (0.4 kg m^{-3}) should be viewed as a best-case scenario in terms of solids loading in bio-oil prior to microfiltration. Drastic decreases in initial permeance were observed when the bio-oil solids loading changed from 0.4 kg m^{-3} to 4.6 or 26.8 kg m^{-3}, which indicates that fouling was significantly reduced when the bio-oil solids loading decreased.

The results obtained from this analysis suggest that increases in microfiltration performance could be realized by combining several solids-removal techniques with microfiltration, such that microfiltration would be a final processing step. For example, pre-filtering the bio-oil at larger pore sizes to remove a significant portion of the solids could dramatically reduce the required filtration area to process a given volume of bio-oil. This process would have to be carefully designed such that the accumulation of the fouling layer is comparatively low relative to a microfiltration process that removes all suspended char particulate in one stage. This strategy is commonly referred to as cascading [60].

Another example could be to implement a clarification system in which the largest char particles are removed prior to introducing to a microfiltration system. Supplementary data is introduced in Appendix E. based on previous work at CE-O, which consistently demonstrated the mass accumulation of suspended char particulate in the top fraction of settled FPBO after seven day standing tests.

3.3.3. Solids and Ash Rejection

Figure 3.10 summarizes the solids and ash rejection from various FPBO cross-flow microfiltration trials as a function of bulk solids and ash content, respectively, and filtration media. The solids rejection data presented below only included bulk permeate samples collected after 2 minutes of processing, and contained mostly bulk permeate samples within the 2-180 minute operating range. This was due to the fact that poor solids rejection (<15%) was demonstrated for 40 µm stainless steel filters during this initial processing time. This was not observed for smaller pore size media, such as the 1 µm stainless steel filter. These findings indicate that there are a considerable number of char particles that fall between the 1-40 µm diameter range, which are not rejected by the larger pore size filtration media, until an adequate cake layer has been formed which subsequently acts as an additional filtration layer.

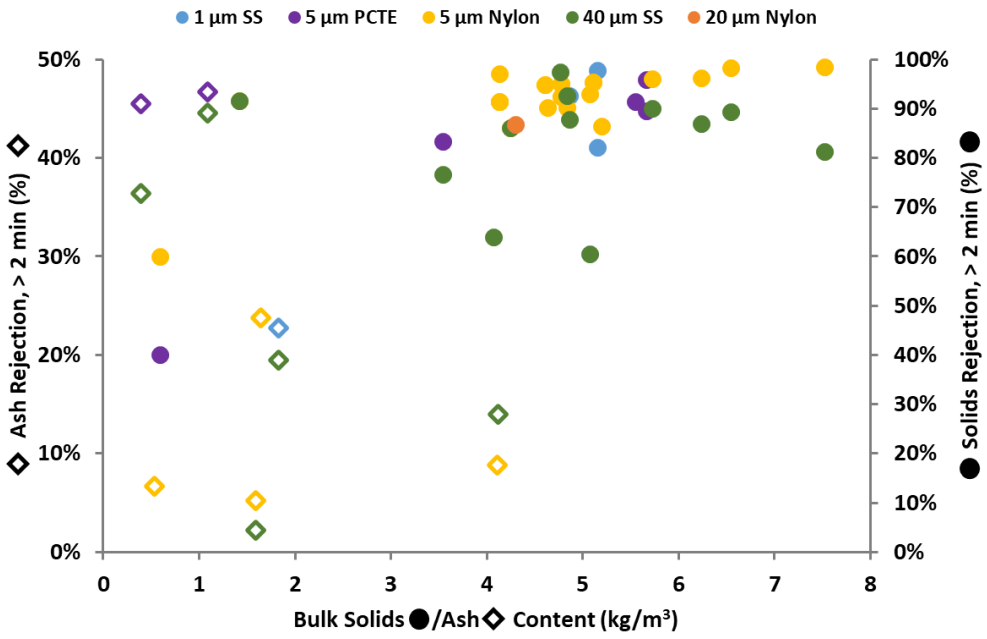

Figure 3.10: Summary of solids and ash rejection from bio-oil cross-flow microfiltration using different filtration media and pore sizes. Solids rejection represented by circles, ash rejection represented by diamonds

The solids rejection using 1, 5, 20 and 40 µm filters/membranes ranged mostly from 80-95%. Solids rejection decreased as the bulk solids content decreased. This could be attributed to lower solids content bio-oil containing smaller particle size distributions of char particles due to greater removal of larger char particles during production (ex. cyclones). Generally, smaller pore size filtration media had superior solids rejection than the large pore size media. As previously discussed, this was very evident in the first two minutes of operation. However, the relative difference in solids rejection between the pore sizes

contained within 1-40 µm after two minutes of operation was typically quite low, which demonstrated that the development of the fouling layers aided in char particulate removal as a primary filtration layer.

Diascopic bright field microscopy was used as a qualitative tool to assess solids removal in this work. An exemplary microscope image of a feed/permeate FPBO sample is demonstrated in Figure 3.11. Additional microscope images are located in Appendix D. along with the procedural steps followed to capture the microscope images. It should be noted that the pink droplets contained in the microscope images are believed to be emulsified hydrocarbon quench fluid from the condensation strategy implemented in CE-O's bubbling fluidized bed fast pyrolysis system. As previously stated, the concentration of the quench fluid is low (<5%).

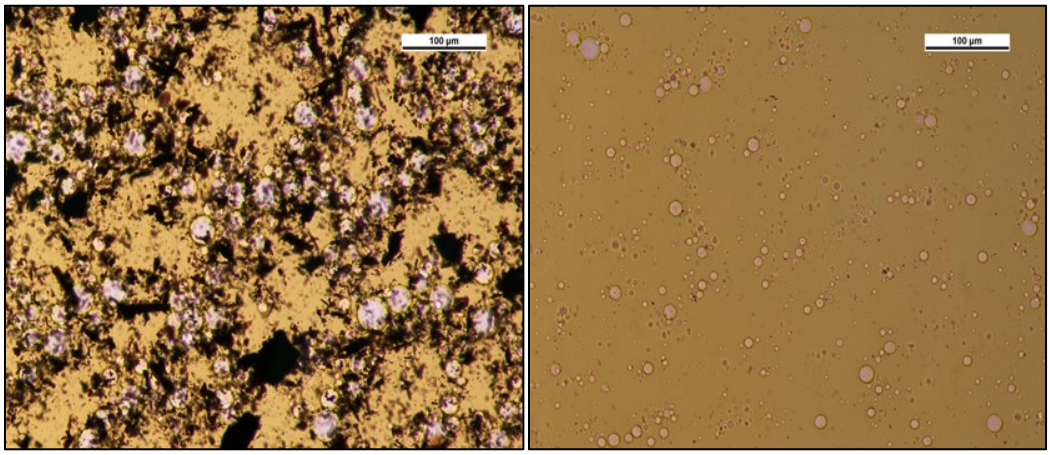

Figure 3.11: Exemplary microscope images (200x magnification) of a 2.3 wt% solids bio-oil (left) feed, with the corresponding low-solids permeate using a 5 µm hydrophilic polycarbonate membrane (right)

The ash rejection is presented for bulk permeate samples collected after the first two minutes of operation. Ash rejection via simple cross-flow microfiltration at pore sizes ranging from 1-40 µm was poor, and ranged from 5-45%. This is lower than previously reported microfiltration of bio-oil (from white oak pellets) using 0.5 µm and 0.8 µm membranes at approximately 60% [90]. Furthermore, this result is inconsistent with previous literature correlating the removal of ash with the removal of suspended char particles from fast pyrolysis bio-oils [52,68,88,97]. This variation could be due to the nature of ash species contained within the fast pyrolysis bio-oils in study. In this work, the bio-oils were produced mostly from sawdust and forest harvest residue, which could be linked to higher concentrations of alkali and alkaline earth metals and other soluble ions relative to other low ash woody feedstock. Thus, many of the ash species could be present dissolved form such that microfiltration is not an adequate separation

mechanism. Furthermore, it is possible that some ash is present at particle diameters less than that of 1-40 µm.

Although the data set is quite limited, it would appear as though the ash rejection was sensitive to the surface properties of the filtration media material. It was demonstrated in a few instances that hydrophobic polycarbonate had the best ash rejection, while hydrophilic nylon had the worst ash rejection, with stainless steel in between. This could be a result of hydrophobic materials better rejecting ionized or solubilized minerals in aqueous components of FPBO. However, more data is required to validate this observation.

3.3.4. Other Properties of Bio-oil Permeate

In addition to the measured solids and ash content of the bio-oils after cross-flow microfiltration, the heating value, density, kinematic viscosity and water content of the low-solids bio-oil were measured in some instances. The properties of the feed and permeate sample streams from various cross-flow microfiltration trials are documented in Table A. 9.

For the most part, changes in water content, kinematic viscosity, density and heating value after cross-flow microfiltration were minor. It was observed that minor reductions in heating value and kinematic viscosity occurred after microfiltration, while minor increases in density were found after microfiltration. These findings are expected to be a direct result from the removal of solid char particulate contained in the bio-oil. This would suggest that the char particulate has a lower density, a higher heating value and contributes to elevated kinematic viscosities in the bio-oil.

In some instances, the water content of the permeated bio-oil was lower than the untreated bio-oil, whereas in other instances, the opposite was found. It is believed that this result is due to a combination of factors, including bio-oil sampling repeatability, the reduction in solids content, or some minor ageing occurring during prolonged heating cycles, of the bio-oil after microfiltration.

3.3.5. Results from Multi-Linear Regression Analysis

To identify the most important factors for FPBO cross-flow microfiltration and the entirety of the datasets, multi-linear regression models were created. The models were developed from over 50 independent experimental trials in which the permeate flux was recorded as a function of processing time without interruption. Interactions between parameters was assumed to be negligible during modelling. Supplementary information related to the procedures undertaken to establish the multi-linear models is

included in Appendix D. The range of operating conditions and fluid parameters used during the development of the multi-linear models are summarized in Table 3.7.

Table 3.7: Range of critical operating parameters used in FPBO cross-flow microfiltration multi-linear modelling exercise

Bio-oil Internal ID (Table 3.1)	1, 2, 5, 6, 7, 8, 9, 10, 11
Solids Content, kg m^{-3}	0.35 – 7.52
Filtration media	1 µm SS, 5 µm PCTE (w/ HB layer) + 40 µm SS support, 5 µm nylon + 40 µm SS support, 20 µm nylon + 40 µm SS support, 40 µm SS
TMP, bar [Pa]	0.34 – 3.06 [34000-306000]
Fluid temperature, °C	40 - 60
Fluid viscosity at operating temperature, $mm^2\ s^{-1}$ [Pa s]	6.3 – 28.5 [0.00756 – 0.0342]
Fluid injection velocity, m s^{-1}	0.24 - 0.93

Once multi-linear regression models were developed for transient state specific cake resistance and pseudo steady-state flux under the range of parameters above, a backward stepwise regression analysis was performed under both scenarios to find the most influential parameters in both operating regions.

3.3.5.1. Transient State Operation

The specific cake resistance, determined by Eq. (4), can be used to calculate the cake thickness, the flux and the permeate volume collected as a function of processing time for dead-end microfiltration under constant pressure. A multi-linear model was developed by performing linear regression analysis on the series of experimental data for which the filtration media pore size, fluid temperature, transmembrane pressure, fluid injection velocity, bulk solids content and fluid viscosity (at operating temperature) were the independent variables, and the calculated specific cake resistance was the response variable. A confidence interval of 95% was used in the statistical analysis. The results from the linear regression modelling of these parameters, along with the backward elimination regression analysis, are summarized in Table 3.8.

Table 3.8: Summary of results from backward stepwise regression analysis of multi-linear specific resistance factor for transient microfiltration modelling. Response variable is specific resistance, $\hat{R}_C$ [m^{-2}] using a confidence level of α=0.05

	Model Coefficients: $\hat{R}_c = a + bx_1 + cx_2 + dx_3 + e\,x_4 + f\,x_5 + g\,x_6$					
Analysis Step	**Units**	**Step 1**	**Step 2**	**Step 3**	**Step 4**	**Step 5**
Linear Intercept	m^{-2}	2.68E+16	2.61E+16	1.96E+16	8.80E+15	1.08E+16
Filtration Media Pore Size (x_1)	see note[a]	-9.51E+14				
Temperature (x_2)	˚C	-2.99E+14	-3.38E+14	-2.51E+14		
Transmembrane Pressure (x_3)	Pa	2.58E+10	2.65E+10	3.36E+10	3.52E+10	
Fluid Injection Velocity (x_4)	m s^{-1}	-2.96E+15	-3.09E+15			
Bulk Solids Content (x_5)	kg m^{-3}	7.64E+14	7.90E+14	7.21E+14	8.25E+14	1.07E+15
Fluid Viscosity (x_6)	Pa s	-4.60E+17	-4.22E+17	-3.92E+17	-4.29E+17	-4.54E+17
Model Fitting Parameters						
Adjusted R^2		0.624	0.607	0.550	0.509	0.380
PRESS		1.18E+33	1.22E+33	1.41E+33	1.30E+33	1.69E+33

[a]Due to limited number of pore sizes used, qualitative coefficients used in placed of quantitative. 40 µm = 0, 20 µm = 1, 5 µm = 2, 1 µm = 3

Overall, the level of fit of the multi-linear model used to predict the specific cake resistance based on the independent parameters was not very strong. One of the indicators of this was the adjusted R^2 value which was at a maximum value of 0.624 when all parameters were included in the model. The predictive error sum of squares (PRESS) was at a minimum when all parameters were included in the model (thus, eliminating any parameters resulted in lower quality model fit). Nonetheless, the multi-linear model that was generated predicted that the most influential were the bulk solids content and fluid viscosity (at operating temperature), while the least influential parameters were the filtration media pore size, the fluid injection velocity, fluid temperature and transmembrane pressure. The specific cake resistance increased with bulk solids content and transmembrane pressure, while it decreased with increasing fluid temperature, filtration media pore size, fluid injection velocity and fluid viscosity (at operating temperature). Many of these outcomes are supported by the experimental data presented in section 3.3.2, with the exception of the fluid viscosity which would have been expected to cause increases in specific cake resistance with increasing fluid viscosity.

3.3.5.2. Pseudo Steady-State Operation

The experimental pseudo steady-state flux was obtained by considering all data points within 20% of the final flux value for each experimental trial, as was described in section 3.3.1.1. The results from the pseudo

steady-state flux linear regression modelling, along with the backward elimination regression analysis, are summarized in Table 3.9.

Table 3.9: Summary of results from backward stepwise regression analysis of multi-linear pseudo steady-state flux modelling. Response variable is permeate flux [m^3m^{-2} s^{-1}] using a confidence level of α=0.05

	Model Coefficients: $J = a + bx_1 + cx_2 + dx_3 + e\,x_4 + f\,x_5 + g\,x_6$					
Analysis Step	**Units**	**Step 1**	**Step 2**	**Step 3**	**Step 4**	**Step 5**
Linear Intercept	m^3 m^{-2} s^{-1}	-9.31E-06	-9.22E-06	-1.08E-05	-1.07E-05	-8.28E-06
Filtration Media Pore Size (x_1)	see note[a]	-3.75E-07	-3.93E-07	-4.04E-07		
Temperature (x_2)	˚C	3.85E-07	3.89E-07	4.10E-07	3.95E-07	3.60E-07
Transmembrane Pressure (x_3)	Pa	-5.33E-12	-5.49E-12			
Fluid Injection Velocity (x_4)	m s^{-1}	2.53E-06	2.53E-06	2.81E-06	2.69E-06	
Bulk Solids Content (x_5)	kg m^{-3}	-8.79E-07	-8.64E-07	-8.20E-07	-8.08E-07	-7.24E-07
Fluid Viscosity (x_6)	Pa s	1.29E-05				
Model Fitting Parameters						
Adjusted R^2		0.807	0.811	0.803	0.791	0.781
PRESS		1.13E-10	1.10E-10	1.09E-10	1.14E-10	1.19E-10

[a]Due to limited number of pore sizes used, qualitative coefficients used in placed of quantitative. 40 µm = 0, 20 µm = 1, 5 µm = 2, 1 µm = 3

The multi-linear model that was used to predict the pseudo steady-state flux had a better level of fit relative to the one used to describe the specific cake resistance, as the adjusted R^2 value ranged from 0.78-0.81. The most suitable regression model eliminated the fluid viscosity based on the PRESS and adjusted R^2.

The predicted steady-state flux increased with fluid temperature, filtration media pore size and fluid injection velocity, while it decreased with increasing transmembrane pressure and bulk solids content. These findings are consistent with the trends that were observed experimentally. Of note, this model supports the observation that lower pressures were more favourable than higher pressures for steady-state microfiltration of fast pyrolysis bio-oils. Furthermore, the fact that the fluid viscosity (at operating temperature) was found to be the least significant parameter, while the fluid temperature was one of the most significant parameters, might again suggest that the viscosity of the gel (or cake) layer adhered to the active filtration, which would be affected by fluid temperature, is an important parameter than can be manipulated to improve bio-oil throughput of the microfiltration process.

It is important to highlight that the pseudo steady-state model developed above should only be used as a predictor when operating parameters are similar to the range provided in Section 3.3.3. Using parameters

outside these ranges may result in the estimate of flux values that are no longer applicable to the model criteria and thus should be approached with caution.

3.4. Conclusions

The removal of suspended solid particles and ash, in many cases, represents an essential processing step prior to direct utilization of fast pyrolysis bio-oils in applications including heat/power generation and catalytic upgrading. This statement is especially true if high ash biomass feedstocks are used to generate these FPBOs. Cross-flow microfiltration represents one of the few available processing operations that can reduce the solids and/or ash content of fast pyrolysis bio-oils to specified levels required for end-use applications. It was determined that excellent solids removal (>95%) can be obtained with the use of filtration media in the 1-40 µm range, while the cake/gel layer that forms on the active filtration surface acts as a primary filtration layer to help improve solids reduction at the cost of significant reductions in flux over time. A collection of stainless steel filters and polymeric membranes in the 1-40 µm range also revealed ash rejection levels ranging from 4-45%.

Flux profiles for FPBO microfiltration follow a rapid decline and intermediate transient decline operating region, as well as a pseudo steady-state operating region, which is common for other microfiltration processes [62]. Studying the key operating parameters determined that low transmembrane pressure operation (<1 bar) lead to higher pseudo steady-state flux relative to higher pressure operation (>1 bar). The use of low viscosity miscible solvents, or higher operating temperatures (up to 60 °C) also caused increases in transient and pseudo steady-state flux. High bulk solids content was found to be detrimental to the throughput of bio-oil microfiltration such that the use of combined solids removal strategies, such as pre-filtration or clarification, should be considered prior to a finishing microfiltration process.

Based on the applicability of a dead-end microfiltration correlation (at constant pressure) for FPBO cross-flow microfiltration in the 1-4 hour operating range, it can be concluded that cake resistance was the dominant resistance mechanism. Given this result, future work should focus on characterizing the cake/gel layer and determining the reversibility of the fouling that is occurring in FPBO cross-flow microfiltration. Additional suggested future work related to this field of study includes a more detailed parametric investigation into the impact of cross-flow fluid velocity and shearing rate on the development of the cake/gel layer and its corresponding resistance.

Furthermore, in addition to what has already been performed in open literature [90], it would be advantageous to perform a similarly detailed study on the effect of key operating parameters on the cross-

flow microfiltration of bio-oil using a tubular, monolithic or spiral-wound microfiltration cell, which may offer processing advantages to the flat-sheet or plate and frame configuration [60] which was represented in this study. Finally, further investigations of the ash rejection from microfiltration, and if necessary, combination with existing ash removal processes (such as ion exchange membranes, for example) are encouraged to achieve high levels of both solids and ash removal from fast pyrolysis bio-oil produced from high ash biomass feedstocks.

Acknowledgements

Funding was provided by Natural Resources Canada's Office of Energy Research & Development through the Program for Energy Research and Development (Project titles: "Pyrolysis Liquids for Immediate Heat and Power Applications" [2015-2019] and "Development and Optimization of Multi-Product Bio-refinery Processes" [2019]). The authors would like to acknowledge Frank Leclair, Evan Shuparski, Jaden Murphy, Simon Lalonde, Berney Chan and the entire staff at the characterization laboratory at CanmetENERGY-Ottawa for their assistance in completing this work.

Chapter 4. Experimental Investigation of Fouling Remediation Strategies for Cross-flow Microfiltration of Fast Pyrolysis Bio-oil

D. Mazerolle[1,2], B. Bronson[1], B. Kruczek[2]*

[1]CanmetENERGY, Natural Resources Canada, 1 Haanel Drive, Nepean, ON, K1A 1M1, Canada

[2]Department of Chemical and Biological Engineering, University of Ottawa, 161 Louis Pasteur Drive, Ottawa, ON, K1N 6N5, Canada

Abstract

As with other microfiltration processes, the overall throughput or performance of fast pyrolysis bio-oil microfiltration for suspended char and/or ash removal is severely hindered by the existence of fouling that occurs over short operating periods. In this work, the fouling residue from cross-flow microfiltration of fast pyrolysis bio-oil was recovered and characterized. Analysis of fouling residue samples indicated that the material was still substantially composed of methanol-soluble organic materials (70-80%) with the balance comprising of char particulate and ash. To improve the throughput from bio-oil cross-flow microfiltration, the use of both on-line and off-line cleaning techniques were evaluated. Both cleaning approaches demonstrated successful regeneration of the flux profiles. Examining on-line cleaning using permeate, solvent and air also demonstrated the reversibility of the fouling layer over the course of continuous operating times exceeding 10 hours and 31 backflushing cycles. Compared to the reference case (no cleaning), on-line compressed air backflushing Increased the overall throughput of low solids permeate by more than 100%. Further opportunity for throughput improvement exists with increased co-optimization of microfiltration operating parameters with backflush downtime. The demonstration of an on-line fouling remediation strategy for bio-oil cross-flow microfiltration increases the likelihood that it could be a viable treatment pathway for suspended solids and/or ash removal in pyrolysis liquids prior to end-use or upgrading.

Keywords:

fast pyrolysis bio-oil; cross-flow microfiltration; fouling remediation, biorefinery membrane processes, on-line backflushing

4.1. Introduction

In previous work by the authors (Chapter 3), cross-flow microfiltration was investigated as a physical treatment pathway to remove suspended char particulate (solids) and ash from fast pyrolysis bio-oils produced from lower quality woody residues. The impact of several key operating parameters, including temperature, transmembrane pressure (TMP) and bulk solids content were evaluated on the performance of such a system. It was found that cake resistance was the dominant mechanism by applying correlations representing dead-end microfiltration at constant pressure to predict the flux and permeate production during the transient and pseudo steady-state operating regions. However, it has not yet been determined whether the observed fouling was reversible. If the fouling is reversible, on-line fouling remediation methods could enhance production capacity of the permeate under the same operating parameters. As such, the work contained below investigates the properties of the fouling residue (cake) that accumulates during cross-flow microfiltration, and explores the use of fouling remediation strategies.

Due to the absence of data for the cross-flow microfiltration of fast pyrolysis bio-oils (FPBO), there are virtually no available literature sources which investigated the use of fouling remediation strategies to improve the overall throughput of such a process. Thus, knowledge and practical guidelines obtained from other common types of membrane separation processes operating in the microfiltration (MF) to the ultrafiltration (UF) range must be leveraged. For example, MF and UF processes commonly used in wastewater treatment, whey (or other proteins) separation, membrane bio-reactor processes, and concentration processes in the food industry have commonalities with respect to bio-oil microfiltration. In comparison to traditional liquid fuels, fast pyrolysis bio-oil is relatively unique; it is acidic, viscous, is typically a bulk mixture of emulsified hydrophilic and hydrophobic components, has limitations on pre-heating due to polymerisation, etc. [21,33,53,98]. A survey through various publications, textbooks, reviews and other sources of literature show common fouling remediation strategies which may be considered for use in a FPBO cross-flow microfiltration system to improve performance.

The use of coagulants or flocculants in wastewater ultrafiltration has been reported to reduce the severity of irreversible pore plugging [62,93]. Combining in-line coagulation and sedimentation have also proven to further reduce fouling in wastewater treatment ultrafiltration. Furthermore, the use of solid additives, termed “filter-aids” to the bulk liquid prior to microfiltration is another strategy which may be used to reduce fouling resistance during processing. Filter-aids, which are typically composed of silicates, can help reduce fouling resistance mechanisms by changing the rheological properties of the filter cake. This can include the cake porosity and cake compressibility [60,61]. The use of filter-aids to improve the removal

of suspended char particles and metals in fast pyrolysis bio-oils has previously been hinted [92]. A common example of a filter-aid which has been previously discussed for MF and UF is diatomaceous earth [61].

Increasing the shear force exerted along the fouling boundary layer is an operational approach which has been linked to reductions in fouling resistance. This includes increasing fluid cross-flow velocity, adopting the use of turbulence promoters such as inserts and channels in the microfiltration cell, creating flow vortices, etc. [99]. More complex strategies to increase shear force along the active filtration surface include the use of mixers, rotating filtration media or cross-rotation filters to disrupt the fouling layer [93].

The use of external fields, such as high frequency vibration, ultrasonication, or the generation of electrical fields to reduce cake formation are other interesting operational strategies that have previously been explored in microfiltration, ultrafiltration and reverse osmosis for colloids, proteins, bacteria, etc. [100,101]. For utilizing an electrical field to help prevent cake fouling in bio-oil microfiltration, the zeta potential of the suspended char particles would need to be quantitatively identified [99]. However, the use of electrokinetic fouling remediation strategies may pose a unique challenge for FPBO cross-flow microfiltration given the viscous and acidic nature of the fluid, as this may influence the electrophoretic mobility of the suspended char particles and the operating life of the anode, respectively.

Membrane cleaning is widely utilized in industrial/commercial membrane separation processes to overcome the economical challenges associated with fouling. Membrane cleaning, as it relates to bio-oil microfiltration, would be categorized under physical cleaning and/or chemical cleaning. Physical cleaning may include permeate or air backflushing, air sparging to create two-phase flow at the filtration surface, sponge ball cleaning (in the case of tubular filtration media), etc. [93,100,102]. Literature review has revealed no existing studies on impacts of physical cleaning on bio-oil cross-flow microfiltration.

Chemical cleaning methods, as the name suggests, requires the use of foreign chemical agents to aid in removing any foulants from within the surface of the filtration media. Some of the considerations with chemical cleaning include the cost and safety associated with their use, the compatibility of the chemical with the filtration media, the necessary down-time, etc. [100]. Previous literature on bio-oil cross-flow microfiltration has revealed a time-intensive cleaning procedure in which tubular ceramic membranes (0.5 µm and 0.8 µm) were cleaned with a combination of methanol, sodium hydroxide and acetic acid soaking in separate stages, up to a total cleaning time of 16 hours [90]. By following the specified procedure, membrane permeance (using methanol as the permeating fluid) was regenerated as high as 90% its original value.

The objective of this study is to better identify the type of fouling (reversible or irreversible) that is occurring during various processing times of FPBO cross-flow microfiltration, and to perform an initial comparison of physical/chemical cleaning methods to increase the throughput of low solids product FPBO from the process.

4.2. Materials and Methods

The FPBO cross-flow microfiltration system, along with the microfiltration cells used in this work, has previously been described in Section 3.2. Supplementary data related to the design of the experimental system is also available in Appendix B. Modifications to the previously reported experimental system were performed which included the addition of vessels on the permeate side of the microfiltration cell which could be used for on-line backflushing, as well as compressed air entry ports. A schematic of the experimental system used in this work is presented in Figure 4.1. Three types of filtration media used in this study which comprised of 40 µm stainless steel (SS), 1 µm SS and 5 µm nylon. The filtration media were circular discs with a diameter of 90 mm. Properties of the filtration media are included in Table A. 4.

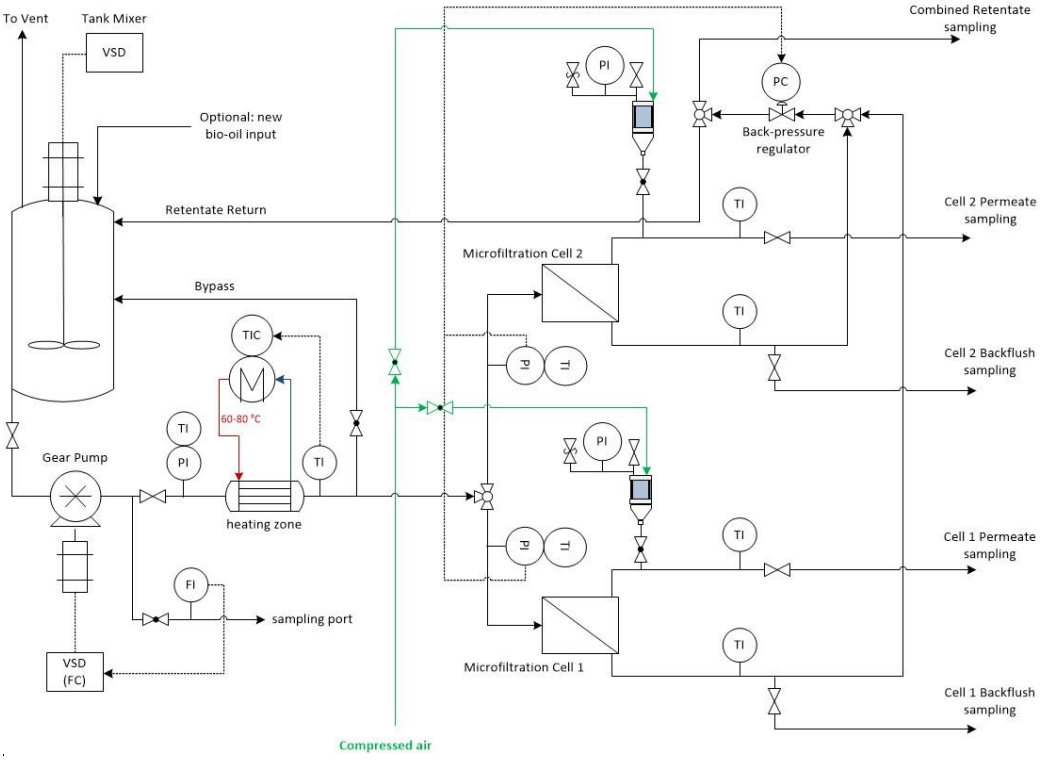

Figure 4.1: Schematic of bio-oil cross-flow microfiltration system (MRK III) used for fouling remediation trials

The fast pyrolysis bio-oils that were used throughout this study were produced at CanmetENERGY-Ottawa, and originated from hardwood flooring sawdust residue or softwood mill residue. Blending of different bio-oils produced under slightly different conditions was necessary to meet the volume requirements for microfiltration study. Blending of bio-oils was catalogued such that the properties of the liquids input into microfiltration experiments were closely monitored. The fluid properties that were analyzed for direct comparison included solids content by ASTM D7579, fluid kinematic viscosity (at operating temperature) by ASTM D445 and in some cases, ash content by ASTM D482. A summary of the fast pyrolysis bio-oils that were used in this work are included in Table 4.1. The properties of the forestry-based biomass feedstocks used to generate the FPBOs are included as supplementary data available in Appendix A.

Table 4.1: Summary of production information and properties of FPBOs used for microfiltration studies

Internal Numerical ID	Original Feedstock	Reactor Temperature Objective (°C)	Age at Use (months)	Solids Content (wt%)	Ash Content (wt%)
7	Hardwood Flooring Sawdust Residue	460 - 480	2-12	0.45	0.13
8	Hardwood Harvest Residue (forest slash)	480	< 1	0.12 - 0.55	0.135 - 0.14
9	Softwood Sawdust (Sawmill Residue)	480	48	0.41	0.154
11	Hardwood Flooring Sawdust Residue	400 - 480	2 - 36	0.35 - 0.63	0.191

Characterization of certain fouling residue samples was performed to better understand some of the physicochemical properties of the accumulated cake layer. To achieve this, samples were physically collected after trials by disassembling the microfiltration cells and collecting the leftover material on the active filtration surface. Selected samples were analyzed for elemental composition, along with solids, ash and moisture content, and in certain cases, ash composition by X-ray fluorescence (XRF). Analyses of the fouling residues were performed similarly to pyrolysis liquids under ASTM D7544, however minor modifications to procedures were required for certain tests due to the differing properties of the fouling residues as compared to fast pyrolysis bio-oil.

For ash determination, samples were placed in platinum crucibles and allowed to air-dry in a fume hood until a constant mass loss (< 0.1 wt% loss per hour) was achieved. Dried samples were then combusted at 775 °C for 16 hours in air, subsequently followed by an additional 2 hours in air for secondary ashing at the same temperature. For water content analysis by Karl-Fischer titration, sample preparation included mixing of residue into methanol at a ratio of 1:1 or 1:2 (fouling residue:methanol). Diluted samples were mixed in a vortex mixer for 30 seconds, followed by ultrasonication for 15 minutes, then additional vortex mixing for 30 seconds prior to any sub-sampling. Density of select fouling residue samples were completed using a helium pycnometer at a residue temperature of 40 °C and a helium pressure of 1.31 bar.

4.2.1. Experimental Procedures

Similar experimental procedures were followed as in previous FPBO microfiltration work at CanmetENERGY-Ottawa as stated in Section 3.2.1. Typically, 6-10 L of bio-oil was used in each trial and pre-heating occurred by circulation through a shell-and-tube heat exchanger with glycol as the heating fluid. Once the appropriate fluid temperature was achieved, a valve was used to direct flow to the microfiltration cells. After passing through the parallel filtration cells, the combined retentate passed through the back-pressure regulator, which was manually adjusted to maintain the desired set point transmembrane pressure. Transmembrane pressure was held constant in each individual trial as to not impact the permeate flux profiles. The combined retentate was then directed back into the mixing vessel.

During processing, the permeate was actively collected in a container located on top of a balance. The instantaneous permeate flux was subsequently approximated by taking the forward-finite difference between the cumulative mass of permeate collected over different time intervals. Permeate weight measurements were taken manually by the operator. Given the typical flux profiles in bio-oil microfiltration, permeate weight measurements were recorded every 1-2 minutes for the first ten minutes of operation, followed by every 5-10 minutes for the subsequent hour of continuous operation. Permeate weight measurements were taken much less frequently after a couple hours of continuous operation. Periodic samples of the circulating liquid medium and retentate (reject) were collected and weighed to obtain mass flow rates during experimental trials and track any changes in solids content over the course of an experimental trial. Baseline flux profiles were generated for each experimental trial by allowing a period of 30-60 minutes of uninterrupted permeation prior to implementing any fouling remediation strategies. This would allow comparison of the baseline flux profile with subsequent flux profiles after regeneration strategies were implemented.

The backflush vessels consisted of a stainless steel conical base, a glass tower and a pressure relief valve connected using sanitary fittings. A compressed air line was installed at the top of the backflush vessel. In the case of solvent and permeate backflushing, the fluids were carefully poured into the backflush vessels, and the vessels were pressurized with compressed air to move the fluid back through the filtration media. In the event of air backflushing, the vessels were simply pressurized with compressed air. A schematic of the backflushing procedure is demonstrated in Figure 4.2.

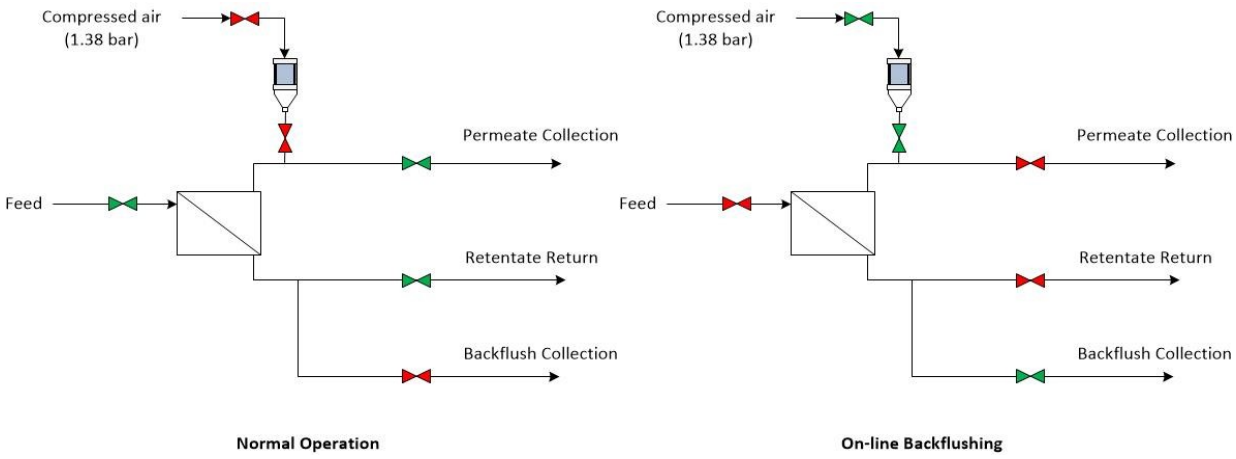

Figure 4.2: Simplified schematic of microfiltration cells during normal operation and with backflushing.

*Red = closed, green = open

4.3. Results and Discussion

4.3.1. Properties of Fouling Residue

A summary of the recorded physicochemical properties of select fouling residue samples, along with critical operating conditions, are included in Table 4.2. Figure 4.3 demonstrates an image of an accumulated fouling layer on the surface of a 5 µm nylon filter after FPBO cross-flow microfiltration for qualitative reference.

Table 4.2: Physicochemical properties of select fouling residue samples collected from FPBO microfiltration trials

	Test Method	Fouling Residue A	Fouling Residue B	Fouling Residue C	Fouling Residue D
Bio-oil Internal ID (Table 4.1)		11	8	9	9
Bio-oil Properties (if available)					
Solids Content, wt%	ASTM D7579	0.37-0.48	0.5-0.64	0.41	0.41
Ash Content, wt%	ASTM D482			0.154	0.154
Water Content, wt%	ASTM E203		13.0-16.0	25.2	25.2
Processing Conditions / Fouling Residue Properties (if available)					
Microfiltration TMP, bar		0.14-1.02	0.34-0.68	0.34-0.68	0.34-0.68
Filtration Media Pore Size, µm		5	5-40	1	40
Carbon, wt%	ASTM D5291	60.3	59.6		
Hydrogen, wt%	ASTM D5291	8.86	8.64		
Nitrogen, wt%	ASTM D5291	0.15	0.23		
Oxygen, wt%	by difference	30.69	31.53		
Ash Content, wt%	ASTM D3174 modified	2.44	1.94	3.25	2.88
Solids Content, wt%	ASTM D7579	26.24	20.87	27.1	27.1
Water Content, wt%	ASTM E203 modified			17.4	18.7
Density, kg/m^3	in-house	1158.4		1208.5	
Ash composition by XRF (ASTM D4326). Units = g / 100 g of ash					
Silicon	ASTM D4326	19.15	18.02		
Aluminum	ASTM D4326	3.79	3.19		
Iron	ASTM D4326	6.65	6.47		
Titanium	ASTM D4326	0.17	0.17		
Phosphorus	ASTM D4326	0.65	0.62		
Calcium	ASTM D4326	9.31	14.33		
Magnesium	ASTM D4326	9.54	9.35		
Sulfur	ASTM D4326	1.02	0.76		
Sodium	ASTM D4326	1.59	0.27		
Potassium	ASTM D4326	2.16	2.49		
Barium	ASTM D4326	0.14	0.15		
Strontium	ASTM D4326	0.05	0.05		
Vanadium	ASTM D4326	0.01	0.01		
Nickel	ASTM D4326	0.14	0.12		
Manganese	ASTM D4326	0.23	0.70		
Chromium	ASTM D4326	0.18	0.16		
Copper	ASTM D4326	1.40	0.18		
Zinc	ASTM D4326	0.10	0.18		
Loss on Fusion	ASTM D4326	0.46	0.67		
Balance[a]	by difference	43.25	42.13		

[a]Balance includes normalized mass contribution of oxygen, since raw XRF data is presented with most elements in oxygenized form

The solids content within the fouling residues produced under the specified operating conditions ranged from 20-28 wt%. Based on the reported density, water and ultimate analysis, it is believed that the non-solid fraction of the fouling residue is mainly composed of bio-oil, likely contained within the pores of the accumulated char particulate. To demonstrate this, the measured water content of fouling residues C and D can be closely approximated using linear blending calculations between the solids content and water content of the bio-oil that was used to generate them. The same can be said with the carbon content of

the residue, assuming that the carbon content of bio-oil is 45-50 wt% (as-received) and the carbon content of the suspended char particulate is 100 wt%. These results would suggest that higher molecular weight components from bio-oil, such as pyrolytic lignin, do not significantly accumulate in the fouling residue. However, more data would be required to substantiate this claim, as well as the possibility exists that smaller pore size filtration media or prolonged processing times could conceivably concentrate heavier fractions in the fouling residue.

The ash content of the fouling residue was concentrated by a factor of 10-20 relative to the ash contained within the bulk pyrolysis liquids that were to be filtered. However, performing a mass balance with the solids and ash content data presented above demonstrates that this corresponds to an ash removal of 20-30% in the permeate relative to the feed. In reality, ash concentration factors on the order of 50-60 (from feed to fouling residue) would be required to achieve ash rejection greater than 90%. This is also not consistent with previous observations indicating a correlation between the solids content and the ash content in FPBO [52,68,89]. This might imply that the bio-oils used in this work had a larger amount of dissolved ash relative to the amount of ash contained within suspended solids as those reported in literature.

Ash composition analysis of certain fouling residues confirms that silicon is the prevalent element contained in the ash. Significant concentrations of calcium and magnesium (9-15 wt% of ash) confirm that these metals likely exhibit a distribution of solid, (filterable) molecules along with an aqueous or oil soluble (non-filterable in the microfiltration range) set of molecules. Elevated iron concentrations within the fouling cake residue could be a result from corrosion and/or erosion of metallic components used in the system during cross-flow microfiltration trials. A significant example was the helical gear pump which experienced material loss over the course of the many experiments.

A qualitative comparison of various laboratory solvents identified that acetone, methanol and ethanol were the most effective at dissolving the non-solid components of the fouling residue, while isopropanol, 1-butanol and diethylene glycol monomethyl ether (DEGMME) were less suitable solvents under the same evaluation criteria. The performance of acetic acid was found to be somewhere in between ethanol and isopropanol.

4.3.2. Off-line Removal of Fouling Layer

It has previously been assumed that absolute value of pore plugging resistance was negligible for FPBO cross-flow microfiltration at extended operating times relative to cake fouling resistance. However, it was

important to determine whether or not there was significant irreversible fouling or pore plugging that was occurring, or if the fouling accumulation on the active filtration surface was reversible. To determine this, two sets of trials were conducted such that each experiment was interrupted after a certain amount of processing time so that the fouling layer could be manually removed prior to resuming microfiltration. If there were forms of irreversible resistance, such as pore plugging, the flux profiles would have been expected to show decreasing performance of flux profiles during both the transient and pseudo steady-state regimes.

In each experimental study, two separate fouling removal methods were investigated. The first fouling layer removal method, at approximately the 120 minute mark of the trials, involved physically removing the fouling layer from the active filtration surface using a scoopula. The second removal method, at approximately the 240 minute mark of the experimental trials, involved the same physical removal method as above, with the addition of soaking the filtration media in methanol for 12-18 hours prior to re-commencement of the trial. An image of the membrane over the course of these trials is shown in Figure 4.3. The added benefit of prolonged soaking of the filtration media would theoretically aid in removing any organic material contained on the surface or within the matrix of the filtration media, which would was not readily removed by the physical removal method described above.

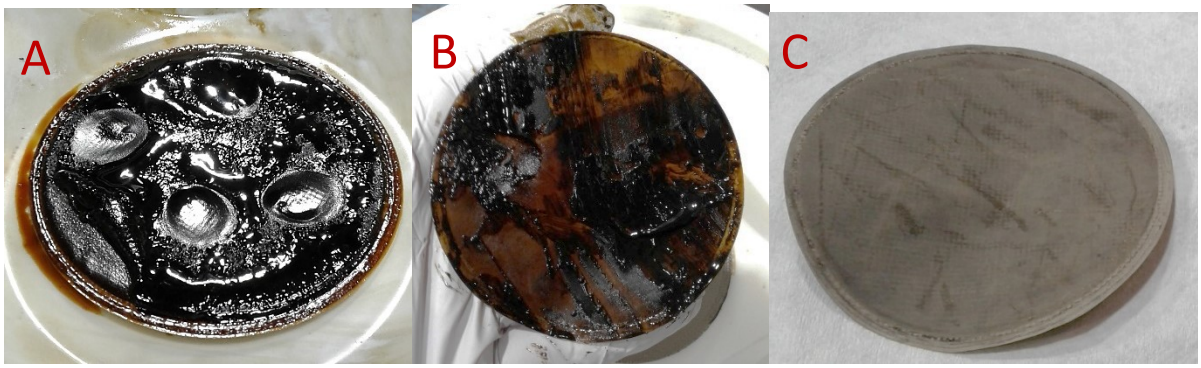

Figure 4.3: Image of 5 µm nylon membrane during off-line fouling removal trials in Section 4.3.2.

*Shown is membrane after 120 minutes of processing (A), membrane with fouling layer physically removed (B) and fouling layer physically removed + membrane soaked in methanol for 18 hours (C)

Figure 4.4 demonstrates the flux as a function of processing time from the two sets of experimental trials with off-line fouling layer removal. Each trial contained in this set also included two parallel microfiltration cells operating under the same conditions, such that each flux profile is the average of both parallel

microfiltration cells. Thus, error bars presented in the plots below represent range of values for each data point. The range of operating conditions for the experimental trials are included in Table 4.3.

Table 4.3: Range of operating conditions in FPBO cross-flow microfiltration trials with off-line cleaning

	Trial 1	Trial 2
Bio-oil Internal ID (Table 4.1)	10	10
Solids Content, kg m^{-3}	4.0-4.6	4.7-5.1
Filtration media	5 µm nylon + 40 µm SS support	5 µm nylon + 40 µm SS support
TMP, bar	0.68 - 0.82	0.62
Fluid temperature, °C	50	40
Fluid kinematic viscosity at operating temperature, mm^2 s^{-1}	25.0	16.0
Observed solids rejection range, %	91-97	93-95
Fluid injection velocity, m s^{-1}	0.4-0.5	0.4 – 0.9

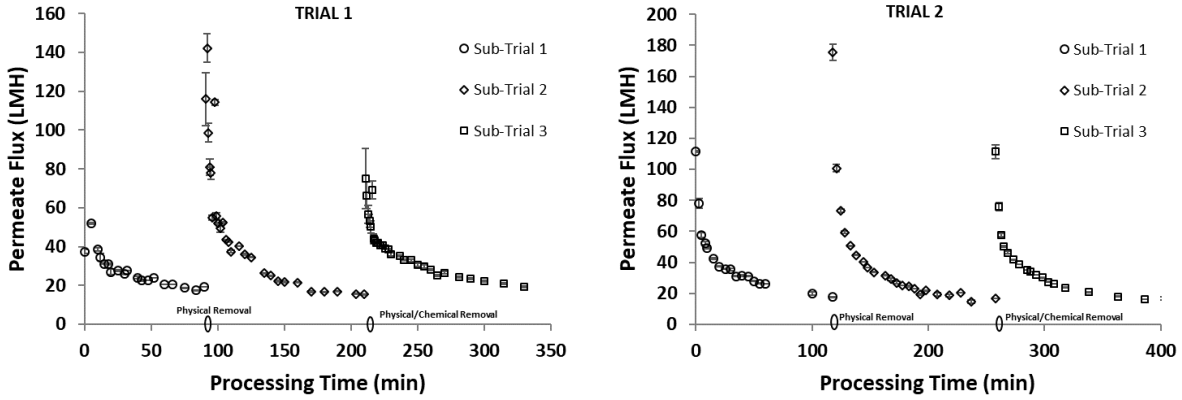

Figure 4.4: Permeate flux as a function of processing time for two separate FPBO cross-flow microfiltration trials with interrupted physical and/or chemical removal of the accumulated fouling layer

The major result obtained from this preliminary investigative study is that removal of the fouling layer (both physically and chemically) lead to seemingly complete regeneration of the flux profile after re-commencement of microfiltration. The specific cake resistance factor was calculated for each sub-trial according to previous methods outlined in Section 3.3.1. A summary of the calculated specific cake resistance factors during the time operating ranges of 0-120 minutes (new filter), 120-240 minutes (physical fouling layer removal) and 240+ minutes (physical + chemical fouling layer removal) are shown in Figure 4.5.

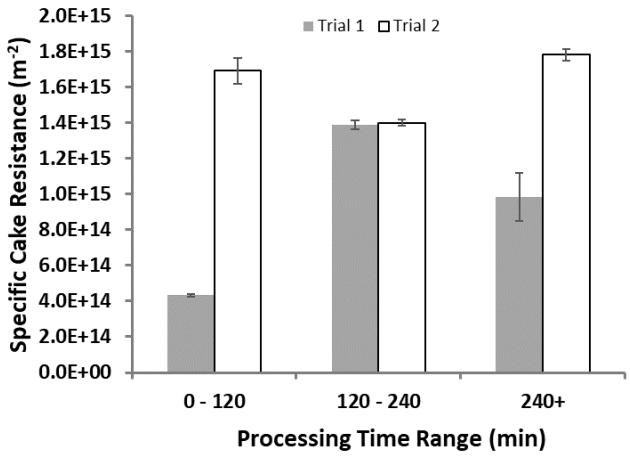

Figure 4.5: Specific cake resistance at different operating points of manual fouling layer removal experimental trials

In reviewing the calculated specific cake resistance as a function of the process time range, it could not be concluded that there were changes to fouling patterns after physical and/or chemical removal of the fouling layer over the course of the experiment. Had irreversible fouling occurred, it would be expected that the specific cake resistance would decrease in response. This result is significant as it introduces the potential of having the capacity to periodically removing the fouling layer that accumulates as a function of processing time to increase the overall throughput of FPBO cross-flow microfiltration.

4.3.3. Fouling Removal Using On-Line Backflushing Techniques

One of the most common practices to achieve on-line cleaning of the filter is through backflushing, such that a fluid is forced from the permeate side of the microfiltration cell through to the feed/retentate side of the cell. By doing so, the goal is to remove any fouling deposits located at the active filtration surface using the backflushing fluid. The backflushing fluids that were investigated included a fraction of the recovered bio-oil permeate, various solvents (ethanol, methanol and DEGMME) and air. Each backflushing fluid was investigated in separate experimental trials in an attempt to compare the relative impact on flux regeneration and operability of the cross-flow microfiltration system.

4.3.3.1. Permeate Backflushing

Since permeate backflushing requires partial consumption of the product to perform fouling remediation, there is a limit on the amount of volume that can be utilized for backflushing. If excessive volumes of permeate are used during permeate backflushing the overall throughput of the cell is greatly decreased. As an example, Chapter 3 demonstrated permeation rates often on the order of 100 L m^{-2} h^{-1} during the

transient region and 20-50 L m^{-2} h^{-1} in the pseudo steady-state region. Thus, using similar permeate backflush fluxes would not be realistic for sustained operation.

For this reason, during an initial study on permeate backflushing, the amount of permeate that was backflushed varied between 25-250 mL, which represents a backflush volume of 3.93-39.3 L permeate per m^2 surface area. The range of operating conditions during the investigation of permeate backflushing are summarized in Table 4.4. The results from this work are summarized in Figure 4.6.

Table 4.4: Range of operating conditions in FPBO cross-flow microfiltration trials with on-line permeate backflushing

Bio-oil Internal ID (Table 4.1)	11
Solids Content, kg m^{-3}	4.3
Filtration media	5 µm nylon + 40 µm SS support **or** 40 µm SS
TMP, bar	0.68 - 0.75
Fluid temperature, °C	50
Fluid kinematic viscosity at operating temperature, mm^2 s^{-1}	28.5
Observed solids rejection range, %	86 (5 µm nylon), 75 (40 µm SS)
Fluid injection velocity, m s^{-1}	0.37
Cleaning sequence	39.3 L m^{-2} air only (1.4 bar) at 50 minutes
	3.9 L m^{-2} permeate (1.4 bar) at room temperature at 105 minutes
	8 L m^{-2} permeate (1.4 bar) at room temperature at 145 minutes
	31.4 L m^{-2} permeate (1.4 bar) at room temperature at 200 minutes for cell 2
	8 L m^{-2} permeate (1.4 bar) at 60 °C at 250 minutes for cell 1
	8 L m^{-2} permeate (1.4 bar) at 60 °C at 265 minutes for cell 2

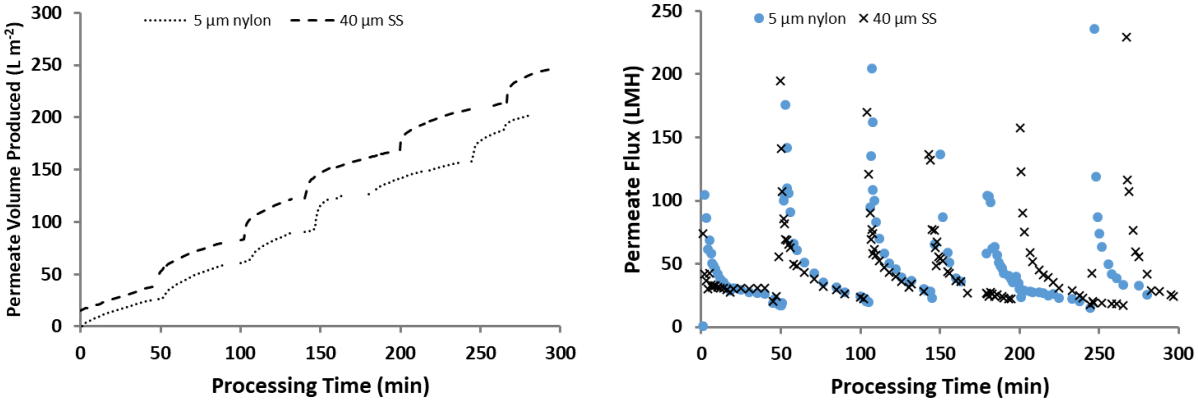

Figure 4.6: Cumulative volume production (left) and permeate flux (right) profiles as a function of FPBO cross-flow microfiltration processing time with periodic permeate backflushing

A preliminary observation upon inspecting the flux and volume profiles is that the fouling was again found to be reversible upon employing on-line permeate backflushing regeneration techniques. It was also found that the general flux decline profiles were repeatable over the course of the experimental trial. However, one of the major differences was the initial flux after each backflushing trial. The y-axis of the plot of the permeate flux as a function of processing time was limited to 250 L m^{-2} h^{-1}, although there are a few data points above that limit (up to a maximum of 1400 L m^{-2} h^{-1}) which represent the initial flux after backflushing. The initial flux profiles that the use of 60 °C permeate (250 and 265 minutes) resulted in the highest initial flux in both the 5 µm nylon and 40 µm SS, while the low volumes (3.93 L m^{-2}) of ambient temperature permeate resulted in the lowest initial flux.

Using ambient temperature permeate for backflushing at 20 psig resulted in rupture of the nylon membrane (at the 160 minute mark) which required replacement of the membrane prior to resuming the trial. This is an important consideration for permeate backflushing as the viscous nature of the liquid, along with moderate backflushing pressures, may be too severe for thin polymeric membrane materials. The use of rigid membrane materials, or the use of additional membrane support layers are recommended for this type of operation.

4.3.3.2. Solvent Backflushing

Although solvent backflushing in FPBO cross-flow microfiltration requires the use of additional material streams into the process, it may be viable to use a low-cost solvent rather than utilize a fraction of the permeate product for fouling remediation if low-cost solvent blending is a quality improvement strategy that is already being considered for FPBO. The use of methanol, ethanol and DEGMME were explored during solvent backflushing. As discussed in Section 4.3.1, methanol and ethanol were found to be some of the most effective solvents for dissolving the organic material contained within the fouling residue, while DEGMME was found to be one of the most ineffective solvents. The results from this study are located in Figure 4.7, while the range of operating conditions for the investigation of solvent backflushing are also presented in Table 4.5.

Table 4.5: Range of operating conditions in FPBO cross-flow microfiltration trial with on-line solvent backflushing

Bio-oil Internal ID (Table 4.1)	11
Solids Content, kg m^{-3}	5.1
Filtration media	5 µm nylon + 40 µm SS support **or** 40 µm SS
TMP, bar	0.68
Fluid temperature, °C	50

Fluid kinematic viscosity at operating temperature, $mm^2\ s^{-1}$	28.0
Observed solids rejection range, %	93 (5 µm nylon), 60 (40 µm SS)
Fluid injection velocity, $m\ s^{-1}$	0.38
Cleaning sequence	40 L m^{-2} air only (1.4 bar) at 35 minutes
	8 L m^{-2} ethanol (1.4 bar) at room temperature at 70 and 100 minutes
	8 L m^{-2} methanol (1.4 bar) at room temperature at 125 and 150 minutes
	8 L m^{-2} DEGMME (1.4 bar) at room temperature at 190 and 215 minutes

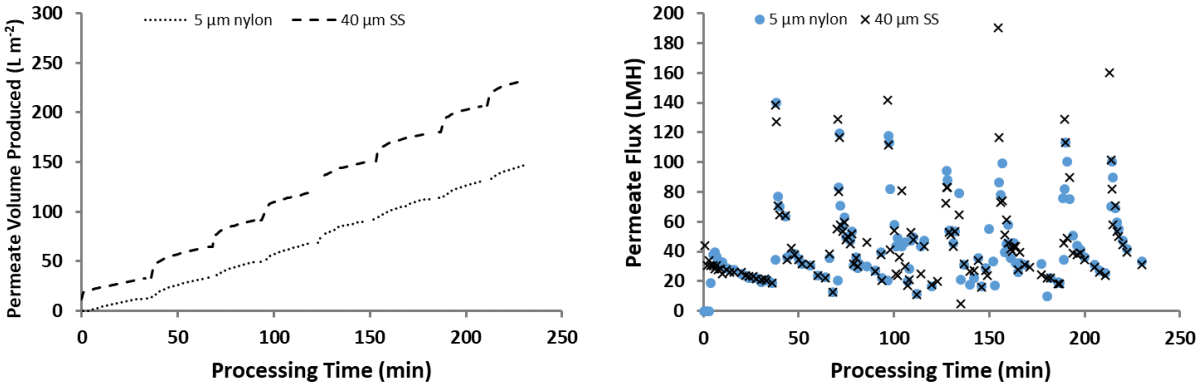

Figure 4.7: Cumulative volume production (left) and permeate flux (right) as a function of FPBO cross-flow microfiltration processing time with periodic solvent backflushing

Similar regenerability of the flux was found with solvent backflushing relative to permeate backflushing for both the 5 µm nylon and 40 µm SS microfiltration cells. Furthermore, the use of ethanol, methanol and DEGMME all have similar impacts on the flux profiles, which indicates that there is no direct evidence within this dataset which indicates that one solvent was more advantageous than the other. This result might suggest that the main mechanism for fouling layer removal by solvent backflushing in the studied processing times is the physical displacement of the accumulated cake layer from moderate pressure injection of solvent back through the filtration media, rather than any chemical dissolution of organic materials at the surface or within the filtration media. However, this may not be the case during prolonged operating times if the fouling were to become more severe, such as the use of prolonged soaking or longer solvent contact times may be required.

In the case of the 40 µm SS filter for this trial, poor solids rejection was observed relative to the 5 µm nylon membrane; however, larger volume throughputs were also observed. This result is likely a function

of the intermittent removal of the fouling layer during backflushing, which temporarily caused poor solids rejection in the case of the 40 µm SS filter, prior to the reformation of the fouling layer which continued to act as a primary filtration layer.

4.3.3.3. Air Backflushing

The use of compressed air as the backflushing fluid was further investigated as it does not require the use of product (permeate) nor supplied solvents. The use of compressed air would rely solely on physical removal of the fouling layer when used as the backflushing fluid, whereas the possibility exists for chemical interaction between the fouling layer and solvent, and to a lesser extent, the permeate. In the preliminary experimental trial using air as the backflushing fluid, with results located in Figure 4.8, the range of operating conditions were as presented in Table 4.6.

Table 4.6: Range of operating conditions in FPBO cross-flow microfiltration trial with on-line air backflushing

Bio-oil Internal ID (Table 4.1)	11
Solids Content, kg m^{-3}	4.8
Filtration media	5 µm nylon + 40 µm SS support **or** 40 µm SS
TMP, bar	0.61 - 0.68
Fluid temperature, °C	50
Fluid kinematic viscosity at operating temperature, mm^2 s^{-1}	25.5
Observed solids rejection range, %	93 (5 µm nylon), 75 (40 µm SS)
Fluid injection velocity, m s^{-1}	0.33
Cleaning sequence	40 L m^{-2} air (20 psig) at 50, 105, 140, 174 and 212 minutes

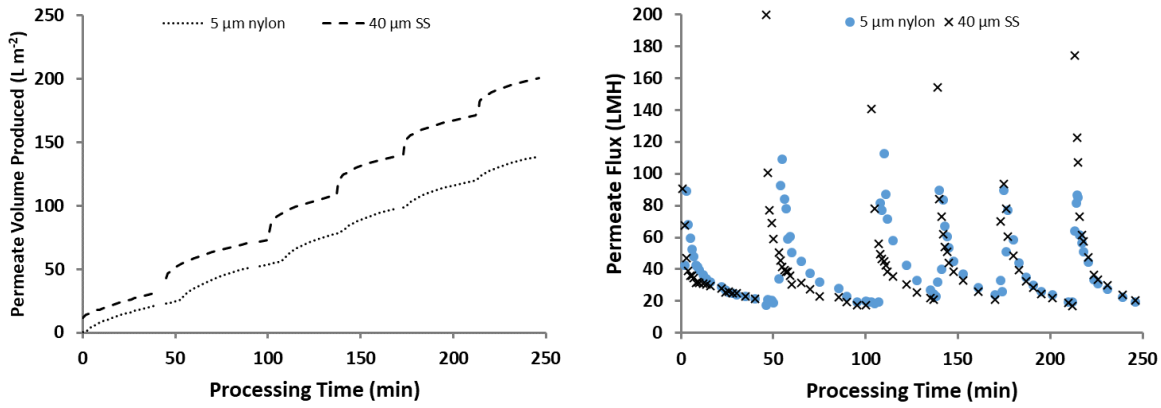

Figure 4.8: Cumulative volume production (left) and permeate flux (right) as a function of FPBO cross-flow microfiltration processing time with periodic air backflushing

Similar to the flux profiles obtained through permeate and solvent backflushing, air backflushing demonstrated good repeatability over the course of the experimental trial. As previously observed, superior initial fluxes were measured with the 40 µm SS filter relative to the 5 µm membrane, at the cost of inferior solids rejection. The permeate solids content was on average 0.03 wt% using the 5 µm nylon membrane with backflushing, while it was around 0.13 wt% using the 40 µm SS filter with backflushing.

4.3.4. Extended Air Backflushing

The results obtained Section 4.3.3 demonstrate promise in increasing the overall throughput of a fast pyrolysis bio-oil cross-flow microfiltration system with the use of intermittent backflushing to actively remove and/or control the accumulated cake fouling layer. However, the processing times and number of backflushes that were explored were quite low, and offer limited insight on the prolonged impact of backflushing on the throughput of such a process. For this reason, exploring extended and frequent air backflushing was performed.

For this work, each backflush sequence lasted approximately one minute. The processing time allowed between backflushes ranged from 10-27 minutes, with the majority ranging from 12-17 minutes. This would represent an approximate regeneration downtime of 6-8% of the total operating time. Similar operating downtimes for fluid backflushing were determined to be optimal in the microfiltration/ ultrafiltration of oily wastewaters [95] and as such as used as reference in this study. A total of 31 backflushing segments were performed. Due to the length of the trial, fresh bio-oil was added, while a purge was removed, on an hourly basis such that the bulk solids content was attempted to maintain constant. The results from this extended trial are presented in Figure 4.9. The range of operating conditions are also presented in Table 4.7.

Table 4.7: Range of operating conditions in extended FPBO cross-flow microfiltration trial with on-line air backflushing

Bio-oil Internal ID (Table 4.1)	7
Solids Content, kg m^{-3}	4.2 – 6.0
Filtration media	1 µm SS
TMP, bar	0.48 - 0.62
Fluid temperature, °C	50
Fluid kinematic viscosity at operating temperature, mm^2 s^{-1}	16.9
Observed solids rejection range, %	92-98 (cell 1), 73-86 (cell 2)
Fluid injection velocity, m s^{-1}	0.32
Cleaning sequence	39.3 L m^{-2} air (20 psig) at ambient temperature at 70, 88, 104, 115, 130, 156, 175, 195, 210, 225, 242, 256, 280, 302, 323, 340,

	366, 385, 401, 416, 430, 445, 470, 483, 496, 513, 530, 548, 563, 577, 598 and 623 minutes.

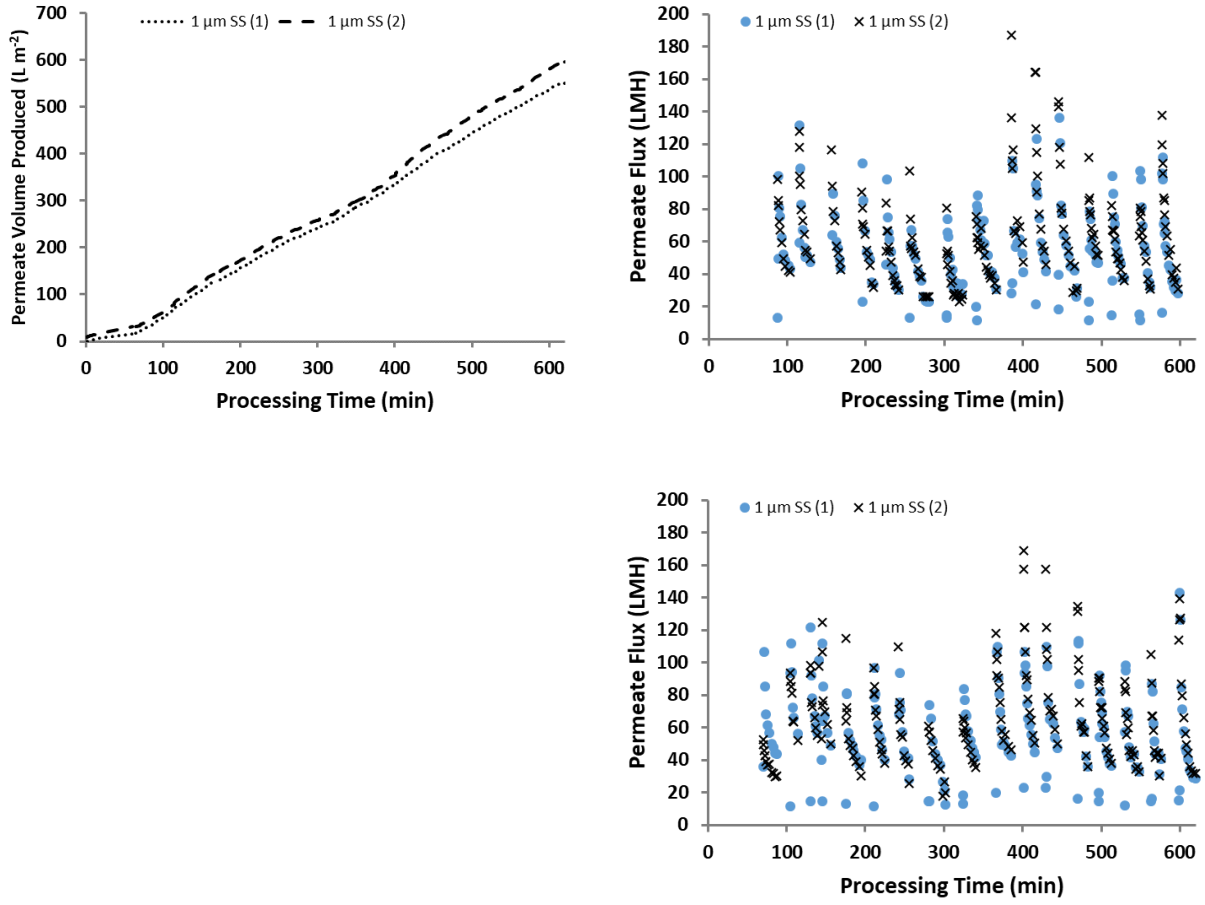

Figure 4.9: Cumulative volume production (left) and permeate flux (right) as a function of processing time with extended air backflushing. Permeate flux plots are split into even-number backflushes (top-right) and odd-number backflushes (bottom-right) for clarity.

The flux profiles continued to demonstrate repeatability over the course of the extended trial, and are comparable at the last backflush sequence relative to the first backflush sequence, which further supports that the dominant fouling mechanism that was occurring remained reversible over this operating range.

By analyzing the cumulative volume production in Figure 4.9, it can be determined that the average flux roughly doubled from 26-32 L m^{-2} h^{-1} to 55-56 L m^{-2} h^{-1} when comparing the baseline operating region to the frequent backflushing operating region. Thus, even though there was a sacrifice of approximately 6% of the operating time to perform air backflushing there still was an increase of overall cumulative volume production of approximately 100% from FPBO cross-flow microfiltration.

The average specific cake resistance and initial flux of both microfiltration cells as a function of consecutive backflush number is also presented in Figure 4.10. Since these data points are an average of two values, the range is provided as error bars. There is no apparent trend observed between the two parameters from this extended backflushing trial. Given this result, along with the observed regenerability in the flux profiles, it can be stated that the fouling continued to exhibit reversible properties over the specified operating parameters and processing time range.

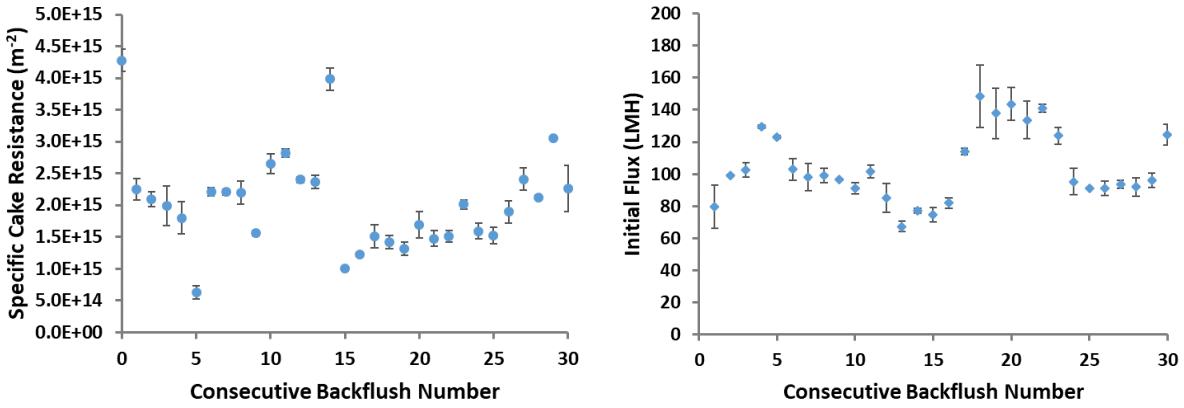

Figure 4.10: Average specific cake resistance, $\hat{R}_C$ (left) and initial permeate flux (right) as a function of consecutive backflush number, for extended air backflushing trial

This result is promising for FPBO microfiltration since the use of more severe filtration media cleaning procedures, such as chemical cleaning and soaking [90] has not yet demonstrated requirement based on the repeated physical fouling removal strategy employed over 31 regeneration cycles and ten hours of processing time.

4.4. Conclusions

The use of off-line cleaning by physical and chemical means determined that fouling was reversible as the permeate flux profile was fully regenerated. Preliminary investigations into on-line cleaning via the use of permeate, solvent and air backflushing also determined the reversibility of the fouling resistance through similar evaluation criteria, while all three fluids had similar regeneration performances.

With continuous operating times exceeding ten hours and 31 backflushing cycles, fouling resistance remained reversible with the use of moderate pressure compressed air as the backflushing fluid and the use of a chemical cleaning agent was not required. By applying intermittent air backflushing with a non-optimized downtime of 6-8%, the overall throughput of FPBO cross-flow microfiltration was improved by over 100% relative to operating at the pseudo steady-state throughput.

In order to continue to improve the performance of FPBO cross-flow microfiltration, the first recommendation includes the co-optimization of operating conditions and regeneration parameters such that the overall throughput of the microfiltration process is maximized. Secondly, the investigation of prolonged operating periods for FPBO microfiltration should continue to be explored such that the time requirement for more severe fouling remediation strategies, such as chemical cleaning, can be specified so that the true operating cost of such a process can be more accurately determined. Finally, the use of advanced fouling remediation strategies that are currently employed in common membrane separation processes, such as wastewater treatment, should be investigated for applicability to microfiltration of fast pyrolysis bio-oils. This may include the use of liquid additives, turbulence promoters and external fields (vibrational, electrical and mechanical).

More in-depth characterization of fouling residues and purge streams from cross-flow microfiltration of fast pyrolysis bio-oils is also recommended. A better understanding of these potential by-product streams will allow the selection of potential uses. Some examples include use as a low quality heating fuel and as a binder for densification for use as an advanced solid biofuel or bioproduct, to name a few.

Acknowledgements

Funding was provided by Natural Resources Canada's Office of Energy Research & Development through the Program for Energy Research and Development (Project titles: "Pyrolysis Liquids for Immediate Heat and Power Applications" [2015-2019] and "Development and Optimization of Multi-Product Bio-refinery Processes" [2019]). The authors would like to acknowledge Frank Leclair and Berney Chan and the entire staff at the characterization laboratory at CanmetENERGY-Ottawa for their assistance in completing this work.

Chapter 5. Improving Ash Removal in Bio-oil with Microfiltration

As reported in Section 3.3.3, ash removal via microfiltration of fast pyrolysis bio-oils produced from lower quality forestry residues in the 1-40 µm range was quite poor at 4-45%. Analysis of select fouling residues in Section 4.3.1 also demonstrated relatively low ash concentration factors in the accumulated fouling layer. This result is likely an effect of the use of higher ash forestry residues as the original material to produce the FPBOs, as the nature of the mineral species contained within the pyrolysis oils were a distribution of solid and dissolved species such that microfiltration was not an effective removal strategy.

Due to the low ash rejections observed by microfiltration, this chapter is intended to disseminate results from preliminary experiments in which detailed ash analysis was performed on the pyrolysis liquids before/after filtration, in an attempt to better understand the cause for poor ash rejection. Furthermore, the use of additives for mineral removal are explored in combination with conventional microfiltration strategies.

5.1. Ash Species Removal via Microfiltration

During selected experimental microfiltration trials outlined in Section 3.3.3, sub-samples of the feed and permeate were collected and analyzed for ash composition. This would allow direct comparison of measurable elements before/after filtration to aid in interpreting the observed poor ash rejection.

Ash composition in the pyrolysis liquids was measured by inductively-coupled plasma optical emission spectrometry (ICP-OES) byFPInnovations, Pointe-Claire laboratory. In preparation for the test, approximately 1 gram of sample was digested in hydrogen peroxide and nitric acid using a microwave digestion unit. The mixture was then diluted to a final volume of 100 mL and analyzed by ICP-OES using standard reference ASTM D7876. Many of the specific ash elements contained in pyrolysis oils were measured as below the reportable detection limit (BRDL). A series of plots are shown in Figure 5.1 which detail the present mineral species (in quantities greater than 10 mg kg^{-1} bio-oil) in the feed and permeate samples for individual microfiltration trials. Plots A-D are from samples obtained from the cross-flow microfiltration system detailed in Section 3.2 while plot E was generated from the dead-end microfiltration system, detailed below in Section 5.2.1.

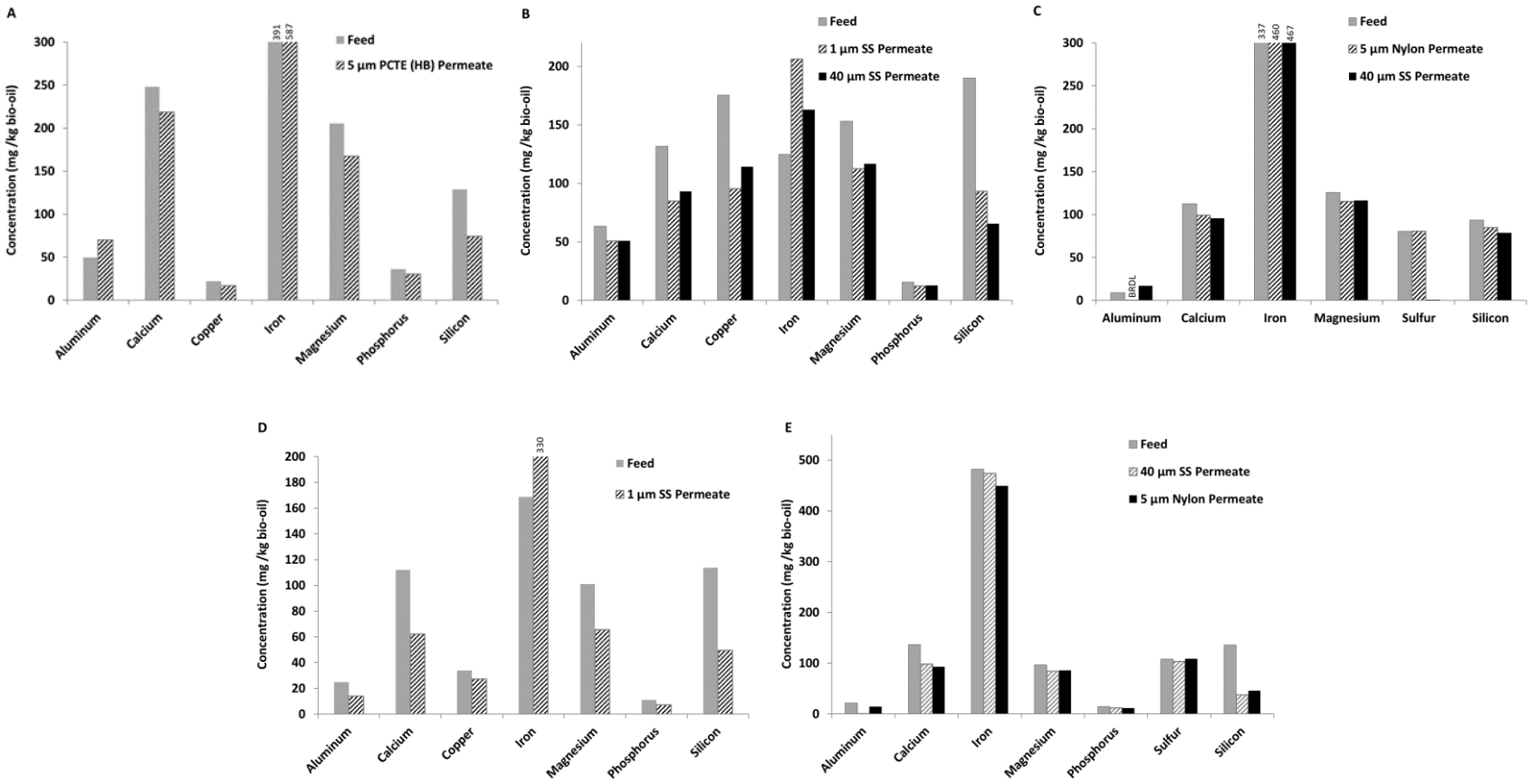

Figure 5.1: Ash composition (by ICP-OES) comparison for feed and permeate samples from cross-flow microfiltration (A-D) and dead-end microfiltration (E) trials for components > 10 mg kg^{-1} in original bio-oil

The analyses showed increased levels of iron after microfiltration in many of the cases. It is suspected that some of this could be explained by gradual material loss from erosion and/or corrosion of metallic components (e.g. from the helical gear pump employed to circulate the bio-oil). This unintended consequence should carefully be considered when interpreting the results from Figure 5.1 and highlights the importance of proper equipment selection for bio-oil handling, even for experimental testing.

The element contained in bio-oil with the highest rejection was consistently silicon. Given that it was discovered in Chapter 4 that the most concentrated element in the fouling residue ash was silicon, this result is not surprising. Typical silicon rejection was on the order of 30-60%. Silicon rejection slightly increased as the pore size of the filtration media decreased. Good rejection of silicon is expected since this element can be introduced into pyrolysis oil either through soil contamination which is common for low quality forestry residues containing surface tissues like bark). Additionally, silicon derivatives are commonly used as a bed material for fluidized beds, such as was the case with CE-O's fluidized bed fast pyrolysis unit. As a small fraction of the bed material is mechanically elutriated during operation, the bed material can also introduce silicon into the bio-oil as a solid [52]. It is possible that some of the silicon contained in the bio-oil falls below the nominal pore diameter of 1-40 µm, such that it was not rejected by the filtration media in these tests. There may also be a fraction of the detectable silicon that is soluble in the aqueous phases of bio-oil such that microfiltration is not a suitable removal strategy.

Similar to silicon rejection, magnesium rejection appeared to increase with decreasing filtration media pore size. However, magnesium rejection varied from 10-30%, which was significantly lower than silicon. Calcium rejection varied from 10-40 wt%, although it was interesting to note that the two stainless steel filters (40 µm and 1 µm) typically had better calcium rejection than the two 5 µm polymeric membranes. Potassium and sodium were not included in the analyses since they were quantified as below their reportable detection limits of 100 mg kg^{-1}. Since the transfer of these alkali metals from biomass to bio-oil through fast pyrolysis is typically less than 5% [52], this result is not surprising. Despite the 1 µm SS filter providing the best ash rejection performance, this was still found to be quite low at less than 50%. To enhance the ash removal capacity of FPBO microfiltration, it was decided to investigate the combined use of solid-phase additives which could subsequently be removed by microfiltration.

5.2. Use of Additives with Microfiltration for Ash Removal

The use of solid-phase additives, such as ion exchange resins, for the removal of contaminants is widely practiced in wastewater treatment, water purification, hydrometallurgy, food and beverage, pharmaceuticals, electronics etc. [60]. There have been a few instances in literature in which the use of solid-phase adsorbents were added to raw bio-oil in an attempt to perform targeted removal of metals. It was previously found that in some cases, the use of 2 wt% thermally-activated and/or chemically-activated silica, followed by microfiltration in the 5-60 µm range was able to reduce the concentration of sodium, potassium, calcium and iron below 1 mg kg^{-1} in bio-oils [103]. However, one of the major findings of this project was that the interaction between the suspended char particles and the additive resulted in poor ash removal performance and variations in detection amounts for the metals contained in the bio-oil by ICP-OES. More recent work was performed which investigated the use of Amberlyst 15 as an additive for the removal of bio-oil blended with isopropanol [104]. Loading ratios as low as 3 wt% were able to remove all detectable amounts of AAEMs, while loading ratios less than 5 wt% was also able to remove all iron. It was found that the removal of cationic metals could be modelled using a pseudo-first order process, with sodium having the fastest removal rate, and iron the slowest.

Patents exist for which the use of ion exchange resins, including Amberlyst 15, for the removal of metallic elements in bio-oil [91,92]. It has been claimed that the use of ion exchange resins are successful in reducing the total metal content in bio-oil to 100 mg kg^{-1} or less. The patents also describe the potential use of temperature, pressure, contact residence time and cleaning conditions to improve the performance of such a system.

The combined use of ion exchange resins and membrane separation processes have lead to the production, development and application of ion-exchange membranes in industries such as wastewater treatment [60]. Combining the use of microfiltration and solid-phase adsorption represents an interesting approach for the removal of char particles and metallic species in fast pyrolysis bio-oils. Experimental trials were performed to study the use of solid-phase additives on the removal performance of metallic species and the resulting impact on the recovery and throughput of a dead-end microfiltration process.

5.2.1. Dead-end Microfiltration System

For this work, a dead-end microfiltration system was used as opposed to a cross-flow microfiltration system. This system was inherently simpler than the cross-flow unit due to no requirements for fluid flow or flow measurement. The dead-end filtration unit comprised of a 2L cylindrical vessel mounted on top of

a single pass shell-and-tube heat exchanger in a vertical configuration, followed by a butterfly valve and a conical drain with an insert for a flat disk filter or membrane. The components of this system were attached by sanitary fittings which allowed easy dismantling in between trials. All wetted components of the system were fabricated from 316 or 304 stainless steel, with the exception of the sanitary fitting gaskets which were fabricated from Viton or Teflon. Heating of the FPBO was achieved by circulating ethylene glycol through the shell-side of the exchanger with the use of a heated circulating bath. Pressurization of the unit was achieved using compressed air to the top of the vessel, while a pressure regulator controlled the transmembrane pressure. Temperature and pressure monitoring was achieved with strategically-placed thermocouples and bourdon tube pressure gauges along with a Graphtec data logger. A diagram and picture of the dead-end filtration unit is shown in Figure 5.2.

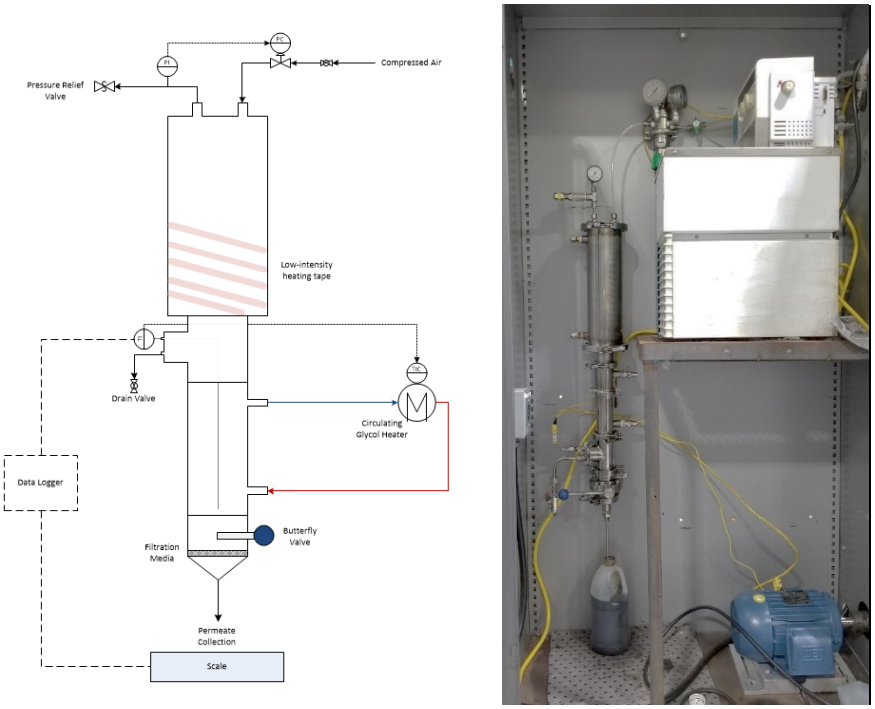

Figure 5.2: Schematic of bio-oil dead-end microfiltration system (left) and image of experimental system (right)

5.2.2. Experimental Procedures

Based on observations and results that were previously found concerning the interaction of suspended char particles and solid-phase additives [103], two bio-oils, including one which had already been filtered, were used in testing for ash removal using additives with microfiltration. The filtered bio-oil was the permeate from a separate cross-flow microfiltration experiment using a 1 µm SS filter, while the other

was a subsample of the original, unfiltered bio-oil used in that test. The bio-oil that was used in this work was a collection of bio-oil samples produced from hardwood flooring sawdust residue using CE-O's fluidized bed fast pyrolysis system, at reactor temperatures ranging from 400-480 °C.

Two different solid-phase additives were tested in this study. The first was Amberlyst 15, which has previously been identified as an effective additive to remove metallic components in FPBOs [92,104], while the second additive was silica gel. Both agents were purchased from Sigma-Aldrich Canada (CAS number 39389-20-3 and 112926-00-8). Prior to use, the silica gel was thermally treated at 360 °C for 3 hours, followed by cooling for a minimum of two hours in a desiccator.

Due to time constraints, only a single loading ratio (5 wt%) and exposure mixing time (22-23 hours) were performed in this work since one of the major objectives was to study the interaction between solid-phase adsorption and dead-end microfiltration. Prior to mixing, approximately 500 mL of bio-oil was added to a round-bottom flask, followed by the addition of the sorbent. The flask was then rotationally mixed in a heated bath at 45 °C for all trials (even without the use of additives for consistency) prior to dead-end microfiltration using a 1 µm SS filter at a fluid temperature of 51 °C ± 1 °C. After agitation, the mixture was added to the dead-end microfiltration system. Once loaded, the system was pressurized to 0.69 barg with the use of compressed air. A summary of the treatment conditions are included in Table 5.1 for reference.

Table 5.1: Summary of treatment conditions used in experimental trials exploring solid-phase adsorbents with microfiltration for ash removal in bio-oil

Treatment ID	Description
Non Filtered-Control **(NF-CON)**	Unfiltered bio-oil mixed at 45 °C for 23 hours
Non Filtered-Amberlyst 15 **(NF-AMB)**	Unfiltered bio-oil mixed with 5 wt% Amberlyst 15 at 45 °C for 22 hours
Non Filtered-Silica **(NF-SIL)**	Unfiltered bio-oil mixed with 5 wt% thermally-activated silica at 45 °C for 23 hours
Pre-Filtered-Control **(PF-CON)**	Pre-filtered (1 µm SS cross-flow microfiltration system at 10 psig, 50 °C) bio-oil at 45 °C for 24 hours
Pre-Filtered-Amberlyst **(PF-AMB)**	Pre-filtered (1 µm SS cross-flow microfiltration system at 10 psig, 50 °C) bio-oil mixed with 5 wt% Amberlyst 15 at 45 °C for 23 hours;
Pre-Filtered-Silica **(PF-SIL)**	Pre-filtered (1 µm SS cross-flow microfiltration system at 10 psig, 50 °C) bio-oil mixed with 5 wt% thermally-activate silica at 45 °C for 23 hours

A collection bottle on top of a balance, which was connected to a data logger, allowed instantaneous measurement of recovered mass (and subsequently flux was approximated by forward finite differentiation) over the course of each trial. Individual trials proceeded until either all of the bio-oil passed through the 1 µm filter or the flux had ceased under constant pressure.

Bio-oil samples were submitted to the characterization laboratory at CanmetENERGY-Ottawa for solids content (ASTM D7579), ash content (ASTM D482), water content (ASTM E203), kinematic viscosity @ filtration temperature (ASTM D445), pH (by titration) and total carbonyls (ASTM E3146). Sub-samples were also submitted to the characterization laboratory at FPInnovations for ash composition by ICP-OES.

5.2.3. Results

A summary of the physicochemical properties of the pyrolysis liquids before/after filtration are included in Table 5.2. Furthermore, the ash composition of the bio-oils, for components present in quantities greater than 10 mg kg^{-1}, are located in Figure 5.3 and Figure 5.4.

Table 5.2: Summary of physicochemical properties of bio-oil during sorbent and/or dead-end microfiltration trials for ash and char removal at CanmetENERGY-Ottawa

ID	units	NF	NF-CON	NF-AMB	NF-SIL	PF	PF-CON	PF-AMB	PF-SIL
Solids Content	wt%	0.69	0.06	0.02	0.03	0.08	0.08	0.05	0.07
Ash Content	wt%	0.122	0.091	0.012	0.096	0.107	0.115	0.013	0.114
Water Content	wt%	20.7	23	24.2	24.1	21.6	21.4	20.7	21.4
Kinematic Viscosity (50 °C)	$mm^2\ s^{-1}$	21.0 ± 1.4	20.0	21.0	21.8	19.4	21.4	22.0	22.8
pH		3.1	2.9	2.6	3.1	3.0	3.1	2.6	3.1
Total Carbonyls	$mol\ kg^{-1}$	4.2	4.5	4.1	4.3	4.4	4.4	3.5	4.1

Excellent solids rejection was observed with the nonfiltered bio-oil, while very small solids rejection was observed with the pre-filtered bio-oil. These results further indicate that the presence of solids, which develop a cake fouling layer on the active filtration surface, act in itself as a primary depth filtration layer to aid in the removal of suspended solid particles [100]. It is interesting to note that there was also a substantial rise in the measured water content of the unfiltered bio-oil after mixing at 45 °C for up to 24 hours, while no observable increase in measured water content was found with the pre-filtered bio-oil. This result corroborates previous findings that the suspended char particles in bio-oil contribute to the instability and condensation reactions occurring during the accelerated ageing process [68,105,106]. Decreases in pH and total carbonyls after treatment with Amberlyst 15 were also experienced.

Analysis of the results above indicate excellent (88-90%) ash removal after using Amberlyst 15 as the sorbent. Evaluating the mineral composition of the liquids after contact with Amberlyst 15 showed virtually complete removal of aluminum, calcium, iron and magnesium on both the unfiltered and pre-filtered bio-oil. Moderate removal of copper was also observed in both cases. Amberlyst 15 was not successful in removing silicon or phosphorus, presumably due to their anionic nature.

It is evident that the thermally-activated silica was not successful in removing ash from the bio-oil, and in fact caused small increases in ash in the pre-filtered bio-oil due to incremental additions of silica to the liquid. It appeared as though the ash removal associated with the silica additive trials were solely based on the microfiltration of the bio-oil. By examining the resulting pH of the bio-oils before/after silica addition, it can also be deduced that it is likely that the goal of producing Si-H bonds was not successful through thermal activation, since the pH of the liquid did not change. Thus, it is recommended that additional treatment pathways, such as chemical activation, are further to be explored with silica gel for superior ash removal.

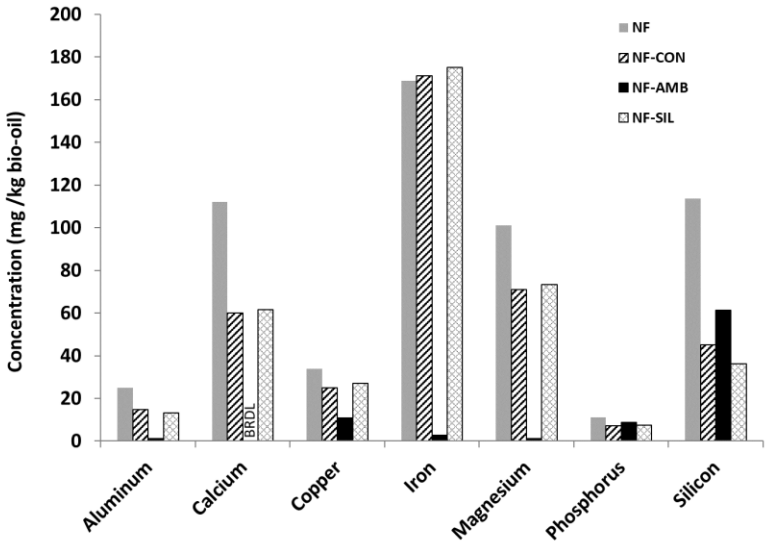

Figure 5.3: Ash composition (by ICP-OES) comparison for dead-end microfiltration trials with unfiltered bio-oil and additives for targeted mineral removal for components > 10 mg kg^{-1} in original bio-oil

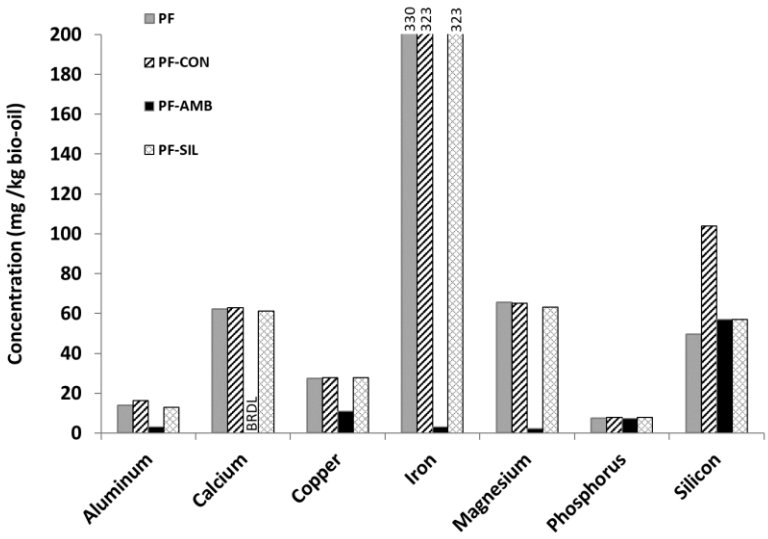

Figure 5.4: Ash composition (by ICP-OES) comparison for dead-end microfiltration trials with 1 µm SS pre-filtered bio-oil and additives for targeted mineral removal for components > 10 mg kg^{-1} in original bio-oil

In addition to the impacts on physicochemical properties of the bio-oil, the resulting impact on dead-end microfiltration throughput was also evaluated. The cumulative volume production from each trial is included in Figure 5.5, as well as the calculated specific cake resistance, as per Eq. (4) previously described in Section 3.3.1.

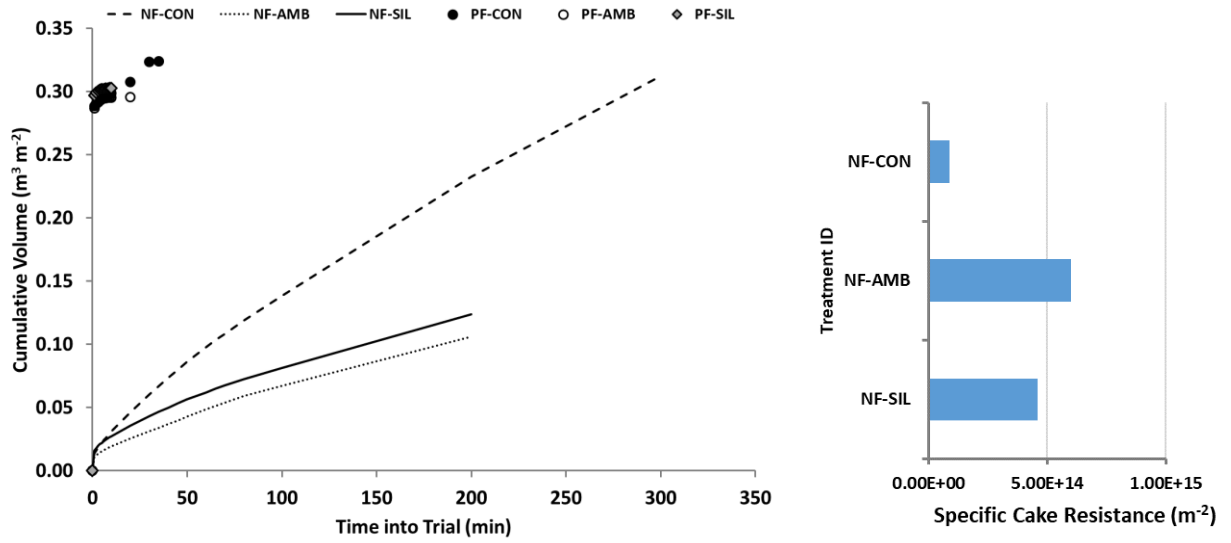

Figure 5.5: Cumulative volume production as a function of processing time for dead-end microfiltration of unfiltered and pre-filtered bio-oil with and without sorbent additives (left) and specific cake resistance of trials with unfiltered bio-oil with and without sorbent additives (right)

In all cases, the use of sorbent additives created a penalty in throughput relative to simple microfiltration. For the case of the pre-filtered FPBO, the use of additives caused the total recovery of bio-oil to decrease from 97% to 91-93%. This result is due to both the physical and chemical entrapment of bio-oil and associated species on the surface and within the pores of the sorbent additives, respectively. Furthermore, the flux decreased slightly relative to the pre-filtered bio-oil at similar processing times, which is due to the presence of the sorbent particles on the active filtration surface which created an additional resistance layer. However, the flux penalty associated with the use of the additives was minor for the pre-filtered bio-oil. The specific cake resistance from the dead-end microfiltration trials using pre-filtered bio-oil could not be reliably calculated. This was because the majority of the fluid had passed through the filter in a very short time period, such that subsequent reductions in flux were caused by lack of additional material to filter rather than the development of a fouling layer.

In the case of the unfiltered bio-oil, the impact of the additives on the flux and throughput was much more severe. It was found that the cumulative volume produced of low-solids/ash bio-oil for the trials with additives was approximately half of that without the use of additives. This result suggests that the sorbent additives interact with the suspended char particles during microfiltration. The specific cake resistance further validated that the use of additives in unfiltered bio-oil causes unproportioned increases in the specific cake resistance from dead-end microfiltration. Furthermore, the specific cake resistance of the unfiltered bio-oil using Amberlyst 15 was higher than that of the silica. This could have been due to the

differences in particle size distribution as the specification sheets of the products indicated that Amberlyst 15 was < 300µm and the silica was 250-500 µm. The compression properties of the sorbents could also have been different which could have changed the cake fouling compressibility at the specific transmembrane pressures. Another possibility is that there was physical/chemical interaction between the sorbent and the liquid components of FPBO, such that either swelling, or additional gel layers could have formed around or within the pores of the sorbent causing an increase in cake resistance properties.

The findings from the work above suggest that if implementing solid-phase sorbent additives for ash removal, it would be necessary to pre-filter the fast pyrolysis bio-oil to realize an increase in throughput relative to pursuing ash removal of the unfiltered bio-oil. To demonstrate this concept, a simulated profile was created in Figure 5.6 in which two scenarios are presented to produce 1 $m^3 m^{-2}$ of low-solids/ash bio-oil; the first includes pre-filtering bio-oil using a 1 µm SS filter followed by contact with sorbent, followed by a secondary filtration to remove the sorbent. The second scenario includes mixing the sorbent with the unfiltered bio-oil, followed by a single microfiltration stage to remove both the suspended char particles and the sorbent.

As the plot demonstrates, it takes approximately half the time to produce 1 $m^3 m^{-2}$ of low-solids/ash permeate by pre-filtering the bio-oil prior to contact with the sorbent relative to mixing the sorbent with the unfiltered bio-oil prior to microfiltration. This result also likely translates to similar applications such as packed-back ion exchange towers, for which the presence of suspended char particulate in the bulk FPBO are theorized to cause low throughputs, accelerate cleaning cycles, elevated pressure operation and/or plugging relative to pre-filtering the bio-oil.

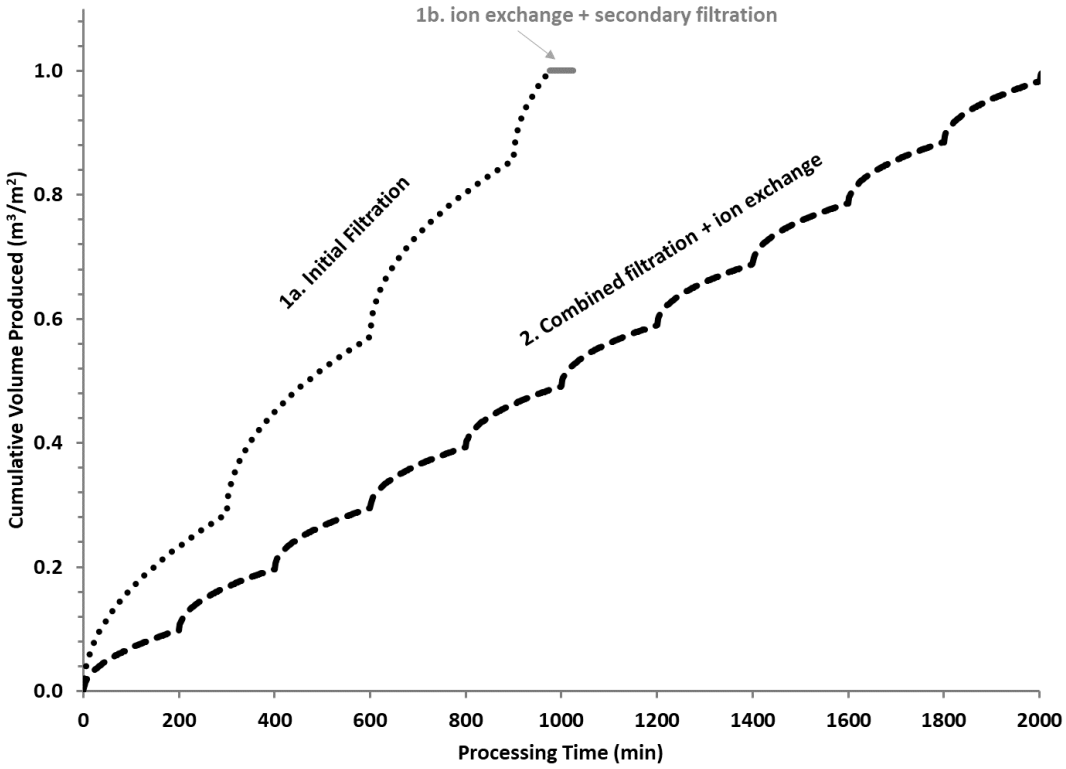

Figure 5.6: Simulated recovery profiles of dead-end microfiltration processes comparing the use of Amberlyst 15 as an additive for targeted metal removal before and after filtration using a 1 µm SS filter

5.3. Conclusions

At a loading ratio of 5 wt%, Amberlyst 15 was successful in removing virtually all cations from unfiltered and pre-filtered (1 µm) FPBO produced from forestry residues. Thermally-activated silica was unsuitable as an additive for ash removal. Although total ash removal was as high as 90% following prolonged contact with Amberlyst 15, considerable levels of silicon remained in the bio-oils. It was also found that adding the sorbents to unfiltered bio-oil caused higher specific cake resistance. This substantially reduced filtration throughput relative to pre-filtered bio-oil. Even though it would employ two filtration steps, it is estimated that overall throughput can be doubled by pre-filtering the bio-oil prior to addition of the sorbent compared to completing the filtration and sorbent removal in a single step.

Although promising results were obtained from a technical standpoint, further study is required. Foremost, it is recommended to perform repeats of select experimental trials to validate the results that were obtained from this work. It was mentioned that only a single loading ratio and exposure time was

used in the set of trials for metal removal using solid-phase adsorbents. However, these are operating parameters that should be more closely studied in an attempt to better optimize such a process for combined mineral and char removal. The use of anionic exchange resin, either independently or with cationic exchange resin, should also be investigated for removal of non-cationic species such as silicon or phosphorus.

It is also of interest to pursue the development of a process that combines the use of solid-phase (or liquid phase) additives with cross-flow microfiltration. This would necessitate the use of a circulating pump capable of handling slurries, such as a rotary lobe or progressive cavity pump. Alternatively, the use of ion exchange membranes may represent an interesting route for similar results. Adsorbent regeneration procedures were not discussed in this work, but are a critical component of such a process. Thus, it is recommend to explore the regeneration of the adsorbents after contact with bio-oil and to identify the associated operational challenges and costs associated with this requirement. Finally, when enough data is available on the process, it would be recommended to complete a cost assessment of the approach such that the incremental processing cost for the use of solid-phase adsorbents for the removal of ash from FPBO could be reasonably estimated.

Chapter 6. Concluding Remarks and Recommendations

The main motivation for this thesis was to help bridge the gap in scientific or design data available in open literature related to the removal of suspended char particulate (solids) and ash from fast pyrolysis bio-oils. The treatment pathways that were experimentally investigated included biomass pretreatment (sieving and acid washing) for ash reduction in a hog fuel prior to liquefaction, as well as cross-flow microfiltration of bio-oils produced principally from harvest and mill residues. A preliminary investigation into the use of solid-phase adsorbents paired with microfiltration was also performed.

Sieving and acid washing of a hog fuel was shown to reduce solids and ash content in the produced bio-oils by as much as 80% and 87%. Furthermore, this pre-treatment approach demonstrated other positive impacts including higher organic liquid yield and reductions in pyrolysis reaction water production during liquefaction. This approach was able to adequately reduce the ash content below that of the 0.15 wt% target specifications, but additional considerations for improved solids removal below 0.25 wt%, as specified by ASTM Grade D [3], would be required.

Alternatively, cross-flow microfiltration of fast pyrolysis bio-oil in the 1-40 µm range was found to reduce the solids content well below the ASTM Grade D limit of 0.25 wt%, and in some cases, the ash content below the limit of 0.15 wt%. However, low ash rejection due to the nature of the ash elements in FPBO (originating from higher ash forestry residuals) necessitated the use of solid-phase adsorbents such as ion exchange resin combined with microfiltration for high ash rejection up to 90%. Fouling in bio-oil cross-flow microfiltration was determined to be dominated by cake resistance, leading to quick and severe reductions in flux. A range of initial bio-oil microfiltration flux values of 100-1000 L m^{-2} h^{-1} were common at transmembrane pressures up to 1.04 bar, while pseudo steady-state flux values in the same trials were on the order of 20-50 L m^{-2} h^{-1} were measured. The use of fluid pre-heating (up to 60 °C), transmembrane pressures ranging from 0.34-0.69 bar, dilution with low viscosity solvents and the consideration for preliminary solids removal strategies were all suggested to improve the process in the transient and pseudo steady-state operating regimes.

The largest throughput of low-solids bio-oil in cross-flow microfiltration was observed in the transient stages of operation. Thus, on-line cleaning procedures were evaluated to disturb the accumulative fouling layer on the active filtration surface to increase throughput of low-solids bio-oil. It was found that the fouling was reversible after repetitive air, solvent and permeate backflush cycling for operating periods of up to 10 hours. Air backflushing procedures were found to increase permeate throughput by up to 100%,

such that the average flux for trials in which non-optimized backflushing was implemented varied from 50-100 L m^{-2} h^{-1}.

Key recommendations resulting from this work are summarized below:

i. Optimize biomass washing procedures in anticipated effort to reduce cost of treatment pathway

Due to the resource intensity required to complete a full experimental campaign in which sieving and nitric acid washing were evaluated as pretreatment pathway prior to pilot-scale fast pyrolysis at CanmetENERGY-Ottawa, only a single washing condition was evaluated. It would be beneficial to perform a multi-level analysis on different washing procedures such that the minimum requirements to achieve satisfactory bio-oil quality and yields are met, depending on the application. Given the variability in mineral contaminants in many biomass feedstocks, washing procedures would have to be adapted for varying qualities of lignocellulosic biomass feedstocks.

ii. Identify the maximum operating time for which severe filtration media cleaning methods, such as chemical soaking, is required in bio-oil cross-flow microfiltration

The cake fouling accumulation on the active filtration surface in FPBO cross-flow microfiltration was reversible over a processing time of 10 hours and up to 31 air backflush cycles. However, it is reasonable to expect that there would eventually be a requirement for more severe cleaning strategies to remove any non-reversible filtration resistances that occur over time. Therefore, evaluating the necessary operating times required until chemical cleaning is essential for estimating the true operating costs of such a process.

iii. Perform additional investigation into ash removal in FPBOs with the use of additives, whether in the solid or liquid phase, which could be combined with microfiltration for virtually complete removal of solids and ash in the optimal number of processing steps

The addition of 5 wt% of Amberlyst 15 was suitable in removing virtually all cations in unfiltered and pre-filtered bio-oil at an exposure time of 24 hours. However, this approach is likely not practical as this would translate to large operating costs in an industrial process due to the cost of the sorbents, the large concentrations of sorbents investigated and prolonged exposure times. Thus, further evaluation of optimal loading ratios, contact times and cleaning procedures is recommended to further improve the feasibility of such an approach.

Master Reference List

[1] A. Brown, P. Le Feuvre, IEA 2017 Technology Roadmap for Delivering Sustainable Bioenergy, Iea. (2017). doi:10.1787/9789264287600-en.

[2] International Renewable Energy Agency (IRENA), Global Energy Transformation: A Roadmap to 2050, 2018. doi:Doi 10.1002/(Sici)1097-0029(19990915)46:6<398::Aid-Jemt8>3.0.Co;2-H.

[3] A. Oasmaa, D.C. Elliott, S. Muller, Quality control in fast pyrolysis bio-oil production and use, Environ. Prog. Sustain. Energy. (2009). doi:10.1002/ep.10382.

[4] A. Drews, Standard Test Method for Ash from Petroleum Products, in: Man. Hydrocarb. Anal. 6th Ed., 2008. doi:10.1520/mnl10845m.

[5] L. Nguyen, B. Bronson, D. Mazerolle, Treatment of Bio-oils from Forest Residues to meet Target Specifications for Immediate Applications, 2017. doi:Unpublished report produced at CanmetENERGY-Ottawa.

[6] R.M. Baldwin, C.J. Feik, Bio-oil stabilization and upgrading by hot gas filtration, Energy and Fuels. 27 (2013) 3224–3238. doi:10.1021/ef400177t.

[7] E. Hoekstra, K.J.A. Hogendoorn, X. Wang, R.J.M. Westerhof, S.R.A. Kersten, W.P.M. Van Swaaij, M.J. Groeneveld, Fast pyrolysis of biomass in a fluidized bed reactor: In situ filtering of the vapors, Ind. Eng. Chem. Res. (2009). doi:10.1021/ie8017274.

[8] J. Scahill, J.P. Diebold, C. Feik, Removal of Residual Char Fines from Pyrolysis Vapors by Hot Gas Filtration, in: Dev. Thermochem. Biomass Convers., 2013. doi:10.1007/978-94-009-1559-6_19.

[9] S. Suttibak, K. Sriprateep, A. Pattiya, Production of Bio-oil from Pine Sawdust by Rapid Pyrolysis in a Fluidized-bed Reactor, Energy Sources, Part A Recover. Util. Environ. Eff. 37 (2015) 1440–1446. doi:10.1080/15567036.2011.631091.

[10] A. Pattiya, S. Suttibak, Fast pyrolysis of sugarcane residues in a fluidised bed reactor with a hot vapour filter, J. Energy Inst. (2017). doi:10.1016/j.joei.2015.10.001.

[11] D.C. Elliott, H. Wang, R. French, S. Deutch, K. Iisa, Hydrocarbon liquid production from biomass via hot-vapor-filtered fast pyrolysis and catalytic hydroprocessing of the bio-oil, Energy and Fuels. 28 (2014) 5909–5917. doi:10.1021/ef501536j.

[12] M. Ikura, M. Stanciulescu, E. Hogan, Emulsification of pyrolysis derived bio-oil in diesel fuel, Biomass and

Bioenergy. 24 (2003) 221–232. doi:10.1016/S0961-9534(02)00131-9.

[13] S.I. Yang, T.C. Hsu, C.Y. Wu, K.H. Chen, Y.L. Hsu, Y.H. Li, Application of biomass fast pyrolysis part II: The effects that bio-pyrolysis oil has on the performance of diesel engines, Energy. 66 (2014) 172–180. doi:10.1016/j.energy.2013.12.057.

[14] R.J.M. Westerhof, D.W.F. Brilman, M. Garcia-Perez, Z. Wang, S.R.G. Oudenhoven, W.P.M. Van Swaaij, S.R.A. Kersten, Fractional condensation of biomass pyrolysis vapors, Energy and Fuels. (2011). doi:10.1021/ef2000322.

[15] A. Tumbalam Gooty, D. Li, C. Briens, F. Berruti, Fractional condensation of bio-oil vapors produced from birch bark pyrolysis, Sep. Purif. Technol. 124 (2014) 81–88. doi:10.1016/j.seppur.2014.01.003.

[16] S. Wang, Y. Gu, Q. Liu, Y. Yao, Z. Guo, Z. Luo, K. Cen, Separation of bio-oil by molecular distillation, Fuel Process. Technol. 90 (2009) 738–745. doi:10.1016/j.fuproc.2009.02.005.

[17] Z.G. Guo, S.R. Wang, Y.Y. Zhu, Z.Y. Luo, K.F. Cen, Separation of acid compounds for refining biomass pyrolysis oil, Ranliao Huaxue Xuebao/Journal Fuel Chem. Technol. 37 (2009) 49–52. doi:10.1016/S1872-5813(09)60010-4.

[18] J.L. Zheng, Q. Wei, Improving the quality of fast pyrolysis bio-oil by reduced pressure distillation, Biomass and Bioenergy. 35 (2011) 1804–1810. doi:10.1016/j.biombioe.2011.01.006.

[19] R.N. Hilten, B.P. Bibens, J.R. Kastner, K.C. Das, In-line esterification of pyrolysis vapor with ethanol improves Bio-oil quality, in: Energy and Fuels, 2010. doi:10.1021/ef900838g.

[20] T. Sundqvist, A. Oasmaa, A. Koskinen, Upgrading fast pyrolysis bio-oil quality by esterification and azeotropic water removal, Energy and Fuels. (2015). doi:10.1021/acs.energyfuels.5b00238.

[21] A. V. Bridgwater, Review of fast pyrolysis of biomass and product upgrading, Biomass and Bioenergy. 38 (2012) 68–94. doi:10.1016/j.biombioe.2011.01.048.

[22] A. Pandey, T. Bhaskar, M. Stöcker, R.K. Sukumaran, Recent Advances in Thermochemical Conversion of Biomass, 2015. doi:10.1016/C2013-0-00403-3.

[23] J. Koppejan, M. Cremers, Biomass pre-treatment for bioenergy, 2019. https://www.ieabioenergy.com/publications/biomass-pre-treatment-for-bioenergy/.

[24] C.C. Dymond, B.D. Titus, G. Stinson, W.A. Kurz, Future quantities and spatial distribution of harvesting residue and dead wood from natural disturbances in Canada, For. Ecol. Manage. 260 (2010) 181–192. doi:10.1016/j.foreco.2010.04.015.

[25] A.H. Zacher, D.C. Elliott, M. V. Olarte, D.M. Santosa, F. Preto, K. Iisa, Pyrolysis of woody residue feedstocks: Upgrading of bio-oils from Mountain-pine-beetle-killed trees and hog fuel, Energy and Fuels. 28 (2014) 7510–7516. doi:10.1021/ef5017945.

[26] D. Bradley, Canadian Report on Bioenergy 2010, 2010. http://www.cancarb.ca/pdfs/pubs/NRCAN canada-report-on-bioenergy-2010-sept-15-2010.pdf.

[27] H.-H. Rogner, R.F. Aguilera, C.L. Archer, R. Bertani, S.C. Bhattacharya, M.B. Dusseault, L. Gagnon, H. Haberl, M. Hoogwijk, A. Johnson, M.L. Rogner, H. Wagner, V. Yakushev, D.J. Arent, I. Bryden, F. Krausmann, P. Odell, C. Schillings, A. Shafiei, J. Zou, Energy Resources and Potentials, in: Glob. Energy Assess., 2012. doi:10.1017/cbo9780511793677.013.

[28] T. Browne, R. Gilsenan, D. Singbeil, M. Paleologou, Bio-energy and Bio-chemicals Synthesis Report, (2011) 54. http://www.fpac.ca/wp-content/uploads/publications/Future_of_forestry/Bio_Energy_Final_En.pdf.

[29] J. Barrette, D. Paré, F. Manka, L. Guindon, P. Bernier, B. Titus, Forecasting the spatial distribution of logging residues across the Canadian managed forest, Can. J. For. Res. 48 (2018) 1470–1481. doi:10.1139/cjfr-2018-0080.

[30] C. Friesen, Biomass availability and supply, in: 2013. https://www.pellet.org/wpac-agm/images/2016/Charles-Friesen-Biomass-availability-and-supply.pdf.

[31] K. Bradburn, CanBio Report on the Status of Bioenergy in Canada, Report. (2014) 89. http://www.bioenergytrade.org/downloads/canada-country-report-2014-Feb-23.pdf.

[32] S. Caillat, E. Vakkilainen, Large-scale biomass combustion plants: An overview, in: Biomass Combust. Sci. Technol. Eng., 2013. doi:10.1533/9780857097439.3.189.

[33] J. Lehto, A. Oasmaa, Y. Solantausta, M. Kytö, D. Chiaramonti, Fuel oil quality and combustion of fast pyrolysis bio-oils (VTT #87), 2013. doi:http://dx.doi.org/10.1016/j.apenergy.2013.11.040.

[34] Wood Energy - List and values of wood fuel parameters - Part 1, (n.d.). http://www.woodenergy.ie/woodasafuel/listandvaluesofwoodfuelparameters-part1/ (accessed August 17, 2019).

[35] A. Oasmaa, C. Peacocke, Properties and fuel use of biomass-derived fast pyrolysis liquids. A guide, 2010. https://www.vtt.fi/Documents/P731.pdf.

[36] J. Lehto, A. Oasmaa, Y. Solantausta, M. Kytö, D. Chiaramonti, Review of fuel oil quality and combustion of fast pyrolysis bio-oils from lignocellulosic biomass, Appl. Energy. (2014).

doi:10.1016/j.apenergy.2013.11.040.

[37] S.D. Stefanidis, K.G. Kalogiannis, A.A. Lappas, Co-processing bio-oil in the refinery for drop-in biofuels via fluid catalytic cracking, Wiley Interdiscip. Rev. Energy Environ. (2018). doi:10.1002/wene.281.

[38] F. de Miguel Mercader, M.J. Groeneveld, S.R.A. Kersten, C. Geantet, G. Toussaint, N.W.J. Way, C.J. Schaverien, K.J.A. Hogendoorn, Hydrodeoxygenation of pyrolysis oil fractions: process understanding and quality assessment through co-processing in refinery units, Energy Environ. Sci. 4 (2011) 985. doi:10.1039/c0ee00523a.

[39] M. Bertero, U. Sedran, Coprocessing of Bio-oil in Fluid Catalytic Cracking, in: Recent Adv. Thermochem. Convers. Biomass, 2015. doi:10.1016/B978-0-444-63289-0.00013-2.

[40] D. Castello, L. Rosendahl, 9 - Coprocessing of pyrolysis oil in refineries, in: Direct Thermochem. Liq. Energy Appl., 2017. doi:10.1016/B978-0-08-101029-7.00008-4.

[41] A.D.R. Pinho, M.B.B. De Almeida, F.L. Mendes, V.L. Ximenes, L.C. Casavechia, Co-processing raw bio-oil and gasoil in an FCC Unit, Fuel Process. Technol. 131 (2015) 159–166. doi:10.1016/j.fuproc.2014.11.008.

[42] A. de R. Pinho, M.B.B. de Almeida, F.L. Mendes, L.C. Casavechia, M.S. Talmadge, C.M. Kinchin, H.L. Chum, Fast pyrolysis oil from pinewood chips co-processing with vacuum gas oil in an FCC unit for second generation fuel production, Fuel. 188 (2017) 462–473. doi:10.1016/j.fuel.2016.10.032.

[43] M. Staš, J. Chudoba, D. Kubička, M. Pospíšil, Chemical Characterization of Pyrolysis Bio-oil: Application of Orbitrap Mass Spectrometry, Energy & Fuels. 29 (2015) 3233–3240. doi:10.1021/acs.energyfuels.5b00407.

[44] X. Hu, D. Mourant, R. Gunawan, L. Wu, Y. Wang, C. Lievens, C.-Z. Li, Production of value-added chemicals from bio-oil via acid catalysis coupled with liquid–liquid extraction, RSC Adv. 2 (2012) 9366. doi:10.1039/c2ra21597g.

[45] Y. Elkasabi, C.A. Mullen, A.A. Boateng, Distillation and Isolation of Commodity Chemicals from Bio-Oil Made by Tail-Gas Reactive Pyrolysis, ACS Sustain. Chem. Eng. 2 (2014) 2042–2052. doi:10.1021/sc5002879.

[46] K.J. Chong, A. V. Bridgwater, Fast Pyrolysis Oil Fuel Blend for Marine Vessels, Environ. Prog. Sustain. Energy. (2016). doi:10.1002/ep.12402.

[47] M. Kass, Z. Abdullah, M. Biddy, C. Drennan, T. Hawkins, S. Jones, J. Holladay, D. Longman, E. Newes, T. Theiss, T. Thompson, M. Wang, Understanding the Opportunities of Biofuels for Marine Shipping, 2018. https://info.ornl.gov/sites/publications/Files/Pub120597.pdf.

[48] R.C. Williams, J. Peralta, K.L.N. Puga, Development of non-petroleum-based binders for use in flexible

pavements-phase, 2015. www.intrans.iastate.edu.

[49] G.M. Fayzrakhmanova, S.A. Zabelkin, A.N. Grachev, V.N. Bashkirov, A study of the properties of a composite asphalt binder using liquid products of wood fast pyrolysis, Polym. Sci. Ser. D. 9 (2016) 181–184. doi:10.1134/S1995421216020052.

[50] J. Lehto, A. Oasmaa, Y. Solantausta, M. Kytö, D. Chiaramonti, Fuel oil quality and combustion of fast pyrolysis bio-oils, VTT Publ. (2013) 79. doi:http://dx.doi.org/10.1016/j.apenergy.2013.11.040.

[51] E. Thiffault, S. Sokhansanj, M. Ebadian, H. Rezaei, E.O.B. Ghiasi, F. Yazadanpanah, A. Asikainen, J. Routa, Biomass pre-treatment for bioenergy, 2018. http://itp-fueltreatment.ieabioenergy.com/publications/biomass-pre-treatment-for-bioenergy-case-study-2-moisture-physical-property-ash-and-density-management-as-pre-treatment-practices-in-canadian-forest-biomass-supply-chains/.

[52] E.J. Leijenhorst, W. Wolters, L. Van De Beld, W. Prins, Inorganic element transfer from biomass to fast pyrolysis oil: Review and experiments, Fuel Process. Technol. 149 (2016) 96–111. doi:10.1016/j.fuproc.2016.03.026.

[53] D. Mazerolle, H. Rezaei, B. Bronson, L. Nguyen, F. Preto, Sieving and Acid Washing as a Pretreatment to Fast Pyrolysis of a High Ash Hog Fuel, Energy & Fuels. (2019) acs.energyfuels.9b00694. doi:10.1021/acs.energyfuels.9b00694.

[54] A. Oasmaa, T. Sundqvist, E. Kuoppala, M. Garcia-Perez, Y. Solantausta, C. Lindfors, V. Paasikallio, Controlling the phase stability of biomass fast pyrolysis bio-oils, Energy and Fuels. 29 (2015) 4373–4381. doi:10.1021/acs.energyfuels.5b00607.

[55] A. Oasmaa, I. Fonts, M.R. Pelaez-Samaniego, M.E. Garcia-Perez, M. Garcia-Perez, Pyrolysis Oil Multiphase Behavior and Phase Stability: A Review, Energy and Fuels. 30 (2016) 6179–6200. doi:10.1021/acs.energyfuels.6b01287.

[56] A. Oasmaa, B. Van De Beld, P. Saari, D.C. Elliott, Y. Solantausta, Norms, standards, and legislation for fast pyrolysis bio-oils from lignocellulosic biomass, Energy and Fuels. 29 (2015) 2471–2484. doi:10.1021/acs.energyfuels.5b00026.

[57] O. Sippula, K. Huttunen, J. Hokkinen, S. Kärki, H. Suhonen, T. Kajolinna, M. Kortelainen, T. Karhunen, P. Jalava, O. Uski, P. Yli-Pirilä, M.R. Hirvonen, J. Jokiniemi, Emissions from a fast-pyrolysis bio-oil fired boiler: Comparison of health-related characteristics of emissions from bio-oil, fossil oil and wood, Environ. Pollut. 248 (2019) 888–897. doi:10.1016/j.envpol.2019.02.086.

[58] M. Beran, L.-U. Axelsson, Development and Experimental Investigation of a Tubular Combustor for Pyrolysis Oil Burning, J. Eng. Gas Turbines Power. (2014). doi:10.1115/1.4028450.

[59] C.R. Shaddix, P.J. Tennison, Effects of char content and simple additives on biomass pyrolysis oil droplet combustion, in: Symp. Combust., 1998. doi:10.1016/S0082-0784(98)80034-9.

[60] W.S.W. Ho, K.K. Sirkar, Membrane Handbook, Springer US, 1992.

[61] M. Cheryan, Ultrafiltration and Microfiltration Handbook, 2018. doi:10.1201/9781482278743.

[62] A. Abdelrasoul, H. Doan, A. Lohi, Fouling in Membrane Filtration and Remediation Methods, Mass Transf. - Adv. Sustain. Energy Environ. Oriented Numer. Model. (2013). doi:10.5772/52370.

[63] D. Mazerolle, H. Rezaei, B. Bronson, L. Nguyen, F. Preto, Sieving and Acid Washing as a Pretreatment to Fast Pyrolysis of a High Ash Hog Fuel, Energy & Fuels. 33 (2019) 5352–5359. doi:10.1021/acs.energyfuels.9b00694.

[64] D. Carpenter, T.L. Westover, S. Czernik, W. Jablonski, Biomass feedstocks for renewable fuel production: a review of the impacts of feedstock and pretreatment on the yield and product distribution of fast pyrolysis bio-oils and vapors, Green Chem. 16 (2014) 384–406. doi:10.1039/C3GC41631C.

[65] W. Elbersen, T.M. Lammens, E.A. Alakangas, B. Annevelink, P. Harmsen, B. Elbersen, Lignocellulosic Biomass Quality, Elsevier Inc., 2017. doi:10.1016/B978-0-12-812303-4.00003-3.

[66] K.L. Kenney, W.A. Smith, G.L. Gresham, T.L. Westover, Understanding biomass feedstock variability, Biofuels. 4 (2013) 111–127. doi:10.4155/bfs.12.83.

[67] B. Livingston, M. Babcock, Ash related Issues in Biomass Combustion, Therm. Work. (2006).

[68] F.A. Agblevor, S. Besler, Inorganic compounds in biomass feedstocks. 1. Effect on the quality of fast pyrolysis oils, Energy and Fuels. 10 (1996) 293–298. doi:10.1021/ef950202u.

[69] J. Huyghe, The role of alkali and earth alkaline metals as intrinsic catalysts in the fast pyrolysis of biomass constituents, (2013) 84. http://lib.ugent.be/fulltxt/RUG01/002/166/525/RUG01-002166525_2014_0001_AC.pdf.

[70] H. Wu, J.I. Hayashi, T. Chiba, T. Takarada, C.Z. Li, Volatilisation and catalytic effects of alkali and alkaline earth metallic species during the pyrolysis and gasification of Victorian brown coal. Part V. Combined effects of Na concentration and char structure on char reactivity, Fuel. 83 (2004) 23–30. doi:10.1016/S0016-2361(03)00238-2.

[71] S.D. Stefanidis, E. Heracleous, D.T. Patiaka, K.G. Kalogiannis, C.M. Michailof, A.A. Lappas, Optimization of bio-oil yields by demineralization of low quality biomass, Biomass and Bioenergy. 83 (2015) 105–115. doi:10.1016/j.biombioe.2015.09.004.

[72] L. Tao, A. Aden, R.T. Elander, V.R. Pallapolu, Y.Y. Lee, R.J. Garlock, V. Balan, B.E. Dale, Y. Kim, N.S. Mosier, M.R. Ladisch, M. Falls, M.T. Holtzapple, R. Sierra, J. Shi, M.A. Ebrik, T. Redmond, B. Yang, C.E. Wyman, B. Hames, S. Thomas, R.E. Warner, Process and technoeconomic analysis of leading pretreatment technologies for lignocellulosic ethanol production using switchgrass, Bioresour. Technol. 102 (2011) 11105–11114. doi:10.1016/j.biortech.2011.07.051.

[73] K.O. Davidsson, J.G. Korsgren, J.B.C. Pettersson, U. Jäglid, The effects of fuel washing techniques on alkali release from biomass, Fuel. 81 (2002) 137–142. doi:10.1016/S0016-2361(01)00132-6.

[74] N. Frederick, N. Zhang, A. Djioleu, X. Ge, J. Xu, D.J. Carrier, The Effect of Washing Dilute Acid Pretreated Poplar Biomass on Ethanol Yields, Intech. (2013) 105–117. doi:10.5772/56129.

[75] S.R.G. Oudenhoven, R.J.M. Westerhof, N. Aldenkamp, D.W.F. Brilman, S.R.A. Kersten, Demineralization of wood using wood-derived acid: Towards a selective pyrolysis process for fuel and chemicals production, J. Anal. Appl. Pyrolysis. 103 (2013) 112–118. doi:10.1016/J.JAAP.2012.10.002.

[76] J. Piskorz, D. Radlein, D.S. Scott, S. Czernik, LIQUID PRODUCTS FROM THE FAST PYROLYSIS OF WOOD AND CELLULOSE, Res. Thermochem. Biomass Convers. (1988) 557–571. doi:10.1081/E-EEE2-120046011.

[77] D. Mourant, Z. Wang, M. He, X.S. Wang, M. Garcia-Perez, K. Ling, C.Z. Li, Mallee wood fast pyrolysis: Effects of alkali and alkaline earth metallic species on the yield and composition of bio-oil, Fuel. 90 (2011) 2915–2922. doi:10.1016/j.fuel.2011.04.033.

[78] H. Rezaei, Efficiency of Metals Removal from Interior Hog Fuel by Means of Water Washing and Acid Washing : Trials and Analyses, Vancouver, 2015. doi:Unpublished internal report produced by FPInnovations and CanmetENERGY-Ottawa.

[79] J.R. Ferrell, M. V. Olarte, E.D. Christensen, A.B. Padmaperuma, R.M. Connatser, F. Stankovikj, D. Meier, V. Paasikallio, Standardization of chemical analytical techniques for pyrolysis bio-oil: history, challenges, and current status of methods, Biofuels, Bioprod. Biorefining. 10 (2016) 496–507. doi:10.1002/bbb.1661.

[80] B. Opalka, Heating fuel from “liquid trees” helps Maine college hit carbon neutrality goal | Energy News Network, (2019). https://energynews.us/2019/06/05/northeast/heating-fuel-from-liquid-trees-helps-maine-college-hit-carbon-neutrality-goal/ (accessed July 13, 2019).

[81] G. Muggen, Fast Pyrolysis Bio-Oil Technology and Production, in: 2018.

https://worldbioenergy.org/uploads/pdf/3 in 1 webinar/Pyrolysis Oil Markets and BTG BTL Global Roll Out - Gerhard Muggen, BTG BTL.pdf.

[82] F. Preto, B. Bronson, E. Harrison, D. Mazerolle, Critical Factors For Operation Of Internal Combustion Engines On Raw About CanmetENERGY, in: Adv. Biofuels Conf. 2017, Gothenburg, Sweden, 2017: pp. 1–26. https://bioenergyinternational.com/app/uploads/2017/05/Preto_Fernando_ABC17-1.pdf.

[83] R. Lødeng, H. Bergem, 7. Stabilisation of pyrolysis oils, Elsevier Ltd., 2018. doi:10.1016/B978-0-08-101029-7.00006-0.

[84] V. Piemonte, M. Capocelli, G. Orticello, L. Di Paola, Bio-oil production and upgrading: New challenges for membrane applications, Membr. Technol. Biorefining. (2016) 263–287. doi:10.1016/B978-0-08-100451-7.00011-6.

[85] ASTM, Standard Test Method for Pyrolysis Solids Content in Pyrolysis Liquids by Filtration of Solids in Methanol, Astm. (2015). doi:10.1520/D7579-09.2.

[86] A. Oasmaa, C. Peacocke, A guide to physical property characterisation of biomass-derived fast pyrolysis liquids, VTT Publ. (2001) 2–65.

[87] D.C. Elliott, Water, alkali and char in flash pyrolysis oils, Biomass and Bioenergy. 7 (1994) 179–185. doi:10.1016/0961-9534(94)00057-Z.

[88] D.C. Elliott, D. Meier, A. Oasmaa, B. Van De Beld, A. V. Bridgwater, M. Marklund, Results of the International Energy Agency Round Robin on Fast Pyrolysis Bio-oil Production, Energy and Fuels. 31 (2017) 5111–5119. doi:10.1021/acs.energyfuels.6b03502.

[89] H.T. Liao, Q. Lu, Z.B. Zhang, C.Q. Dong, Overview of Methods to Remove Solid Particles from Biomass Fast Pyrolysis Oils, Adv. Mater. Res. 608–609 (2012) 265–268. doi:10.4028/www.scientific.net/AMR.608-609.265.

[90] A. Javaid, T. Ryan, G. Berg, X. Pan, T. Vispute, S.R. Bhatia, G.W. Huber, D.M. Ford, Removal of char particles from fast pyrolysis bio-oil by microfiltration, J. Memb. Sci. 363 (2010) 120–127. doi:10.1016/j.memsci.2010.07.021.

[91] S.J. Frey, R. Gattupalli, T.A. Brandvold, UOP patent method and apparatus for forming low-metal biomass derived pyrolysis oil (filtration and ion exchange).pdf, 2012.

[92] S.J. Frey, R. Marinangeli, T.A. Bandvold, M. Koch, V. Abrahamian, J.A. Noga, T. Traynor, UOP patent method for forming low metal biomass derived bio-oil (ion exchange and azeotropic distillation).pdf, 2013.

[93] A.C.M. Franken, Prevention and control of membrane fouling : practical implications and examining recent innovations, Prev. Control Membr. Fouling. (2009) 47. http://www.ispt.eu/media/CS-01-02-Final-report-Prevention-and-reduction-of-membrane-fouling.pdf.

[94] M.D. Kass, C.J. Janke, R.M. Connatser, S.A. Lewis, J.R. Keiser, K. Gaston, Compatibility Assessment of Fuel System Elastomers with Bio-oil and Diesel Fuel, (2016). doi:10.1021/acs.energyfuels.6b01138.

[95] H. Peng, A.Y. Tremblay, Membrane regeneration and filtration modeling in treating oily wastewaters, J. Memb. Sci. 324 (2008) 59–66. doi:10.1016/j.memsci.2008.06.062.

[96] F.Z. Ashtiani, H. Rezaei, A. Fouladitajar, Fouling behavior and performance of microfiltration membranes for whey treatment in steady and unsteady-state conditions, Brazilian J. Chem. Eng. 31 (2014) 503–518. doi:10.1590/0104-6632.20140312s00002521.

[97] Q. Lu, W.Z. Li, X.F. Zhu, Overview of fuel properties of biomass fast pyrolysis oils, Energy Convers. Manag. 50 (2009) 1376–1383. doi:10.1016/j.enconman.2009.01.001.

[98] D. Mohan, C.U. Pittman, P.H. Steele, Pyrolysis of Wood / Biomass for Bio-oil : A Critical Review, Energy & Fuesl. 20 (2006) 848–889. doi:10.1021/ef0502397.

[99] S.N. Jagannadh, H.S. Muralidhara, Electrokinetics Methods To Control Membrane Fouling, Ind. Eng. Chem. Res. 35 (1996) 1133–1140. doi:10.1021/ie9503712.

[100] Z. Yan-jun, W. Kai-fen, W. Zheng-jun, Z. Liang, L. Shu-shen, Fouling and cleaning of membrane - a literature review, J. Environ. Sci. 12 (2000) 241–251. doi:1001-0742(2000)02_0241-11.

[101] F. Meng, S. Zhang, Y. Oh, Z. Zhou, H.S. Shin, S.R. Chae, Fouling in membrane bioreactors: An updated review, Water Res. (2017). doi:10.1016/j.watres.2017.02.006.

[102] X. Shi, G. Tal, N.P. Hankins, V. Gitis, Fouling and cleaning of ultrafiltration membranes: A review, J. Water Process Eng. 1 (2014) 121–138. doi:10.1016/j.jwpe.2014.04.003.

[103] B. Kruczek, Investigation of Removal of Alkali Elements from Biofuel by Silica Additives and Microfiltration; Report no. 4 (Final), 2002. doi:Unpublished report produced at University of Ottawa.

[104] G. Zhou, S. Roby, Study on the Removal of Metals from Pyrolysis Oil with Ion-Exchange Resins at Ambient Conditions, Energy and Fuels. 30 (2016) 1002–1005. doi:10.1021/acs.energyfuels.5b01896.

[105] K. Naske, Caitlin & Speed, Jason & Wynne, Zach & E. Crosby, Sarah & Walters, Effects of Char Particles On the Aging of Bio-Oil Produced From Timber Biomass Pyrolysis, in: 2009 AlCHE Annual Meeting, 2009.

[106] J.P. Diebold, A review of the chemical and physical mechanisms of the storage stability of fast pyrolysis bio-oils, 1999. doi:10.2172/753818.

[107] J. Sullivan, M. Douek, Determination of carbohydrates in wood, pulp and process liquor samples by high-performance anion-exchange chromatography with pulsed amperometric detection, J. Chromatogr. A. (1994). doi:10.1016/0021-9673(94)80259-9.

[108] BOPP, Precision woven stainless steel filter mesh, (2012). http://www.bopp.ch/Bopp2012/media/boppLibrary/Download-Center/English/brochures/Bopp_FI_Metallfiltergewebe-e_2012.pdf.

[109] W.S Tyler, Wire cloth handbook, (2018).

[110] Sterlitech, POLYCARBONATE TRACK ETCH (PCTE) MEMBRANE FILTERS, (2016) 1.

[111] Sterlitech, Nylon Membrane Filters, (2018) 2. http://www.sterlitech.com/filters/membrane-disc-filters/nylon-membranes.html.

[112] G.C.R. Douglas C. Montgomery, Applied Statistics and Probability for Enginnering - 5th Edition, 2011. doi:10.1017/CBO9781107415324.004.

[113] N.K. Shammas, L.K. Wang, H.H. Hahn, Fundamentals of Wastewater Flotation, in: Flotat. Technol., Humana Press, Totowa, NJ, 2010: pp. 121–164. doi:10.1007/978-1-60327-133-2_4.

Appendices

Appendix A. Supplementary Data - Chapter 1.

Table A. 1: Properties of various exemplary Canadian forestry residues characterized at CanmetENERGY-Ottawa

	Test Method	Hardwood Sawdust	Mill Softwood Sawdust	Beetle-Kill Wood	Hardwood Harvest Residue	Softwood Harvest Residue	Mill Bark	Mill Hog Fuel	Salt-Laden Hog Fuel	Coastal Hog Fuel
Province		Ontario	Ontario	British Columbia	Quebec	Quebec	Quebec	British Columbia	British Columbia	British Columbia
Proximate Analysis (wt%, dry basis)										
Ash[a]	ASTM D7582	0.3	0.7	0.7	1.9	1.2	6.4	9.5	11.8	20.3
Volatile	ISO 562	85.4	82.1	83.6	81.9	80.4	76.5	71.6	64.9	62.0
Fixed Carbon	ASTM D7582	14.3	17.2	15.8	16.3	18.4	17.1	19.0	23.2	17.6
Ultimate Analysis (wt%, dry ash-free basis)										
Carbon	ASTM D5373	49.3	51.8	51.3	50.4	52.5	54.6	52.9	54.4	54.4
Hydrogen	ASTM D5373	6.0	6.0	6.2	6.1	6.3	6.4	6.1	5.9	6.2
Nitrogen	ASTM D5373	0.2	0.2	0.2	0.3	0.3	0.7	0.4	0.3	0.4
Sulfur	ASTM D4239	<0.05	<0.05	<0.05	<0.05	<0.05	<0.05	0.2	0.1	0.3
Oxygen	by difference	44.5	42.0	42.2	43.2	40.9	38.4	40.9	39.9	38.7
Heating Value (MJ/kg)										
HHV	ISO 1928	18.47	20.50	20.43	20.07	20.69	20.76	19.03	18.48	16.98
Biochemical Composition (wt%, dry basis)										
Acetone Extractives	TAPPI T-204	1.7			2.0	3.4	6.7		2.4	
H_2O Extractives	TAPPI T-207				5.9	7.4				
Acid Insoluble Lignin	TAPPI T-222	21.4			23.4	30.7	31.1		23.7	
Acid Soluble Lignin	NREL/TP-510-42617	2.7			2.3	0.5	2.0		0.9	
Cellulose	TAPPI T-204	38.6			39.1	34.4	25.3		27.4	
Hemicellulose	TAPPI T-204	22.3			26.0	25.5	18.6		19.1	
Arabinan	[107]	0.7			1.4	2.4	1.5		1.8	
Xylan	[107]	1.6			18.7	5.8	13.6		3.3	
Mannan	[107]	2.2			2.1	9.9	0.8		8.6	
Galactan	[107]	0.7			1.0	3.0	0.9		1.9	
Glucan	[107]	4.1			42.0	38.9	27.0		31.0	

***It is important to note that the list of biomass feedstocks above should not be treated as an exclusive list or dataset, but rather exemplary data points from different types of Canadian biomass feedstocks.**

[a]In accordance with ash composition included in Table A. 2; [b]Whole tree

Table A. 2: Ash composition of various exemplary Canadian forestry residues characterized at CanmetENERGY-Ottawa

	Hardwood Sawdust	Mill Softwood Sawdust	Beetle-Kill Wood, Whole Tree	Hardwood Harvest Residue	Softwood Harvest Residue	Mill Bark	Mill Hog Fuel	Salt-Laden Hog Fuel	Coastal Residue
Province	Ontario	Ontario	British Columbia	Quebec	Quebec	Quebec	British Columbia	British Columbia	British Columbia
Composition of Ash (wt% of ash, dry) by ASTM D4326									
Chlorine	0.0027	0.0155	0.0092	0.0046	0.0045	0.0057	N/A	0.39	0.0465
SiO_2	2.06	9.75	11.39	2.23	4.09	11.14	25.48	19.64	26.24
AL_2O_3	0.25	2.39	3.45	0.43	1.59	1.96	4.70	4.74	5.83
Fe_2O_3	0.43	1.67	0.65	0.78	1.47	1.30	4.87	4.70	5.46
TiO_2	<0.0003	0.11	0.10	<0.0003	0.09	0.10	0.21	0.23	0.32
P_2O_5	2.66	2.12	11.69	3.67	6.37	2.43	10.34	8.13	8.92
CaO	29.07	39.33	24.34	45.17	34.74	40.14	27.82	27.20	23.35
MgO	5.90	4.53	11.25	3.25	5.26	3.42	13.90	11.95	12.35
SO_3	2.62	0.87	2.12	1.76	2.56	0.85	3.40	3.08	2.21
Na_2O	0.37	1.41	0.77	<0.002	<0.002	0.42	1.11	5.23	1.22
K_2O	25.50	9.73	15.59	8.82	15.20	7.62	6.57	4.55	5.42
Barium	0.26	0.26	0.07	0.41	0.44	0.22	0.07	0.03	0.03
Nickel	<0.005	0.01	0.02	<0.005	0.01	<0.005	<0.005	0.01	< 0.005
Manganese	1.40	1.46	1.52	1.43	3.64	0.13	0.29	0.36	0.16
Chromium	<0.005	0.04	0.04	<0.005	0.02	0.01	0.01	0.01	0.01
Loss on Fusion	29.20	25.96	14.76	31.54	23.98	29.84	1.1	10.05	8.38

***It is important to note that the list of biomass feedstocks above should not be treated as an exclusive list or dataset, but rather exemplary data points from different types of Canadian biomass feedstocks.**

Appendix B. Development of Bio-oil Cross-Flow Microfiltration System

To study the microfiltration profiles of fast pyrolysis bio-oils for suspended char particulate (solids) and ash removal, a bench scale cross-flow microfiltration system was designed and assembled at CE-O. The system was designed to produce as much as 1 L h^{-1} (LPH) of bio-oil permeate. Over the course of the project, the cross-flow microfiltration system was modified in response to lessons learned and to incorporate process improvements to better achieve research objectives. There was a total of three versions of the cross-flow microfiltration systems, abbreviated as MRK I (2016), MRK II (2017) and MRK III (2018-2019).

An image of the MRK I version of the system is included below.

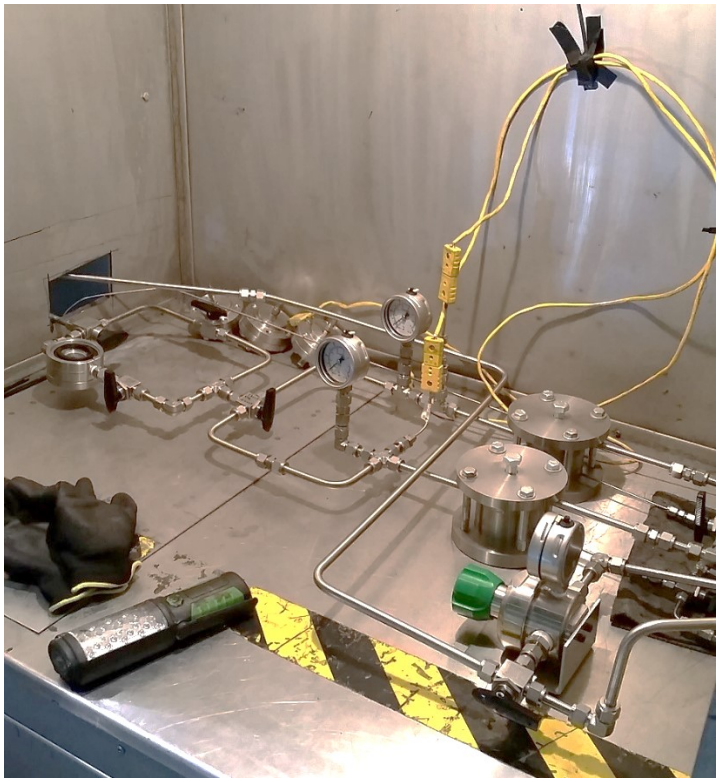

Figure A. 1: Picture of experimental cross-flow FPBO microfiltration system (MRK I) in 2016

After the proof-of-concept stage, the system was modified to create the MRK II version. The most significant changes included new, larger microfiltration cells with larger active filtration areas (discussed further below). The major experimental objective of the MRK II unit was to explore the impact of operating parameters on the flux profiles for FPBO cross-flow microfiltration, which was explored in Chapter 3. An image of the MRK II version of the system is found in Figure A. 2.

Figure A. 2: Picture of experimental cross-flow FPBO microfiltration system MRK II (2017)

The largest operational difference between the MRK II and MRK III systems was that the MRK III version included the addition of pressurized vessels mounted on the top of the microfiltration cells which were used for on-line backflushing. These vessels contained an internal volume of approximately 500 mL, and allowed pressurized backflushing of solvents or air to aid in the removal of the fouling layer on the active surface of the filters. An image of the back-end of the MRK III system is shown in Figure A. 3.

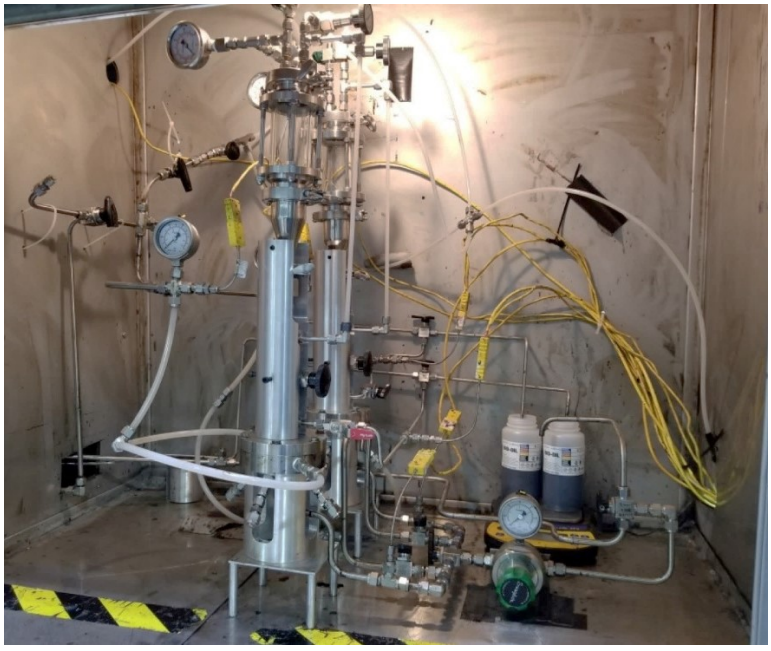

Figure A. 3: Picture of experimental cross-flow FPBO microfiltration system MRK III (2018)

There were three different microfiltration cells used over the course of this work. During proof-of-concept trials, two smaller microfiltration cells were used. One was fabricated at CanmetENERGY-Ottawa based on an old design from National Research Council, Canada, and the University of Ottawa (cell 1). The other, cell 2, was recovered from storage at CanmetENERGY-Ottawa. Although the original applications of each microfiltration cell were unknown, both were deemed suitable for preliminary testing based on their relative simplicity. These are shown in Figure A. 4.

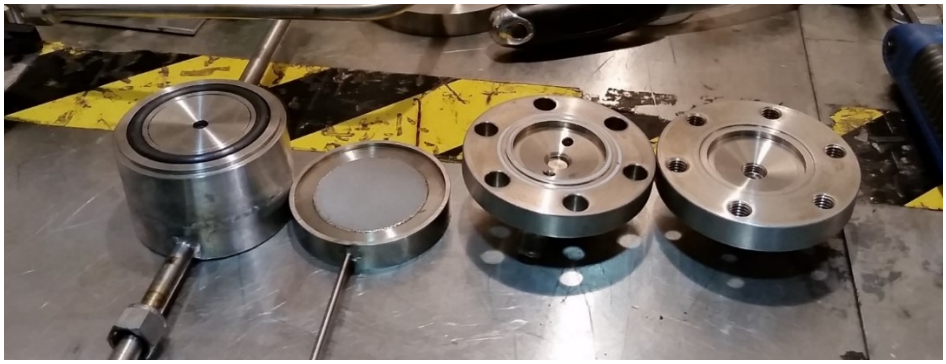

Figure A. 4: Filtration cells used in early proof-of-concept experimental trials with the MRK 1 microfiltration system; disassembled cell 1 on the left, disassembled cell 2 on the right

After the proof-of-concept trials, design of a new microfiltration cell was performed based on lessons learned from the preliminary work. This new microfiltration cell (cell 3) was larger than the previous ones, such that more permeate could be produced for analysis. Other important design changes include the inversion of the feed/permeate such that the feed was introduced from the bottom of the active filtration surface, while the internal volume on the feed side of the cell was increased, and multiple inlet ports for fluid injection were added. The main considerations for these design changes included the intention to facilitate the removal of the accumulated fouling on the active filtration cell, as well as increasing the shear force acting on the fouling layer. This microfiltration cell design was used for the vast majority of the experimental work that was included in Chapters 3 and 4. A drawing and some additional images of microfiltration cell 3 are included below.

Figure A. 5: Side view of different flow configurations for prototype filtration cell used in bio-oil microfiltration studies with the MRK II and MRK III experimental system

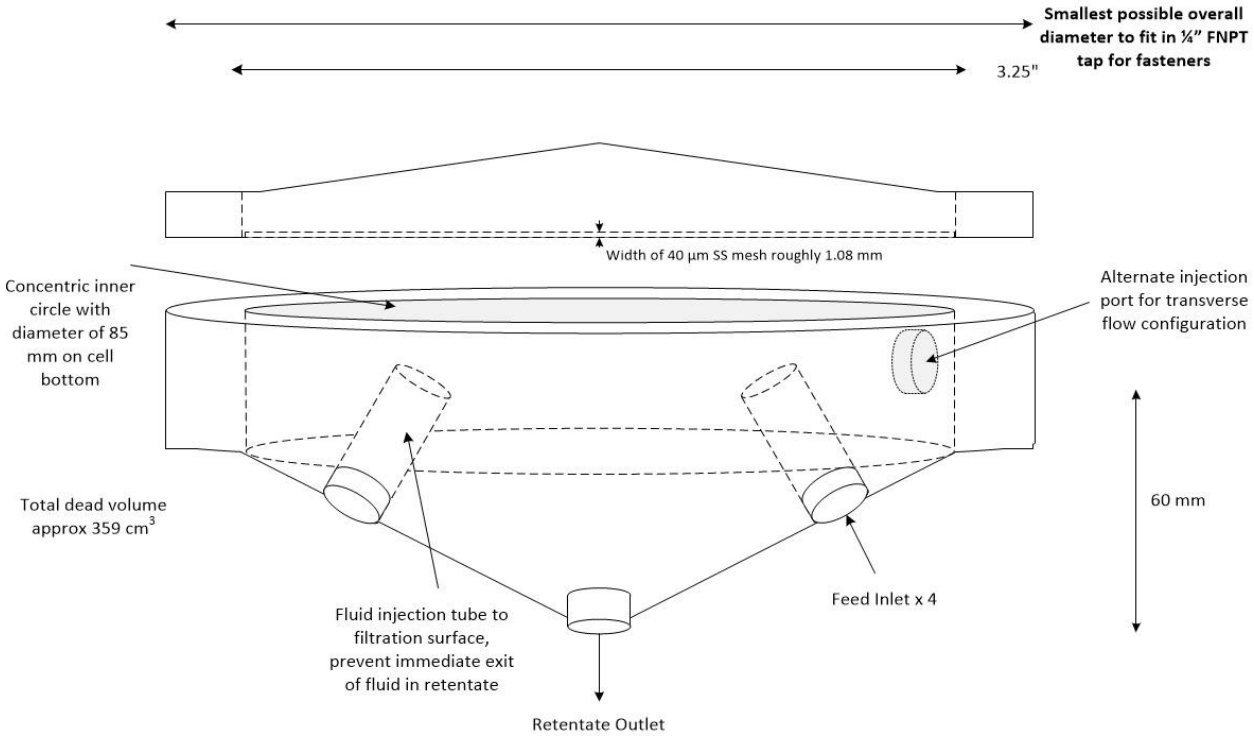

Figure A. 6: Simplified drawing of customized filtration cell fabricated at CanmetENERGY-Ottawa for bio-oil microfiltration studies

Based on lessons learned from the third microfiltraiton cell, a prototype CAD drawing of a fourth microfiltration cell was performed. The major design change for this new microfiltration cell was to change the configuration to a flat-sheet cell, as well as increase the active filtration surface so that it could process 5-10 kg h^{-1} of low-solids permeate. Theoretically, such a unit could relatively easily be attached to CanmetENERGY-Ottawa's kg h^{-1} fluidized bed fast pyrolysis system. The system was also designed such that the tangential velocity of the circulating fluid across the active filtration surface was maximized and to limit low-flow zones. Ultimately, this prototype cell has not yet been constructed.

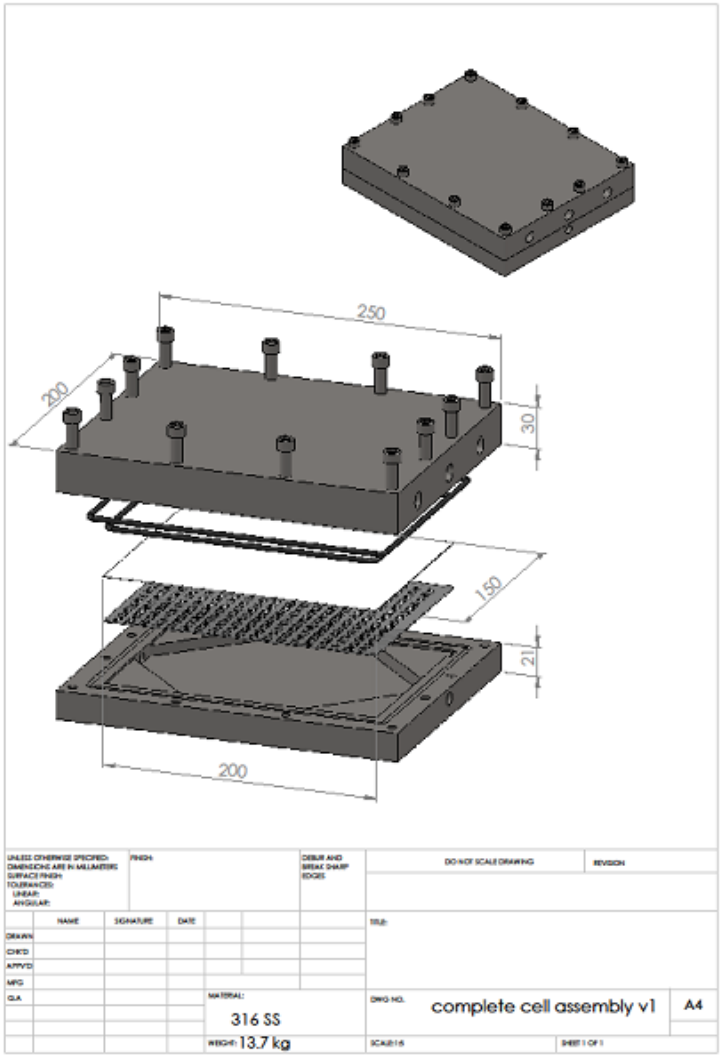

Figure A. 7: Concept CAD drawing of new filtration cell to process 5-10 kg h^{-1} of low-solids bio-oil permeate

Appendix C. Supplementary Data - Chapter 2.

A. Experimental Facilities

CanmetENERGY-Ottawa's 5-10 kg h^{-1} bubbling fluidized bed fast pyrolysis unit was the principal experimental unit used in the investigation of sieving and nitric acid washing on the fast pyrolysis of hog fuel outlined in Chapter 2. The experimental system is described in detail in Section 2.2.

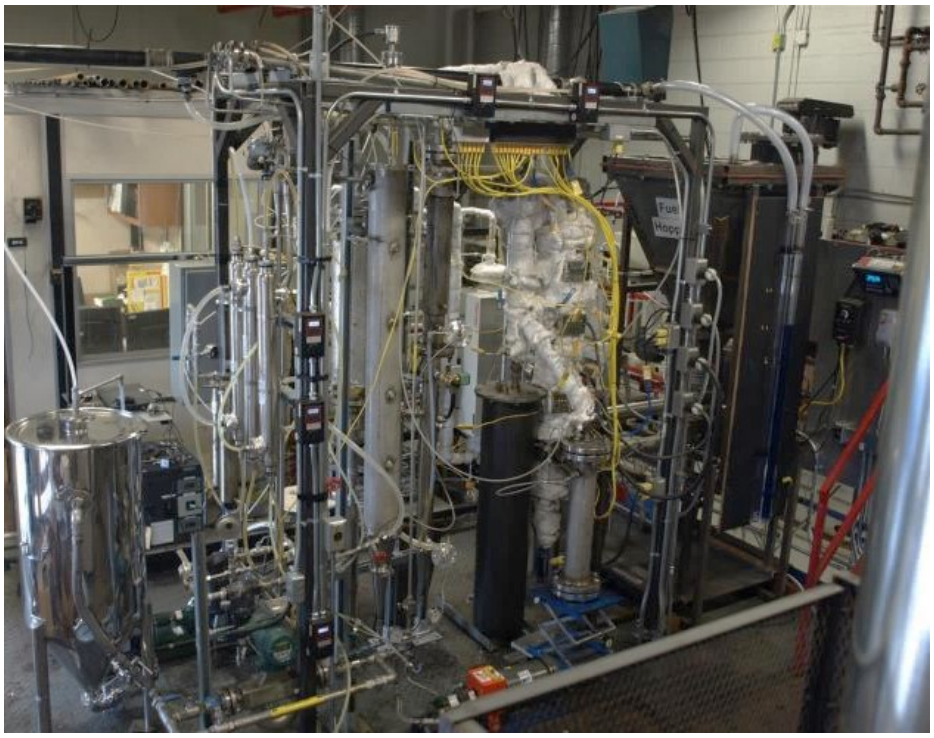

Figure A. 8: Image of CanmetENERGY-Ottawa's 5-10 kg h^{-1} bubbling bed fluidized fast pyrolysis system

B. Ash Removal by Sieving and Nitric Acid Washing

Although the total amount of ash removed via sieving and nitric acid washing was discussed in Chapter 2, the composition of removed ash was not explored. A summary of the ash composition of the produced pyrolysis liquids from the various hog fuel-based feedstocks in the Chapter 2 study are included in Figure A. 9, along with low a bio-oil produced from a hardwood sawdust feedstock for reference.

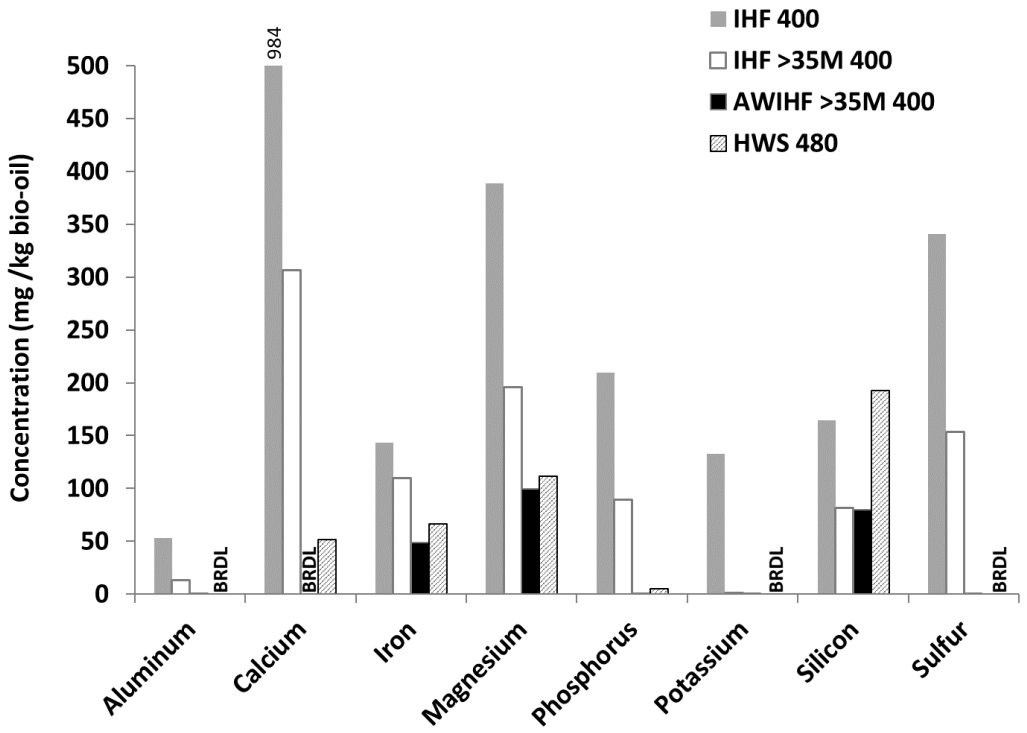

Figure A. 9: Ash composition (by ICP-OES) comparison in produced bulk pyrolysis liquids from series of sieving + nitric acid washing trials along with bio-oil produced from low ash hardwood sawdust as reference for components > 10 mg kg^{-1} in original hog fuel bio-oil

*BRDL = Below reportable detection limit

C. Chemical Quantification of FPBOs

An expanded dataset from the chemical quantification data presented in Section 2.3.3.3 is presented below in Table A. 3. The procedures for sample preparation and analysis are described in Section 2.2.

Table A. 3: Summary of chemical composition data of fast pyrolysis bio-oils from hog fuel pretreatment study

Sample ID	Group Classification	units	IHF 400	>35M 400	AW>35M 400	IHF 480	>35M 480	AW>35M 480
Furfural	furan	g kg^{-1}	2.6	4.0	4.4	3.0	2.5	3.5
2(5H)-Furanone	furan	g kg^{-1}	6.4	7.7	2.4	3.7	3.9	1.8
5-Methylfurfural	furan	g kg^{-1}	0.9	1.2	1.2	0.8	0.8	0.7
3-Methyl-2(5H)-furanone	furan	g kg^{-1}	0.1	0.1	0.0	0.6	0.6	0.3
5-Hydroxymethylfurfural	furan	g kg^{-1}	4.3	4.6	12.3	3.1	2.9	6.7
Guaiacol (2 methoxyphenol)	Guaiacols and syringols	g kg^{-1}	2.5	2.8	1.8	2.0	2.9	1.7
Creosol	Guaiacols and syringols	g kg^{-1}	3.0	4.2	3.7	1.7	2.4	2.5
4-Ethylguaiacol	Guaiacols and syringols	g kg^{-1}	0.8	0.9	0.7	< LOQ	0.5	0.5
Syringol	Guaiacols and syringols	g kg^{-1}	0.4	0.5	0.7	1.1	< LOQ	1.0
Eugenol	Guaiacols and syringols	g kg^{-1}	1.2	1.4	1.2	0.6	0.9	0.8
Vanillin	Guaiacols and syringols	g kg^{-1}	2.2	2.7	2.5	2.0	2.3	2.2
Apocynin	Guaiacols and syringols	g kg^{-1}	1.5	1.7	1.6	1.1	1.2	1.2
Syringylaldehyde	Guaiacols and syringols	g kg^{-1}	< LOQ	< LOQ	< LOQ	0.4	0.3	0.4
Acetosyringone	Guaiacols and syringols	g kg^{-1}	< LOQ	< LOQ	0.6	0.2	< LOQ	< LOQ
Levoglucosan	Levoglucosan	mg g^{-1}	24.7	30.0	127.1	19.5	16.7	97.4
Glycolaldehyde	Other volatile oxygenates	g kg^{-1}	81.3	89.4	74.5	56.4	59.3	28.1
Hydroxyacetone (Acetol)	Other volatile oxygenates	g kg^{-1}	31.9	35.3	11.0	22.6	23.4	10.3
3-Hydroxy-2-butanone	Other volatile oxygenates	g kg^{-1}	0.6	0.5	< LOQ	< LOQ	0.2	< LOQ
2-Cyclopenten-1-one	Other volatile oxygenates	g kg^{-1}	1.0	1.0	0.5	1.5	1.4	0.7
3-Methyl-1,2-cyclopentenone	Other volatile oxygenates	g kg^{-1}	5.0	5.4	4.1	3.7	3.9	2.9
Maltol	Other volatile oxygenates	g kg^{-1}	1.9	1.9	1.9	1.0	1.0	1.0
Phenol	Phenol	g kg^{-1}	0.1	0.2	0.1	0.5	0.6	0.3
o-Cresol	Phenol	g kg^{-1}	< LOQ	< LOQ	< LOQ	< LOQ	< LOQ	0.1
p-Cresol	Phenol	g kg^{-1}	0.1	0.1	0.2	< LOQ	< LOQ	0.3
m-Cresol	Phenol	g kg^{-1}	< LOQ	< LOQ	< LOQ	< LOQ	< LOQ	0.1
2,4-Xylenol	Phenol	g kg^{-1}	< LOQ	0.0	0.1	< LOQ	< LOQ	0.1
Hydroquinone	Phenol	g kg^{-1}	0.5	0.7	0.2	0.6	0.7	0.2
Acetic acid	Volatile acids	g kg^{-1}	21.6	30.3	15.4	23.0	18.8	19.4
Propanoic acid	Volatile acids	g kg^{-1}	1.7	1.8	1.0	1.8	1.6	1.1
Butanoic acid	Volatile acids	g kg^{-1}	1.0	1.0	0.8	1.0	0.9	0.8

Appendix D. Supplementary Data - Chapter 3.

A. Properties of Filtration Media

The properties of the various filtration media that were used over the course of the bio-oil microfiltration experiments are listed in Table A. 4 for reference, along with the estimated membrane resistance as calculated by a derivative of the Kozeny-Carmen equation for laminar flow through a packed bed [60] as shown in Eq. (11).

Table A. 4: Specifications of filtration media used in experimental testing for bio-oil microfiltration

Filtration Media	Sintered Stainless Steel	Twilled Stainless Steel	Polycarbonate Hydrophilic	Polycarbonate Hydrophobic	Nylon
Manufacturer	BOPP	W.S. Tyler	Sterlitech	Sterlitech	Sterlitech
Reference	[108]	[109]	[110]	[110]	[111]
Nominal Pore size (µm)	1	40	5	5	5
Abbreviation	1 µm SS	40 µm SS	5 µm PCTE HP	5 µm PCTE HB	5 µm nylon
Nominal Weight (mg cm^{-2})	**779.3[d]**	**332.9**	**1.1**	**1.1**	**6.1**
Nominal Thickness (µm)	2305	1219	3 - 24	3 - 24	65 - 125
Maximum Temperature (°C)	> 200	> 200	140	140	180
Pure Water Permeance (L h^{-1} m^{-2} bar^{-1})	N/A	N/A	6.17E+05	6.17E+05	2.92E+05
Pure Air permeance (L h^{-1} m^{-2} bar^{-1})	N/A	N/A	5.29E+07	5.29E+07	N/A
Bubble point (psi)			1.2[a]	1.2[a]	6[b]
Number pores per m^2	7.00E+11	2.39E+08	4.07E+09	4.07E+09	4.33E+10
Porosity	0.55	0.3	0.08	0.08	0.85
Assumed Thickness (µm)	**2305**	**1219**	**12**	**12**	**152.4**
Specific Surface Area (m^2 m^{-3})	4.89E+06	4.29E+04	6.96E+04	6.96E+04	4.53E+06
Estimated Resistance[c] (m^{-1})	1.34E+11	8.13E+07	1.92E+08	1.92E+08	2.29E+08

[a]Measured with isopropanol; [b]Measured with purified water; [c]Assuming uniform cylindrical pores [60]; [d]Filtration media properties in bold measured experimentally in repeats

$$R_m = \frac{2(1-\varepsilon_m)^2 \, {S_m}^2 l}{{\varepsilon_m}^3} \quad (11)$$

$$\varepsilon_m = n_p \, \pi \, {r_p}^2 \quad (12)$$

$$R_m = \frac{2 \, \pi \, n_p \, r_p}{(1-\varepsilon_m)} \quad (13)$$

where ε_m is the porosity of the membrane, S_m is the specific surface area, n_p is the number of pores per unit area and l is the membrane thickness

B. FPBO Cross-flow Model Validation

Further FPBO cross-flow microfiltration modelling validation was performed to what is currently included in Section 3.3.1. This includes additional experimental trials, as well as a slightly wider range of operating parameters as described below. The flux and volume profiles for this set of data are included in Figure A. 10.

Table A. 5: Range of operating conditions in cross-flow microfiltration trials used to validate model

Bio-oil Internal ID (Table 3.1)	7, 10
Solids Content, kg m^{-3}	4 - 5
Filtration media	1 µm SS (+ 40 µm SS support), 5 µm nylon (+ 40 µm SS support) **or** 40 µm SS
TMP, bar	0.5 - 0.82
Fluid temperature, °C	50
Fluid kinematic viscosity at operating temperature, $mm^2 \, s^{-1}$	16.5 – 28.5
Observed solids rejection range, %	60 - 98
Fluid injection velocity, m s^{-1}	0.4 ± 0.098

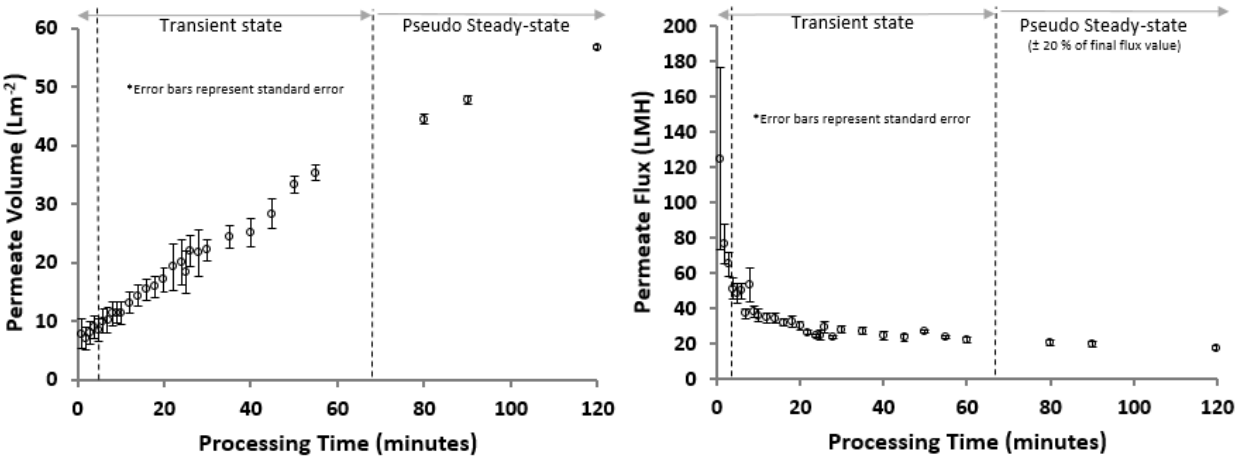

Figure A. 10: Average cumulative volume production (left) and permeate flux (right) and as a function of processing time for various FPBO cross-flow microfiltration trials at CanmetENERGY-Ottawa without any operational interference

Similar to as presented in Section 3.3.1.1, the range of data from above were manipulated to form a plot of V/A vs. tV/A in an attempt to determine the specific cake resistance of each trial. The results form this exercise are included below.

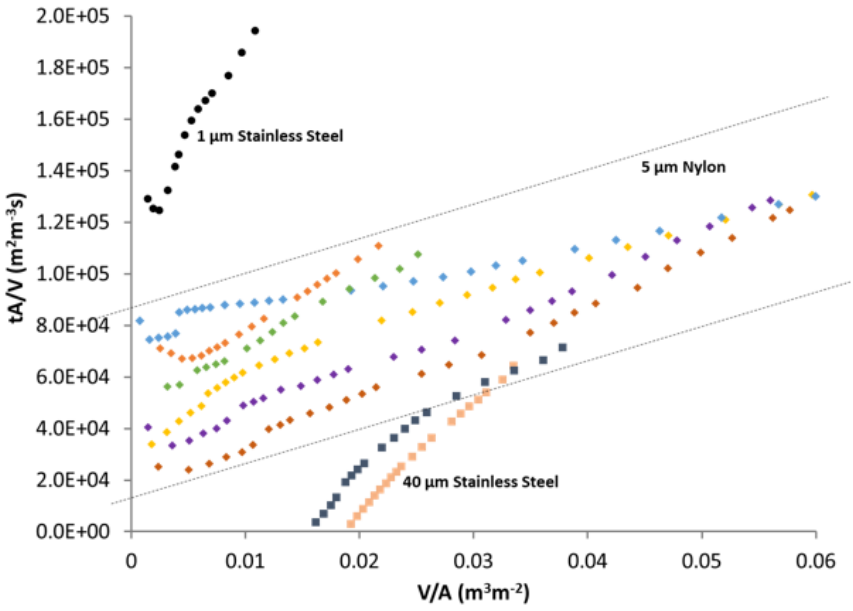

Figure A. 11: Plot of V/A vs. tA/V for various FPBO cross-flow microfiltration trials to determine the specific cake resistance during model development

It is evident from the plot above that the slope from the plots above is sensitive to the filtration media that was used. Furthermore, the intercept from the plots using 40 µm SS filters displayed a negative y-intercept, indicating that the membrane resistance value obtained did not correlate well with the model.

This result is likely a function of the high initial fluxes observed when using a 40 µm SS filter, which would translate to either very low or negligible membrane resistance value compared to the cake resistance.

The average (along with standard error) of calculated values from the model validation are also presented in Figure A. 12. This includes the specific cake resistance, the cake resistance at pseudo steady-state, the experimental and model flux, etc.

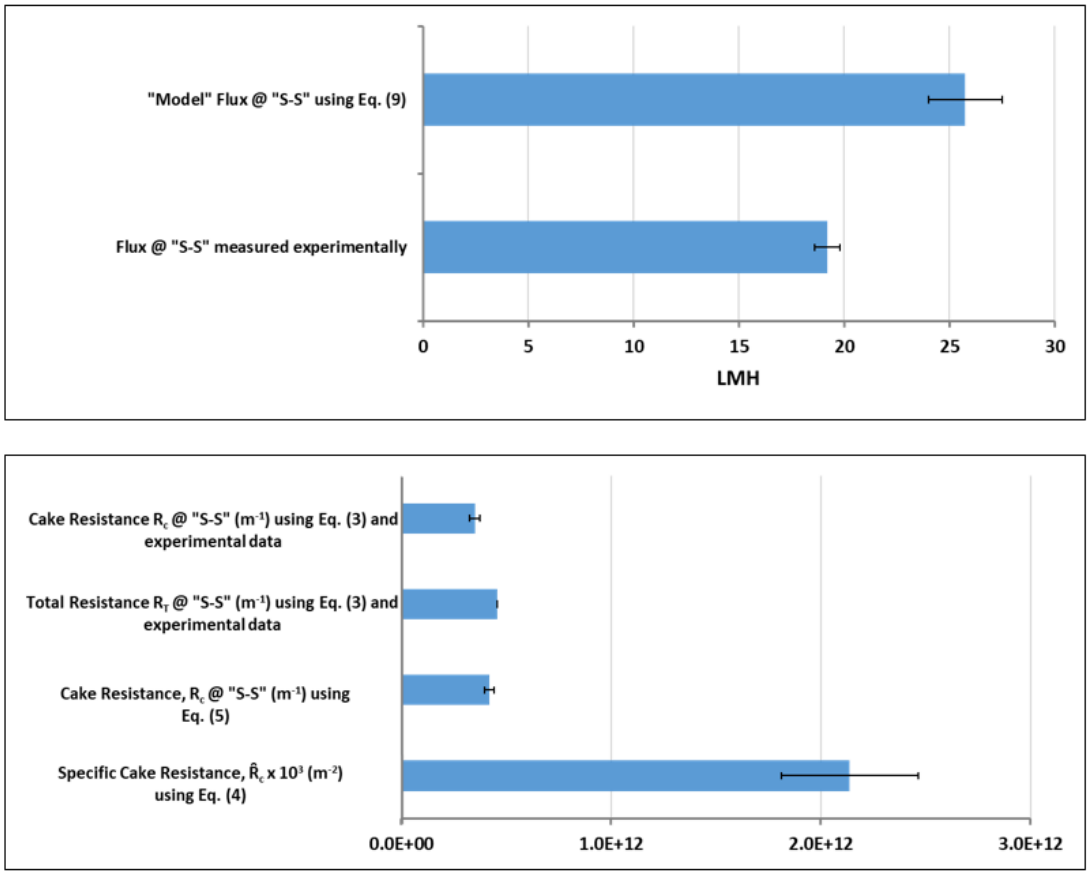

Figure A. 12: Comparison of flux (top) and resistance (bottom) values with associated standard error obtained from model development with range of operating conditions described above

C. Effect of operating parameters

Complementary plots which may be used to help describe the impacts of cross-flow microfiltration operating parameters and fluid properties on system performance and flux are described below.

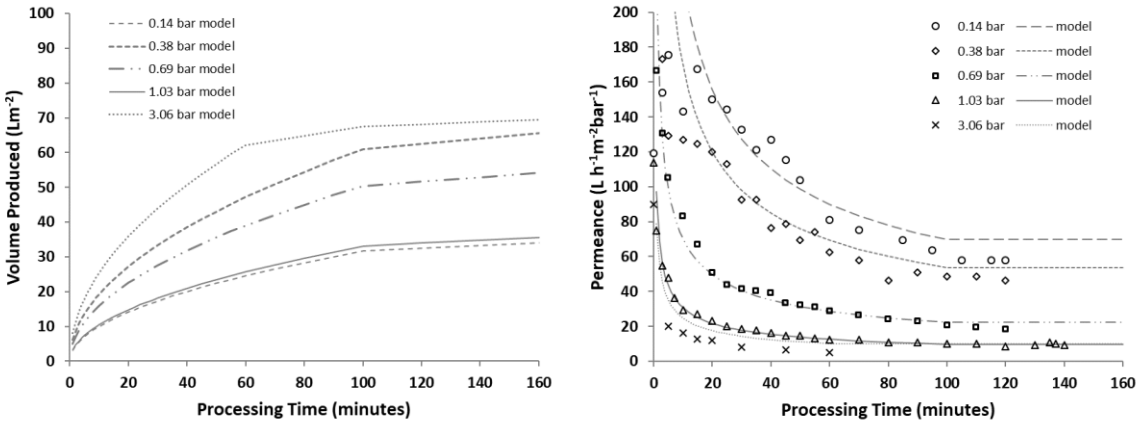

Figure A. 13: Cumulative volume production (left) and permeance (right) and as a function of processing time for five separate trials comparing the impact of transmembrane pressure, as described in Section 3.3.2

The initial permeate flux increased quite dramatically as the TMP increased. However, the decline in flux associated with processing time also increased substantially as the TMP increased. This is exemplified by comparing the reduction in flux after five minutes of operation. Reductions in permeate flux as low as 5% were observed at a TMP of 0.14 bar after this time, while as high as a 78% reduction in flux was observed at 3.06 bar. The pseudo steady-state flux was comparable between the lowest and highest TMP trials, and was 1.5-2 times larger at the intermediate TMP trials of 0.34-0.68 bar (5-10 psi).

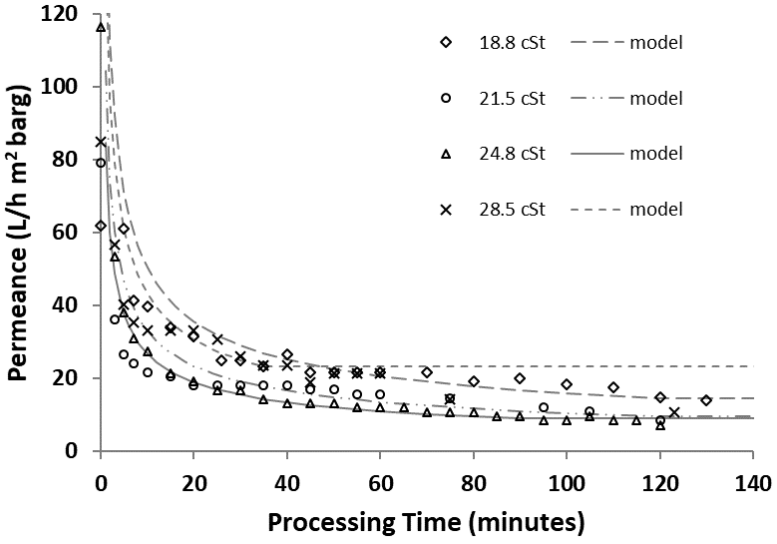

Figure A. 14: Permeance as a function of processing time for four separate trials comparing the impact of fluid kinematic viscosity by solvent addition, as described in Section 3.3.2.2

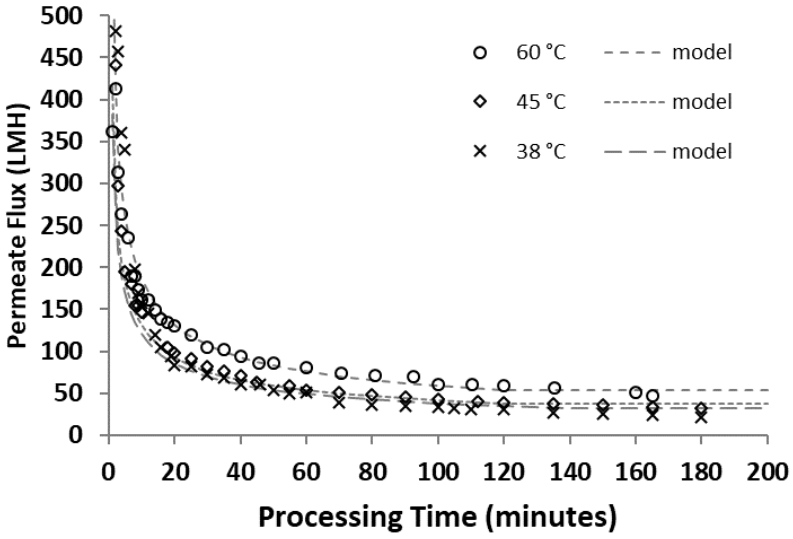

Figure A. 15: Permeate flux as a function of processing time for three separate trials comparing the impact of fluid temperature, as described in Section 3.3.2.2

Increasing the pre-heat temperature did not result in increased flux in the rapid decline transient region of the flux profile. However, it is apparent that the flux increases with pre-heat temperature during the intermediate decline transient and steady-state operating regions. Given this result, it may be possible that increasing the fluid temperature has a more profound impact on microfiltration by reducing the fouling cake (or "gel layer") viscosity, such that the cake fouling resistance decreases and causes larger pseudo steady-state permeate flux values relative to rapid decline transient operating region flux values.

D. Use of diascopic bright field microscopy to assess solids removal

During early experimental testing of cross-flow microfiltration with fast pyrolysis bio-oils, microscope imaging was used as a qualitative indicator for solids removal. Similar procedures were followed in existing literature on the subject [90]. Some select microscope images are included below to visually demonstrate the removal of suspended char particles in FPBO from cross-flow microfiltration. A Nikon ECLIPSE 50i POL diascopic bright-field microscopy unit was used to capture the images below.

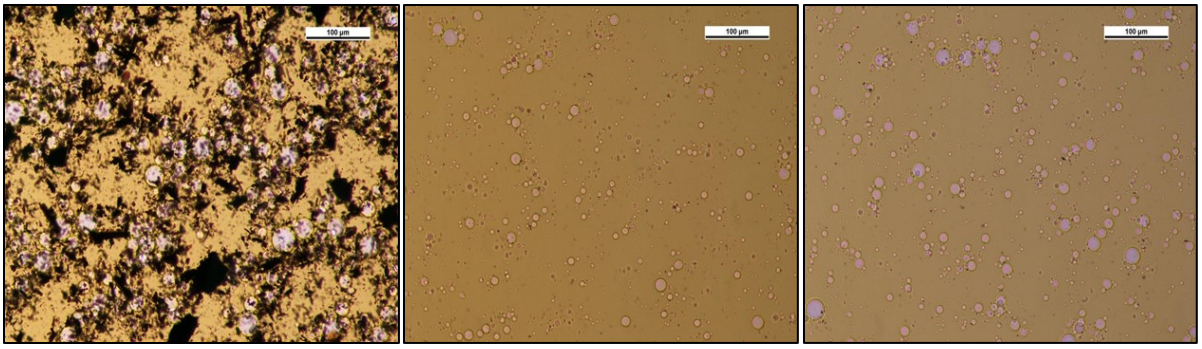

Figure A. 16: Microscope images (200x magnification) of a 2.3 wt% solids bio-oil (left) feed, with the permeate using a 5 µm hydrophilic polycarbonate membrane (middle) and a 5 µm hydrophobic polycarbonate membrane (right)

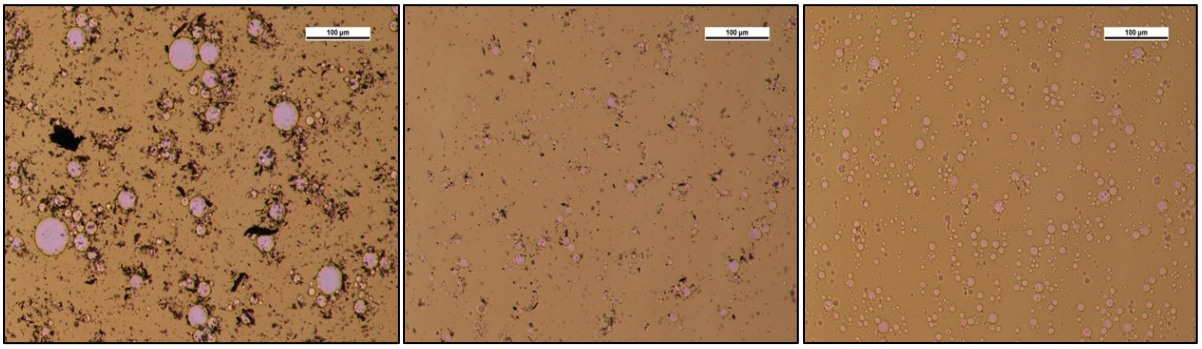

Figure A. 17: Microscope images (200x magnification) of a 0.3 wt% solids bio-oil (left) feed, with the permeate using a 40 µm stainless steel filter (middle) and a 5 µm hydrophobic polycarbonate membrane (right)

An important note here is that what appears to be air bubbles in the images above is actually emulsified droplets of the quench fluid that is used during condensation of the pyrolysis vapours in the pilot scale fast pyrolysis unit at CanmetENERGY-Ottawa.

A few procedural steps were followed to capture the microscope images:

i. Representatively sub-sample the bio-oil sample into a vial (in this case, 30 mL vials were used)
ii. Clean the microscope slides and cover slips with lint-free wipes. Use solvent to clean if necessary.
iii. Prior to sampling, ensure the aliquot of FPBO is well-mixed such that the solids may be assumed as evenly dispersed.
iv. As soon as possible after mixing, use a clean pipette to remove a small volume (1-5 mL) of the bio-oil. It is recommended to remove the sample from the middle section of the vial, and not the top/bottom.

v. Prior to depositing a drop of the bio-oil on the microscope slide, allow 1-2 drops of the sample to pass through the pipette to avoid any air bubbles. Once this is ensured, place 1-2 drops of the bio-oil on the microscope slide.

vi. Place the cover slip on the bio-oil sample. This is best done by applying the slip at approximately a 30° angle from the microscope slide plane, and done very slowly.

vii. Depending on the kinematic viscosity of the bio-oil, viscosity reduction may be required prior to sampling using a pipette. This may be done by adding a low viscosity diluent, or pre-heating the sample to appropriate temperatures (40-60 °C).

In addition to microscope images of the bio-oils before and after filtration, some microscope imaging was performed on the filtration media in an attempt to better understand the fouling that was occurring. An image of a PTFE membrane before/after bio-oil microfiltration is demonstrated below for reference.

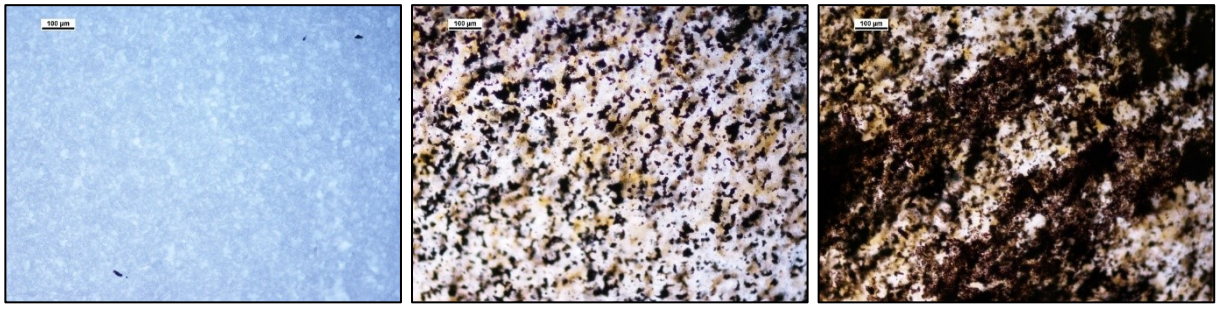

Figure A. 18: Optical microscope image of 5 µm PTFE membrane at 100x magnification before (left) and after bio-oil microfiltration (middle and right) showing different levels of fouling on surface of membrane

E. Multi-Linear Regression Modelling

As discussed in Section 3.3.3, the use of multi-linear regression models were used to verify the experimental observations with the entire range of FPBO cross-flow microfiltration data captured in this thesis. For transient operation, the specific cake resistance, as calculated by Eq. (4), was used as the response parameter. Meanwhile, for pseudo steady-state operation, the experimentally-measured flux was used as the response parameter. These response variables were tabularized with the independent parameters, which were the operating conditions under investigation, and included the fluid temperature, the transmembrane pressure, the fluid viscosity (at operating temperature), the filtration media pore size, the fluid injection velocity and the measured solids content. An excerpt of the data matrix used for regression analysis of the specific cake resistance is included below in Table A. 6.

Table A. 6: Excerpt of data matrix used to generate multi-linear regression model of specific cake resistance of FPBO cross-flow microfiltration under range of operating parameters included in Table 3.7

units	µm	°C	Pa	m s^{-1}	kg m^{-3}	Pa s	m^{-2}
Observation	**Pore Size**	**Average Temperature**	**Average TMP**	**Tube Exit Velocity**	**Solids Content**	**Viscosity (at operating temperature)**	**Specific RC , $\hat{R}C$**
1	5	40	310332	0.425	0.826	0.01048	2.164E+16
2	5	40	310332	0.425	0.826	0.01048	3.898E+16
3	40	40	310332	0.292	3.54	0.02294	1.623E+16
4	5	40	310332	0.292	3.54	0.02294	5.097E+15
5	40	40	310332	0.375	26.786	0.02721	3.133E+16
6	5	40	310332	0.375	26.786	0.02721	1.750E+14
7	5	40	13793	3.672	5.546	0.01746	1.220E+15
8	5	40	34481	2.768	5.664	0.01888	7.451E+14
9	5	40	68963	0.847	5.664	0.01770	2.329E+15
10	5	40	103444	0.508	4.366	0.01770	1.049E+16
n	40	40	34481	0.870	4.768	0.01955	1.077E+15
. . .	. . .	. . .	. . .	. . .	. . .	. . .	. . .
56	1	50	55860	0.316	5.1525	0.01932	2.690E+15

After developing the matrices, there was a total of 56 sample observations (independent trials) for each scenario. Outliers were removed from the dataset, by applying methods prescribed by Cook's distance parameter [112]. A total of five outlier trials were found, which included a few trials with high solids content (> 10 kg m^{-3}) as well as high fluid injection velocity (> 3 m s^{-1}). Thus, the matrix of results used in regression modelling included 51 sample observations in both cases.

The development of the multi-linear regression models followed procedures outlined in Chapter 12 of Montgomery et al, 2011 [112]. Alternatively, the use of the regression feature in the data analysis pack of Microsoft Excel provided a shortcut method to achieve the same result. At the conclusion of the regression modelling exercise, each response variable had an associated intercept value and associated regression parameter value for each independent variable. Furthermore, probability values (p-values), at a 95% confidence interval, for each regression parameter were found, along with a coefficient of determination (r^2) for the model fit.

Backward stepwise regression analysis was performed to identify the least significant independent variables based on procedures further outlined in Montgomery et al, 2011 [112]. The regression parameter with the lowest t-statistic value (the highest p-value) was eliminated from the model. The development of the regression model was then repeated with the remaining regression parameters.

However, the use of a single variable model is most often not suitable. Thus, the use of other evaluation criteria, such as the adjusted coefficient of determination (r^2), Mallow's Cp and the predictive sum of squares (PRESS) were used [112]. The adjusted r^2 evaluates the fit of the model, but is normalized for the number of parameters (since the unadjusted r^2 value cannot increase when a regression variable is removed). Mallow's Cp is used to determine the precision of a model, and the calculated value should decrease as the model precision increases. Finally, the PRESS for a given regression model is minimized when the optimal number of parameters have been removed. The complete backward stepwise elimination regression analyses for the specific cake resistance and pseudo steady-state flux are presented below in Table A. 7 and Table A. 8.

Table A. 7: Results from backward stepwise elimination regression for response variable specific cake resistance, at a confidence interval of 95%

	Model Coefficients: $\hat{R}_c = a + bx_1 + cx_2 + dx_3 + e\,x_4 + f\,x_5 + g\,x_6$					
Analysis Step	**Units**	**Step 1**	**Step 2**	**Step 3**	**Step 4**	**Step 5**
Linear Intercept	m^{-2}					
Model Coefficient		2.68E+16	2.61E+16	1.96E+16	8.80E+15	1.08E+16
P-Value		3.03E-05	4.96E-05	1.12E-03	3.79E-04	7.36E-05
Filtration Media Pore Size (x_1)	see note[a]					
Model Coefficient		-9.51E+14				
P-Value		1.54E-01				
Temperature (x_2)	˚C					
Model Coefficient		-2.99E+14	-3.38E+14	-2.51E+14		
P-Value		1.62E-02	6.20E-03	4.30E-02		
Transmembrane Pressure (x_3)	Pa					
Model Coefficient		2.58E+10	2.65E+10	3.36E+10	3.52E+10	
P-Value		7.63E-03	6.63E-03	9.45E-04	7.62E-04	
Fluid Injection Velocity (x_4)	$m\ s^{-1}$					
Model Coefficient		-2.96E+15	-3.09E+15			
P-Value		1.24E-02	9.81E-03			
Bulk Solids Content (x_5)	$kg\ m^{-3}$					
Model Coefficient		7.64E+14	7.90E+14	7.21E+14	8.25E+14	1.07E+15
P-Value		1.50E-04	1.04E-04	5.96E-04	1.08E-04	2.91E-06
Fluid Viscosity (x_6)	Pa s					
Model Coefficient		-4.60E+17	-4.22E+17	-3.92E+17	-4.29E+17	-4.54E+17
P-Value		4.36E-06	1.01E-05	6.73E-05	2.11E-05	4.25E-05
Model Fitting Parameters						
Adjusted R^2		0.624	0.607	0.550	0.509	0.380
PRESS		1.18E+33	1.22E+33	1.41E+33	1.30E+33	1.69E+33
C-p		25.6	24.5	23.0	13.1	14.5

[a]Due to limited number of pore sizes used, qualitative coefficients used in placed of quantitative. 40 µm = 0, 20 µm = 1, 5 µm = 2, 1 µm = 3

Table A. 8: Results from backward stepwise elimination regression for response variable pseudo steady-state flux, at a confidence interval of 95%

	Model Coefficients: $J = a + bx_1 + cx_2 + dx_3 + e\,x_4 + f\,x_5 + g\,x_6$					
Analysis Step	**Units**	**Step 1**	**Step 2**	**Step 3**	**Step 4**	**Step 5**
Linear Intercept						
Model Coefficient	$m^3\ m^{-2}\ s^{-1}$	-9.31E-06	-9.22E-06	-1.08E-05	-1.07E-05	-8.28E-06
P-Value		3.97E-04	3.79E-04	1.63E-05	2.77E-05	7.79E-05
Filtration Media Pore Size (x_1)	see note[a]					
Model Coefficient		-3.75E-07	-3.93166E-07	-4.04247E-07		
P-Value		7.79E-02	5.80E-02	5.58E-02		
Temperature (x_2)	˚C					
Model Coefficient		3.85E-07	3.89E-07	4.10E-07	3.95E-07	3.60E-07
P-Value		3.16E-11	8.08E-12	6.85E-13	2.58E-12	2.05E-12
Transmembrane Pressure (x_3)	Pa					
Model Coefficient		-5.33E-12	-5.49E-12			
P-Value		1.12E-01	9.82E-02			
Fluid Injection Velocity (x_4)	$m\ s^{-1}$					
Model Coefficient		2.53E-06	2.53E-06	2.81E-06	2.69E-06	
P-Value		8.44E-02	8.22E-02	5.69E-02	7.59E-02	
Bulk Solids Content (x_5)	$kg\ m^{-3}$					
Model Coefficient		-8.79E-07	-8.64E-07	-8.20E-07	-8.08E-07	-7.24E-07
P-Value		6.14E-09	2.94E-09	8.26E-09	2.04E-08	6.20E-08
Fluid Viscosity (x_6)	Pa s					
Model Coefficient		1.29E-05				
P-Value		6.42E-01				
Model Fitting Parameters						
Adjusted R^2		0.807	0.811	0.803	0.791	0.781
PRESS		1.13E-10	1.10E-10	1.09E-10	1.14E-10	1.19E-10
C-p		24.1	21.3	16.2	13.7	11.4

[a]Due to limited number of pore sizes used, qualitative coefficients used in placed of quantitative. 40 µm = 0, 20 µm = 1, 5 µm = 2, 1 µm = 3

F. Properties of feed and permeate samples in FPBO cross-flow microfiltration

In some instances, the physicochemical properties of the produced low-solids permeate samples were compared to the unfiltered bio-oil. Previous literature has found that the chemical composition of the bio-oil was largely unchanged, with the exception of hydroxyacetaldehyde doubling after microfiltration, although no explanation for this phenomenon was offered [90]. Furthermore, it was found that there were small increases in the water-soluble fraction (and necessarily small reductions in the water-insoluble fraction) of bio-oil after microfiltration. It was believed that this was due to the removal of the char particles, which are hydrophobic in nature. A summary of relevant physicochemical properties of FPBO

before/after microfiltration is shown in Table A. 1. Note that chemical analysis of the FPBO was not performed in this work.

Generally, the low-solids permeate bio-oil displayed marginal increases in water content and density, while also demonstrating marginal reductions in kinematic viscosity relative to the unfiltered bio-oil. This result is most likely linked to the physical removal of the char particles. It is also interesting to note that the density increases after microfiltration, which validates that the density of the suspended char particles is lower than that of the fast pyrolysis bio-oil. However, it is important to note that the changes in these properties are quite small, and thus is may be applicable to assumed that the physicochemical properties of filtered bio-oil (with the exception of solids and ash) are quite comparable to that of unfiltered bio-oil. This result could theoretically change depending on the filtration media and pore size used, as the rejection of individual components in bio-oil could significantly change the bulk properties of the low-solids permeate.

Table A. 9: Summary of select physicochemical properties of fast pyrolysis bio-oils before and after cross-flow microfiltration

Bio-Oil Used[b]	Filter Type	Fluid Temperature (°C)	Average TMP (bar)	Solids Content (wt%)		Ash Content (wt%)		Water Content (wt%)		Kinematic viscosity @operating temperature ($mm^2 s^{-1}$)		Heating Value ($MJ kg^{-1}$)		Density ($kg m^{-3}$)	
Stream[a]				F	P	F	P	F	P	F	P	F	P	F	P
6	5-6 µm PTFE	40	0.69	0.14	0.12	0.018	0.014			13.85	13.21				
6	5-6 µm PTFE	40	0.69	0.05	0.13	0.014	0.016			34.15	33.88				
2	5-6 µm PTFE	40	1.72	0.4	0.09	0.078	0.041			26.57	24.62				
2	40 µm SS	40	1.72	0.4	0.11	0.078	0.031								
2	5-6 µm PTFE	40	1.03	0.27	0.08	0.067	0.001								
2	40 µm SS	40	1.03	0.27	0.11	0.067	0.012			11.9	11.02				
2	40 µm SS	40	0.69	0.25	0.22	0.059	0.057			13.45	13.41				
2	40 µm SS	40	0.69	0.29	0.1	0.068	0.054								
2	40 µm SS	40	0.69	0.29	0.2	0.068	0.06	17.8	18.0	28.05	27.83	19.78	19.26		
2	5 µm HP PCTE	40	3.10	0.27	0.07	0.065	0.044	16.8	17.0	26.12	25.66	19.81	18.81	1185	1204
2	5 µm HB PCTE	40	3.10	0.27	0.05			16.8	17.3	26.12	26.05	19.81	18.72	1185	1205
2	5 µm HP PCTE	40	3.10	0.25	0.06	0.061	0.048	16.8	17.2	23.83	22.76	19.45	18.29	1182	1201
2	5 µm HB PCTE	40	3.10	0.25	0.06	0.061	0.044	16.8	17.2	23.83	22.84	19.45	18.27	1182	1202
1	5 µm HP PCTE	40	3.10	0.16	0.05	0.171	0.187			9.0	8.9			1149	1147
1	5 µm HB PCTE	40	3.10		0.08		0.166				9.0				1153
3	5 µm HP PCTE	40	3.10	2.3	0.04	0.119	0.046			24.35	19.84			1156	1202
2	40 µm SS	40	3.10	0.3	0.07	0.033	0.021							1188	1204
2	5 µm HB PCTE	40	3.10	0.3	0.05	0.033	0.018							1188	1197
3	40 µm SS	40	3.10	2.27	0.03	0.092	0.051							1153	1198
3	5 µm HB PCTE	40	3.10	2.27	0.04	0.092	0.049							1153	1188
2	40 µm SS	40	3.10	0.3	0.07	0.033	0.021			19.4					
2	5 µm PCTE HB	40	3.10	0.3	0.05	0.033	0.018			19.4					
3	40 µm SS	40	3.10	2.27	0.03	0.092	0.051			23.1					
3	5 µm PCTE HB	40	3.10	2.27	0.04	0.092	0.049			23.1					
10	40 µm SS	40	0.34	0.4	0.01					16.4	15.9				
4	40 µm SS	40	0.34	0.36	0.13	0.364	0.313			6.6	6.6				
4	5 µm nylon	40	0.34	0.41	0.04	0.364	0.332			6.7					
4	20 µm nylon	40	0.34	0.38	0.05		0.391			6.8					
5	40 µm SS	40	0.34	0.64	0.12			16.2	16.1	28.5					
5	5 µm nylon	40	0.34	0.64	0.01			16.2	16.2	28.5					
5	5 µm nylon	40	0.69	0.56	0.01			15.5	15.1	24.8					
5	40 µm SS	40	0.69	0.56	0.06			15.5	15.4	24.8					
5	40 µm SS	40	0.69	0.54	0.07			14.3	14.5	21.5					
5	5 µm nylon	40	0.69	0.54	0.02			14.3	14.6	21.5					
5	40 µm SS	40	0.48	0.5	0.05			13.2	13.5	18.8					
5	5 µm nylon	40	0.69	0.5	0.02			13.2	13.4	18.8					

Bio-Oil Used[b]	Filter Type	Fluid Temperature (°C)	Average TMP (bar)	Solids Content (wt%)		Ash Content (wt%)		Water Content (wt%)		Kinematic viscosity @operating temperature ($mm^2\ s^{-1}$)		Heating Value ($MJ\ kg^{-1}$)		Density ($kg\ m^{-3}$)	
Stream[a]				F	P	F	P	F	P	F	P	F	P	F	P
8	5 µm nylon	40	0.34	0.44	0.06	0.139	0.106	24.4		20.3					
8	5 µm nylon	45	0.34	0.12	0.01	0.135	0.142			19.9					
8	40 µm SS	45	0.34	0.12	0.01	0.135	0.138			19.9					
6	5 µm nylon	47.5	0.34	0.05	0.02	0.045	0.048	23.5		16.8					
6	5 µm PCTE HB	47.5	0.34	0.05	0.07		0.048			16.8					
11	5 µm nylon	50	0.69	0.43	0.03		0.02			28.0					
11	40 µm SS	50	0.69	0.43	0.17		0.18			28.0					
11	5 µm nylon	50	0.34	0.41	0.01	0.191	0.167			28.0					
9	1 µm SS	50	0.59	0.41	0.01	0.154	0.119	25.2	23.8	13.1					
9	40 µm SS	50	0.59	0.41	0.06	0.154	0.124	25.2	24.1	13.1					
11	1 µm SS	51.4	0.69	0.69	0.06	0.122	0.091	20.7	23	21.0	20.0				
11	1 µm SS	52.1	0.69	0.08	0.08	0.107	0.115	21.6	21.4	19.4	21.4				

[a]F = feed, P = permeate; [b]Refer to Table 3.1

Appendix E. Segregation of Suspended Char Particulate During Fast Pyrolysis Bio-oil Settling

A. Settling Apparatus

The elevated presence of suspended solid particles in FPBO can lead to sludge formation in holding vessels for applications including heat and power, as well as catalytic upgrading [36]. Previous work by CanmetENERGY-Ottawa has attempted to determine a standardized method for assessing bio-oil "uniformity". One such approach attempts to characterize the uniformity of FPBO by its propensity to segregate during undisturbed settling for 7 days. A similar approach has been identified as a tool to define homogeneity (or alternatively, heterogeneity) by VTT [35]. To accomplish this, a vertical "vessel" with strategically-placed valves was assembled, such that four distinct fractions of settled bio-oil could be separated and collected independently after a specified duration (7 days in this case) settling test. The apparatus has purposely been constructed from common components and fittings to be easily replicable and available at a low cost. It has been previously described in a delivered conference presentation [82] but not published in written form. A schematic of the device is included below for reference.

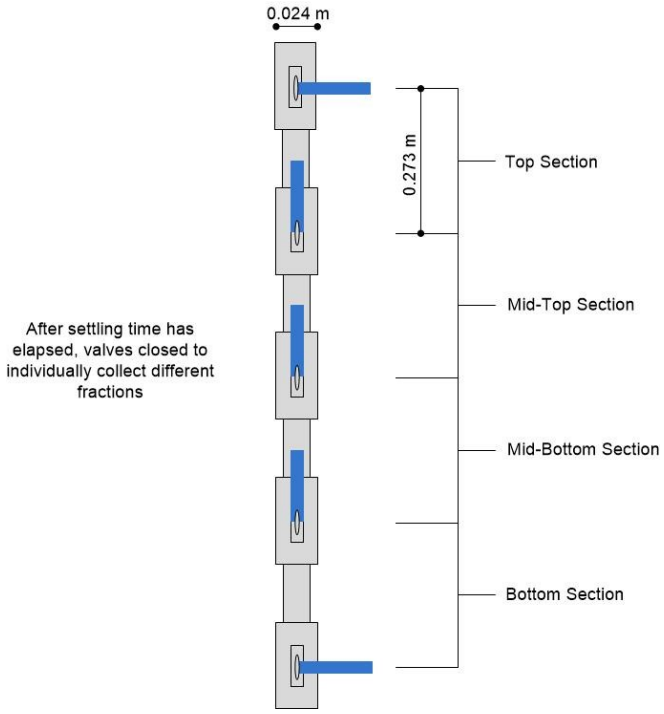

Figure A. 19: Schematic of bio-oil settling apparatus

B. Results from Settling Tests

A series of results from 7-day settling tests with various fast pyrolysis bio-oils are summarized in Figure A. 20 in which the solids content was specifically investigated. For each 7-day settling test, approximately 500 mL of FPBO was loaded into the settling apparatus. After 7 days, each fraction was collected separately and submitted for solids content (ASTM D7579) performed at the characterization laboratory at CanmetENERGY-Ottawa. Additional results exist for water content and kinematic viscosity (40 °C) under the same test criteria, although are not included below.

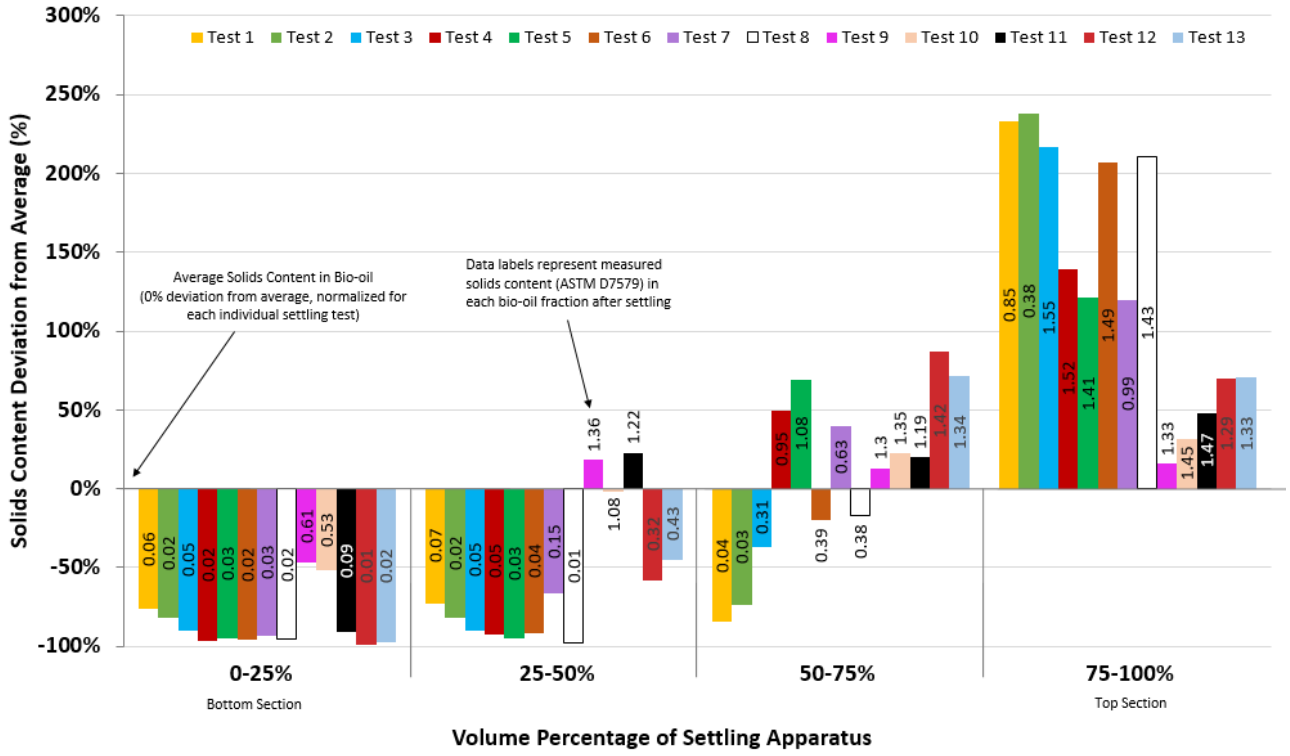

Figure A. 20: Summary of results from fast pyrolysis bio-oil 7-day settling tests describing the relative deviation in solids content based on volumetric region of settling apparatus

From the results above, the accumulation of solids in the top section after 7 days in the settling apparatus is evident. Furthermore, the majority of the top section settled bio-oil samples contain a suspended char concentration of greater than 1.0 wt%. Meanwhile, it is apparent that the solids content in the two bottom sections of the apparatus is consistently low (< 0.1 wt%). In many cases, the solids content of the 50-75 vol% of the apparatus also falls within the < 0.1 wt% criteria. These results suggest that allowing sufficient settling time for fast pyrolysis bio-oil in itself appears to be a technically-feasible method for significant reductions of solids content from the bulk liquid, if an effective sludge removal strategy could be implemented.

C. Comparison of Uniformity of Filtered and Non-Filtered Bio-oils

It was also of interest to perform settling tests with filtered fast pyrolysis bio-oils to determine any significant differences in solids accumulation after a seven day settling test. A summary of settling results from filtered bio-oils are included below in Figure A. 21, along with the median results from unfiltered bio-oil for comparison.

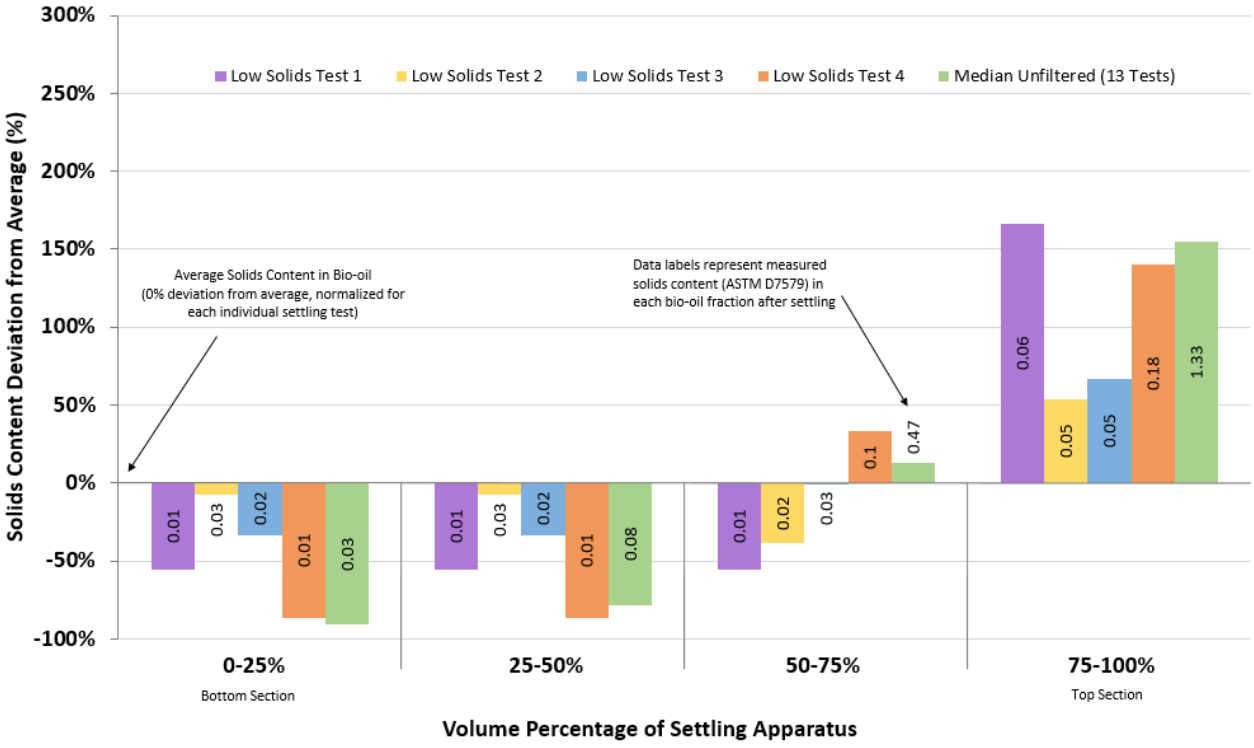

Figure A. 21: Relative deviation in measured solids content from 7-day settling test with filtered, low-solids bio-oil relative to median results from unfiltered bio-oils 7-day settling test

The stratification of solids in the settled FPBOs follow similar trends between the filtered and unfiltered samples, despite the solids content in filtered bio-oil being much lower. In many cases, the filtered bio-oil shows a concentration of solid particulate below 0.1 wt% in all stages, whereas the median value for unfiltered bio-oil at the top section exceeds 1.0 wt%. These results demonstrate some of the practical advantages of applying solids removal techniques, such as microfiltration, to bio-oil prior to direct utilization applications. In this case, significantly less stratification of solids is observed relative to unfiltered bio-oil.

D. Conclusions

The results from this subset of data indicate that it may be worthwhile to investigate the removal of solids from fast pyrolysis bio-oils using methods in which accelerated the settling of the suspended char particles is performed. Many of these clarification techniques are employed as preliminary processing strategies in wastewater treatment and mineral processing (among other industries), and could include air sparging, use of hydrophobic additives to capture biochar particles (similar to air sparging), advanced settling vessels, application of electric fields, etc. [113].